Mid- to late Holocene climate variability of the Maritime Continent

Dissertation zur Erlangung des Doktorgrades der Naturwissenschaften

Dr. rer. nat.

im Fachbereich Geowissenschaften

der Universität Bremen

vorgelegt von

Cornelia Regula Kwiatkowski

Bremen, September 2016

Tag des öffentlichen Kolloquiums

28.10.2016

10 Uhr s.t.

Gutachter der Dissertation

Prof. Dr. Dierk Hebbeln

Prof. Dr. Heiko Pälike

Prüfer

Prof. Dr. Tobias Mörz

Dr. Mahyar Mohtadi

Weitere Mitglieder des Prüfungsausschusses

Dr. Jeroen Groeneveld

Adrian Baumeister

Cornelia Regula Kwiatkowski

Marum – Zentrum für marine Umweltwissenschaften

Datum: 13.09.2016

ERKLÄRUNG

Hiermit versichere ich, dass ich

1. die Arbeit ohne unerlaubte fremde Hilfe angefertigt habe,

2. keine anderen al die von mir angegebenen Quellen und Hilfsmittel benutz habe und

3. die den benutzen Werken wörtlich oder inhaltlich entnommenen Stellen als solche kenntlich gemacht habe.

Bremen, den 13.09.2016

…….
(Unterschrift)

Danksagung

Ich möchte mich sehr herzlich bei Prof. Dr. Dierk Hebbeln und Dr. Mahyar Mohtadi für die Vergabe dieser Arbeit und für die sehr gute Betreuung während meiner Promotion bedanken.

Ich danke Prof. Dr. Heiko Pälike für die Erstellung des Zweitgutachtens.

Vielen Dank an mein Thesis Komitee für die jahrelange Unterstützung, hilfreiche Diskkussionen und viele gute Ratschläge.

Ein besonderer Dank gilt Dr. Stephan Steinke und Dr. Jeroen Groeneveld, die meine Begeisterung für Foraminiferen als Werkzeug zur Klimarekonstruktion schon während des Studiums geweckt haben und von deren Erfahrung und Fachwissen ich sehr profitiert konnte.

Vielen Dank an die gesamte AG Hebbeln, im Besonderen an Dr. Claudia Wienberg und Dr. Jürgen Titschack für die Unterstützung, die 10:00 h Kaffee-Runde mit jeder Menge Kekse und die gute Zeit während meiner Promotion.

Ein herzlicher Dank gebührt meinen Zimmerkollegen Florian Boxberg und Sandy Böhnert für die ein oder andere Tanz- und Showeinlage und eine allzeit sehr gute Arbeitsatmosphäre.

Ich möchte mich auch bei meinen Co-Autoren, besonders bei Dr. Matthias Prange, Dr. Ann Holbourn und Prof. Dr. Wolfgang Kuhnt, aber auch bei unsere indonesischen Kooperationspartnern Dr. Haryadi Permana, Dr. Rina Zuraida und Dr. Susilohadi Susilohadi für die gute Zusammenarbeit und viele hilfreiche Kommentare bedanken.

Für die Unterstützung im Labor möchte ich mich bei Dr. Jürgen Titschack, Dr. Monika Segl, Dr. Henning Kuhnert, Birgit Meyer-Schack, PD Dr. Matthias Zabel, Silvana Pape, Christina Gnade, Volker Diekamp, Kai Grumbt, Elena Metang und Olaf Winkler bedanken. Vielen Dank für den IT Support von Jutta Bülten und Hilfe bei allen administrativen und logistischen Belangen von Carmen Murken, Dr. Nico Dittert und Götz Ruhland.

Dem Bremer Graduierten Kolleg ‚Global Change in the Marine Realm - GLOMAR' möchte ich für viele hilfreiche und interessante Lehrveranstaltungen, Seminare und Workshops danken.

Die vorliegende Arbeit wurde im Rahmen des Projekts CAFINDO (03F0645A) als Teil des Deutsch-Indonesischen Kooperationsprojektes SPICE III finanziell vom Bundesministerium für Bildung und Forschung (BMBF) gefördert und von dem DFG-Research Center / Cluster of Excellence „The Ocean in the Earth System" unterstützt.

Vielen Dank an all meine Freunde, vor allen an Nadine Rippert, Martina Hollstein, Wiebke Grewe, Arne Schwab, Hiske Fink und Andi Wanger für stets offene Ohren und die unglaubliche Unterstützung während der gesamten Promotion. Ihr seid die Besten!

Ein ganz besonderer Dank gilt meiner Familie, im Besonderen meinen Schwiegereltern, Karin und Jürgen Kwiatkowski, die sich während Konferenzen oder langen Arbeitstagen liebevoll um unseren kleinen Hannes gekümmert haben.

Auch möchte ich Hannes für herrliche Ablenkung und viele erholsame Kuschelstunden danken!

Zu guter Letzt möchte ich mich ganz besonders bei meinem Mann, Henning Kwiatkowski, für seinen Rückhalt und seine Unterstützung während des Studiums und während der Promotion bedanken. Ein unendliches Glück, dass es dich gibt!

Table of Contents

Abstract

The Maritime Continent is located within the Indo-Pacific Warm Pool (IPWP) which is described as the largest area of warm sea surface temperatures with the highest rainfall on Earth. Serving as the largest source of atmospheric water vapor and latent heat, it is of crucial importance to global atmospheric and hydrologic circulation. The regional climate is controlled by large-scale phenomena such as the seasonal migration of the Intertropical Convergence Zone (ITCZ), the Australian-Indonesian monsoon system as well as climate anomalies like the Indian Ocean Dipole (IOD) and or oscillations such as El Niño-Southern Oscillation (ENSO). Due to the complex topography of the Maritime Continent and very local air-sea interactions, the environmental influence of these phenomena strongly varies across the region today and may have done so during the past.

Environmental reconstructions have been conducted by using proxy records from speleothems, corals as well as marine and lacustrine sediments revealing a complex history of climate variations of the Maritime Continent during the Holocene. Mid-to late Holocene sea surface conditions were reconstructed by using trace elements and stable isotopes as well as relative abundances of planktic foraminifera. Additionally, the amount, composition and grain size distribution of bulk sediment was investigated. Based on multi-proxy reconstructions from four marine sediment cores from western, central, and southern Indonesia, this thesis outlines variations in rainfall and upper water column conditions in response to large-scale climate phenomena as the IOD, the Australian-Indonesian monsoon system and ENSO from mid- to late Holocene.

In the eastern tropical Indian Ocean (western Indonesia), thermocline temperatures, the thermal gradient of the upper ocean as well as the relative abundances of planktic foraminifera reveal a deeper thermocline between 8 and 3 ka and an uplift of the thermocline for the past 3 ka off western Sumatra. The recorded shoaling of the thermocline and the deduced increased occurrence of upwelling likely results from a more-positive IOD-like mean state of the Indian Ocean during the late Holocene. A transient Holocene climate model simulation reproduces anomalous surface easterly winds over the equatorial eastern Indian Ocean that support the interpretation of more positive IOD-like mean state during the late Holocene compared to the mid-Holocene.

In the Makassar Strait (central Indonesia) cooler and fresher sea surface coincide with an increase in terrigenous runoff from eastern Borneo and point to an intensified Australian-Indonesian summer monsoon (AISM) during the late Holocene. Contemporaneously, periods

characterized by freshwater pulses recorded off eastern Borneo might be related to a strengthened ENSO with intensified El Niño and La Niña conditions.

Sediment composition within the Java Sea (southern Indonesia) suggest variations in precipitation in southern Borneo and eastern Java in response to the Australian-Indonesian monsoon system and ENSO. Drier conditions in southern Borneo but relatively unchanged rainfall in Java around ~2 ka indicate more frequent and/or intensified El Niño events which are masked by an intensified AISM in Java. Present-day variations in rainfall over Java reveal a close relationship of monsoonal rainfall to northern high latitude climate variations which may have persist also during the past and contributed to the late Holocene intensification of the AISM over the Maritime continent.

Zusammenfassung

Der maritime Kontinent befindet sich im Indo-Pacific Warm Pool. Der Indo-Pacific Warm Pool gilt weltweit als das größte Gebiet warmer Oberflächenwassertemperaturen mit dem höchsten Niederschlag und dient somit als größte Quelle atmosphärischen Wasserdampfes und latenter Wärme. Diese Region ist daher von entscheidender Wichtigkeit für die globale atmosphärische und ozeanische Zirkulation. Das regionale Klima wird bestimmt durch großräumige Klimaphänomene wie die saisonale Verschiebung der Intertropischen Konvergenzzone (ITCZ), dem australisch-indonesischen Monsunsystem, sowie Klimaanomalien wie den Indian Ocean Dipole (IOD) und Zirkulationssysteme wie die El Niño-Southern Oscillation (ENSO). Die komplexe Topographie und lokale, atmosphärisch-ozeanische Wechselwirkungen führen dazu, dass der Einfluss dieser Klimaphänomene auf die heutige, und möglicherweise auch auf die frühere Umwelt, regional stark variiert.

Umweltrekonstruktionen anhand von Proxies aus Speläothemen, Korallen sowie marinen und lakustrinen Sedimenten zeigen eine komplexe Geschichte holozäner Klimaveränderungen des Maritimen Kontinentes. Es wurden mittel- bis spät-holozäne Oberflächenwasserbedingungen mit Hilfe von Spurenelementen, stabilen Isotopen und relative Vorkommen planktischer Foraminiferen rekonstruiert. Darüber hinaus wurden Menge, Zusammensetzung und Korngrößenverteilung des abgelagerten Sedimentes untersucht. Basierend auf Multiproxy-Rekonstruktionen an vier marinen Sedimentkernen aus West-, Zentral- und Süd-Indonesien, befasst sich diese Arbeit mit mittleren und spät-holozänen Veränderungen des Niederschlages und der Oberflächenwasserbedingungen als Folge von Veränderungen in großräumigen Klimaphänomene wie dem Indian Ocean Dipole, El Niño-Southern Oscillation (ENSO) und dem Australisch-Indonesischen Monsunsystem.

Im östlichen, äquatorialen Indischen Ozean (West-Indonesien) zeigen Thermoklinentemperaturen, der Temperaturgradient innerhalb der oberen Wasserschichten sowie das relative Vorkommen planktischer Foraminiferen eine tiefere Thermokline zwischen 8.000 und 3.000 Jahren vor heute und eine Hebung der Thermokline vor Sumatra während der vergangenen 3.000 Jahre. Die aufgezeichnete Thermoklinenverflachung und das davon abgeleitete verstärkte Auftreten von Auftrieb könnte auf eher positive IOD-ähnlichen Bedingungen im Indischen Ozean während des späten Holozäns zurückzuführen sein. Eine transiente Klimasimulation bildet eine Zunahme ungewöhnlicher Ostwinde entlang der Oberfläche über dem östlichen, äquatorialen Indischen Ozean über die letzten 8.000 Jahre ab und unterstützt damit die Interpretation von eher positiven IOD-ähnlichen Bedingungen im späten Holozän gegenüber dem mittleren Holozän.

In der Straße von Makassar (Zentral-Indonesien) stimmt eine kühlere und weniger-saline Meeresoberfläche mit einem Anstieg des terrigenen Eintrags aus Ostborneo überein und deutet somit auf einen verstärkten, australisch-indonesischen Summermonsun im späten Holozän hin. Zeitgleich sind Perioden, die sich durch Süßwasserimpulse auszeichnen, vor Ostborneo aufgezeichnet und stehen vermutlich mit einem verstärkten ENSO mit stärkeren El Niño- und La Niña-Bedingungen in Zusammenhang.

Die Sedimentzusammensetzung in der Java See (Süd-Indonesien) zeigt Veränderungen im Niederschlag über Süd-Borneo und Java im Zusammenhang mit dem australisch-indonesischen Monsunsystem und ENSO. Trockenere Bedingungen in Süd-Borneo und relativ gleichbleibender Niederschlag über Java lassen sich auf ein erhöhtes Auftreten und/oder verstärkte El Niño-Bedingungen und deren Überlagerung durch einen verstärkten Summermonsun über Java zurückführen. Gegenwärtige Änderungen im Niederschlag über Java zeigen eine enge Beziehung des Monsunregens zu Klimaveränderungen in den höheren, nördlichen Breiten, welche womöglich auch während des Holozäns existierte und zur spät-holozänen Verstärkung des australisch-indonesischen Summermonsuns über dem Marinen Kontinent betrug.

1. Introduction

1.1. Motivation

Indonesia as part of the Maritime Continent is located around the equator within the Indo Pacific Warm Pool (IPWP) between the Pacific and Indian Oceans and between the Asian and Australian continents (Fig. 1).

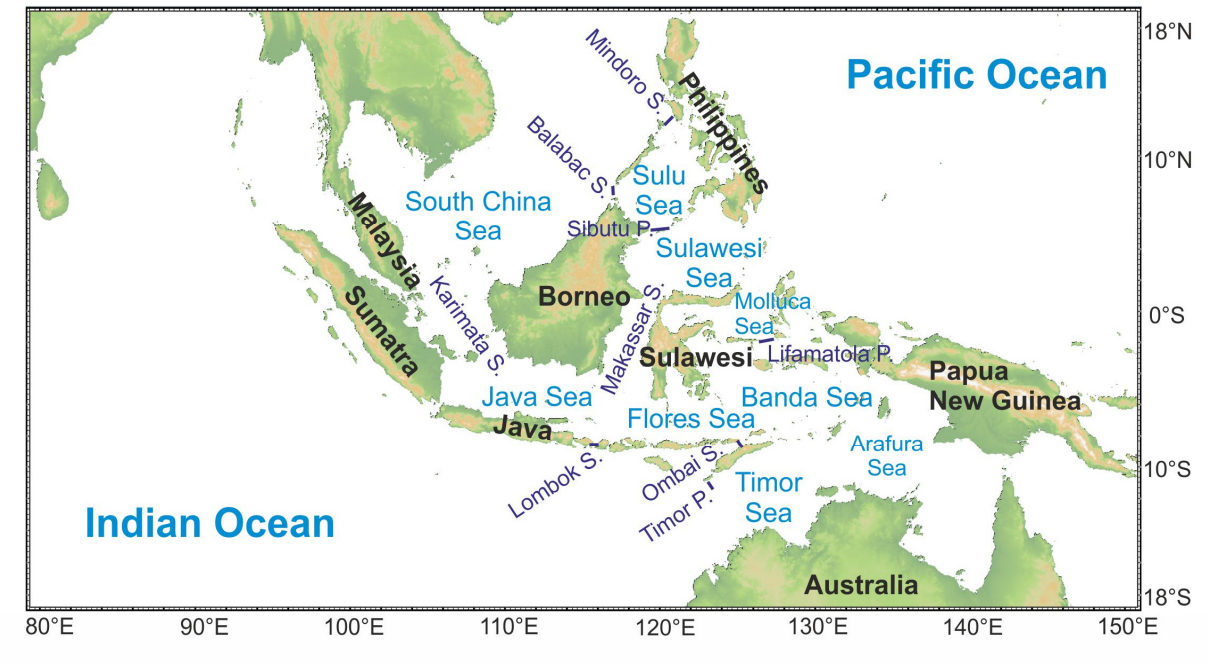

Figure 1: Map of the Maritime Continent with names of oceans, adjacent seas (blue), sea passages (purple) and islands (black) created by using GeoMapApp.

In 2016, approximately 260 Mio. inhabitants live in Indonesia (http://worldpopulationreview.com/countries/indonesia-population/) strongly depending on agriculture, fisheries and mining in terms of employment, food security, and global trades. Thus, a healthy ecosystem in Indonesia is essential for the local population.

Marine and terrestrial ecosystems in Indonesia are strongly dependent on the global and regional climate evolution. Today, the seasonal cycle of the Indonesian climate is controlled by the migration of the Intertropical Convergence Zone (ITCZ) passing Indonesia twice a year and the Australian-Indonesian monsoon system predominated by southeasterly winds during austral winter and northwesterly winds during austral summer (Wyrtki, 1961; Robertson et al., 2011). The seasonal cycle is affected by climate anomalies such as the Indian Ocean Dipole (IOD, Saji et al., 1999; Webster et al., 1999) or the El Niño – Southern Oscillation (ENSO, Philander, 1983, 1985) acting on an interannual scale. Generally, drier conditions and prolonged dry

seasons are often associated with a positive IOD (Saji et al., 1999) or/and an El Niño event (Rasmusson and Carpenter, 1982). These oscillatory modes interact with each other resulting in a very complex climatic system over Indonesia and hence, the Maritime Continent. In addition to the strong entanglement of these climate phenomena, their influence varies across the region due to island topography and ocean–atmosphere fluxes, which are mainly imposed by sea-surface temperature (SST) variability (Aldrian and Susanto, 2003).

Facing global climate change, Indonesia will likely suffer from a rising sea level, an increase in average SST, and a decrease (increase) in average rainfall in southern (northern) Indonesia (Pachauri et al., 2014). In response to a rising SST it is very likely that extreme precipitation events will become more frequent (Pachauri et al., 2014). Future environmental changes may lead to intensified monsoonal rainfall (Jourdain et al., 2013; Pachauri et al., 2014) and probably a shift to predominant El Niño conditions (Collins, 2005). Therefore, climate change will have a dramatic effect on marine ecosystems (Pachauri et al., 2014) as well as on agricultural activities in Indonesia and other tropical countries (Naylor et al., 2007) strongly affecting food security and nutrients supply to local people.

To adapt to a changing ecosystem, the prediction of possible environmental changes and their implications for society are very important. By using climate simulations, effects of environmental changes can be determined and future climate evolution can be projected. Thus, climate models are of crucial importance to simulate future climate scenarios and to illustrate potential interactions of climate phenomena as well as the evolution of these phenomena in response to changes in environmental boundary conditions such as atmospheric CO_2, solar radiation or sea level. Furthermore, climate models help to identify dynamics and possible forcing mechanisms of environmental changes and provide a good basis to understand how climatic phenomena are interconnected in past, present, and future times. However, climate models are only reliable to predict future variations when they reproduce past climatic changes confidently.

Therefore, proxy-based climate reconstructions build the basis of climate modelling and are essential to validate the outcome of complex climate simulations. By using observational data from the past centuries or proxy reconstructions from various climatic archives such as marine sediments, past climate variations can be reconstructed over centennial to geologic time scales. Recent climate models that reflect the spatial and seasonal distribution of rainfall over the Maritime Continent are very inconsistent in reproducing the future evolution of the monsoonal system over the Maritime Continent (Jourdain et al., 2013). The land-sea heterogeneity and the complex topography with high narrow mountain ranges result in large differences in the model

outputs (Jourdain et al., 2013). Furthermore, potential bias of local air-sea interactions and interannual variations in response to ENSO and IOD might complicate possible predictions.
Within this study, mid- to late Holocene climate variability of the Maritime Continent is elucidated by using marine proxy records from different regions in Indonesia indicating centennial to millennial variations in precipitation and sea surface conditions. The recorded signals vary with the study site and the used proxy highlighting the need of more reconstructions from different regions in Indonesia to build a reliable, highly resolved fundament for climate modelling focusing on the IPWP region. Thus, proxy reconstructions, especially resolving centennial to millennial climate variations within the Holocene, from various regions of the Maritime Continent are indispensable to draw a complete picture of past climate variability in response to IOD, ENSO and the monsoonal system to enable the prediction of future climate evolution in Indonesia.

1.2. Scientific Objectives and Approach

Centennial to millennial-scale changes in Holocene over-land precipitation and sea surface conditions in Indonesia have been studied by using lacustrine (Konecky et al., 2013; Russell et al., 2014) and marine sediment cores (e.g. Linsley et al., 2010; Mohtadi et al., 2011), corals (Abram et al., 2009), speleothem records (e.g. Partin et al., 2007; Griffiths et al., 2009; 2010). Lacustrine and marine sediment cores provide decadal to millennial resolution using a variety of proxies such as the elemental composition of bulk sediments or foraminifera tests reflecting environmental changes on land and in the ocean, respectively. Trace elements and stable isotopes from corals are linked to environmental changes in the water column and impress by a seasonal resolution. However, coral based reconstructions only span the lifetime of a coral, thus a couple of years. On longer time scales, different specimens are needed to reconstruct the climate variations far back in time providing discontinuous but highly resolved climate reconstructions. Speleothems are mineral deposits formed by cave drip water and are highly sensitive to environmental changes within the cave, the soil and vegetation cover above the cave and in the atmosphere (Fairchild and Baker, 2012). The physical and chemical parameters of speleothems allow the estimation of environmental parameters such as air temperature, the amount of rainfall, type or amount of vegetation and the atmospheric circulation in an annual to millennial resolution (Fairchild et al., 2006a). However, variations in karstic aquifer, crystal growth and secondary alteration often complicate the interpretation of speleothem records (Fairchild et al., 2006b).

While speleothem records from northern Borneo indicate more humid conditions during the mid-Holocene and drier conditions during the late Holocene (Partin et al., 2007), speleothem records from southern Indonesia indicate dry conditions during the mid-Holocene and a wetter late Holocene (Griffiths et al., 2009; 2010; Ayliffe et al., 2013). Latter is supported by the elemental composition in marine sediments retrieved from southern Indonesia which indicate an increase in terrestrial runoff during the late Holocene (Mohtadi et al., 2011; Steinke et al., 2014; Kuhnt et al., 2015). The isotopic composition of plant fragments reflect more humid conditions from Lake Towuti, central Sulawesi (Russell et al., 2014), relatively stable amount of rainfall south of Sulawesi (Tierney et al., 2012) and prolonged dry periods off Sumba during the late Holocene (Dubois et al., 2014). Deuterium isotopes from Lake Lading on Java, southern Indonesia, indicate a steadily increased precipitation over the past millennium (Konecky et al., 2013). Thus, climate reconstructions appear to draw an inconsistent picture of Holocene precipitation history of the Maritime Continent caused by the application of different proxies which may be seasonally biased and which are affected by different drawbacks. Furthermore, these reconstructions were performed at different regions in the Maritime Continent which are controlled by large-scale climate phenomena such as ENSO or the monsoonal system to a different extend as it is observed today (Aldrian and Susanto, 2003). However, the reconstructions showed that the monsoonal system (Mohtadi et al., 2011), ENSO and the IOD (Abram et al., 2009; Niedermeyer et al., 2014) may have changed over time. They interact with each other today, and may have done so during the past resulting in amplified or erased climatic signals recorded in the climatic archives. Furthermore, the dominance of climate phenomena may have varied across the region due to the complex geographical setting as it is observed today (Aldrian and Susanto, 2003) and may have resulted in potential masking or diminishing of paleo-climatic signals.

Proxy records from marine sediments off Sumatra, western Indonesia, from the Makassar Strait, central Indonesia, and the Java Sea, southern Indonesia, are used to reconstruct variations in sea surface conditions, changes in upper water stratification and precipitation-related terrigenous runoff in response to different climatic forcing mechanisms during the Holocene.

This study intends to investigate the climate evolution of western, central and southern Indonesia on centennial to millennial time-scales from mid- to late Holocene in order to test the following hypotheses:

1. Subsurface water conditions off western Sumatra during the past 8 ka were related to variations in IOD.

2. Late Holocene changes in sea surface water conditions within the Makassar Strait are primarily caused by a strengthening Australian Indonesian summer monsoon.

3. Precipitation over eastern and southern Borneo and eastern Java varied in response to changes in the Australian-Indonesian monsoon system and ENSO during the mid- to late Holocene.

To test these hypotheses four marine sediment cores retrieved from the eastern Indian Ocean off western Sumatra, the Makassar Strait off the Mahakam Delta, and the Java Sea off the Solo Delta, Java and the Seruyan Delta, Borneo have been studied (Fig. 2). These continuous high resolution proxy records provide an important insight into mid- to late Holocene climate history of Indonesia and hence the Maritime Continent and essentially contributes to the data basis which can be used to validate climate models.

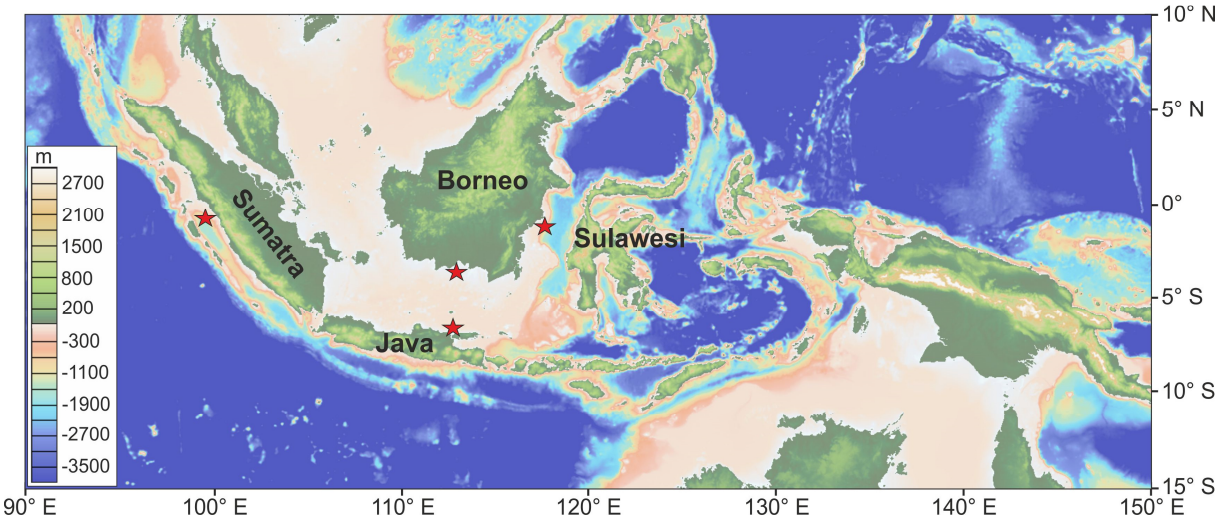

Figure 2: Map indicating the topography and bathymetry of the Maritime Continent created by using GeoMapApp. The red stars represent the core sites of the sedimentary records investigated in this thesis.

2. The Maritime Continent

2.1. Geography of the Maritime Continent

The Maritime Continent is located in the tropics between the Pacific and Indian Oceans and is bordered by the Asian and Australian continents. It comprises, amongst other countries, Indonesia, the Philippines, and Papua New Guinea (Ramage, 1968). The western Pacific is bordered by the Philippine archipelago in the North and by the island of Papua New Guinea in the East. The islands of Borneo and Sulawesi form the center of the Maritime Continent. The Sunda Arc along the Sunda Trench in the eastern Indian Ocean consist of the islands Sumatra with its characteristic fore-arc islands, Java and the Lesser Sunda Islands forming the western and southern margin of the Maritime Continent (Fig. 2). The Maritime Continent consist auf thousands of islands and various shallow and deep ocean basins, also referred to as the Indonesian Seas, providing a very complex geographical setting. The topography of the Maritime Continent is characterized by narrow high mountain ranges of volcanic origin facing the Indian Ocean and reaching altitudes of more than 3,500 m (Fig. 2, Tab. 1). The mountains in Borneo extend from the Iran Mountains in the Northeast to the Schwaner Mountains in the Southwest reaching altitudes of ~4,000 m while southern Borneo is mainly characterized by wide plains (Fig. 2, Tab. 1). Also Sulawesi and the smaller islands of Indonesia are characterized by high mountains (Fig. 2). On Papua New Guinea, a high mountain range extends from West to South East with highest elevations of ~5,000 m (Fig. 2, Tab 1).

Table 1: Largest islands of the Maritime Continent with size and altitude (http://islands.unep.ch/Tiarea.htm).

Island	Area (km^2)	Altitude (m)
Papua New Guinea	785,753	5,030
Borneo	748,161	4,175
Sumatra	443,066	3,804
Sulawesi	180,681	3,455
Java	138,794	3,676

The Indonesian Seas are connected to the Pacific and Indian Ocean and interconnected via sea passages (Fig. 1, 2, Gordon, 2005). The Sulu Sea is located south of the Philippines with a shallower basin in the Northwest (< 2,000 m water depth) and a deep basin in the Southeast (> 3,500 m) exchanging ocean water with the South China Sea mainly via the Mindoro and the Balabac Straits and with the Sulawesi Sea via the Sibutu Passage (Fig. 1, 2, Gordon, 2005). The deep Sulawesi Sea (> 3,500 m) builds the entrance to the Makassar Strait between the islands of Borneo and Sulawesi. The southern South China Sea and the Java Sea in the West are located

on the flooded Sunda shelf and hence, very shallow with water depths < 300 m (Fig. 1, 2). The Java Sea is connected to the South China Sea via the Karimata Strait in the West and to the Banda Sea via the Flores Sea in the East. The Banda Sea is located south of Sulawesi and is connected to the Molucca Sea via the Lifamatola Passage in the North. The Banda Sea reaches water depths of more than 7,000 m (Tomczak and Godfrey, 1994) and merges into the Arafura and Timor Sea in the South. The Arafura Sea and the Timor Sea are shallow ocean basins with average depths of less than 300 m north of Australia (Fig. 1, 2). The main passages towards the Indian Ocean are the Timor Passage and the Ombai Passage connecting the Banda Sea to the open Indian Ocean and the Lombok Strait between Bali and Lombok connecting the Java and Flores Sea to the open Indian Ocean (Fig. 1, 2, Gordon, 2005).

2.2. Oceanography of the Maritime Continent

Western Pacific coastal currents, the surface oceanography of the Maritime Continent itself and the current system of the eastern Indian Ocean vary in response to seasonal variations of monsoonal surface winds. During austral summer (boreal winter), the New Guinea Coastal Current (NGCC) flows eastward along the coast of Papua New Guinea (Fig. 3, Wyrtki, 1961). The North Equatorial Current (NEC) flows westward around 10°N which splits into the Philippines Current (PC) flowing northward and a southward component feeding the Mindanao Eddy (Fig. 3, Tomczak and Godfrey, 1994). The return flow, the North Equatorial Counter Current (NECC), is fed by the Halmahera and the Mindanao Eddies and flows eastward just north of the equator (Tomczak and Godfrey, 1994). Parts of the PC enter the Indonesian Seas by passing the Luzon Strait to the South China Sea and split up into a southward component flowing as the Sibutu Passage Throughflow (SPTF) through the Mindoro Strait and the Balabac Strait into the Sulu Sea and enters the Sulawesi Sea by the Sibutu Passage (Fig. 3, Gordon et al., 2012). The other component becomes the South China Sea Throughflow (SCSTF) and flows southward as well but enters the Indonesian Seas by passing the Karimata Strait into the Java Sea (Wyrtki, 1961; Gordon et al., 2012). The Java Sea is a shallow sea located on the flooded Sunda shelf in central Indonesia with an average depth of 40 m resulting in a vertically homogeneous water column (Wyrtki, 1961). The current system in the Java Sea flows in eastward direction during austral summer (Fig. 3, Wyrtki, 1961). Pacific surface water fed by the Mindanao Eddy flows southward entering the Indonesian Seas by passing the Sulawesi Sea and forms the main source of the Indonesian Throughflow (ITF, Tomczak and Godfrey, 1994). About 80% of the ITF flows through the Makassar Strait (Gordon, 2005) splitting into two

components: the first one flows southward and enters the Indian Ocean by passing the Lombok Strait and the second one flows eastward entering the Flores and Banda Seas (Fig. 3, Gordon et al., 2012). By passing the Ombai Strait and Timor Passage, the ITF flows into the Indian Ocean in westward direction forming the South Equatorial Current (SEC, Schott et al., 2009).

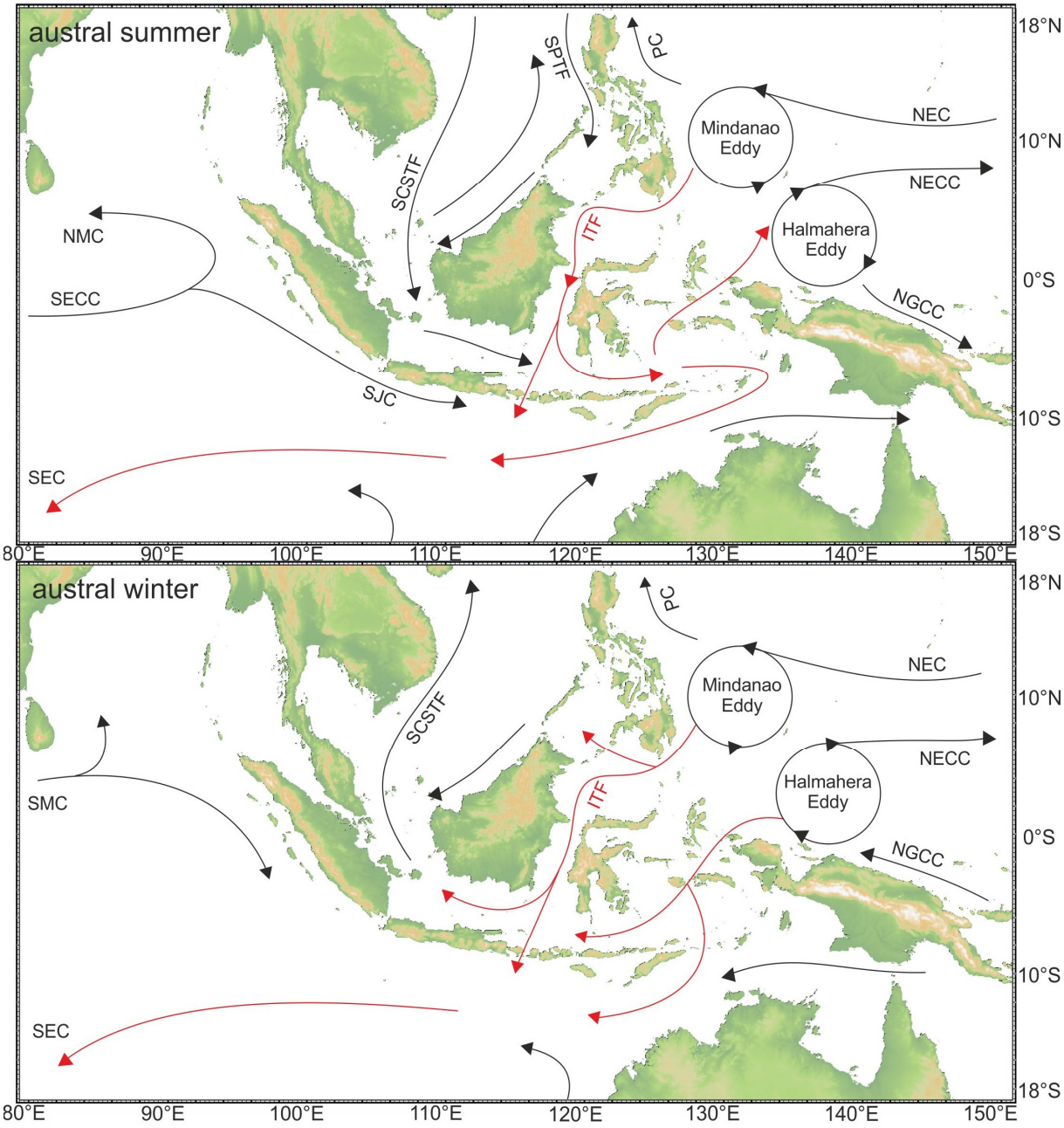

Figure 3: Schematic representation of the surface current system during austral summer (top) and austral winter (bottom). The black branches indicate the North Equatorial Current (NEC), North Equatorial Countercurrent (NECC), the Mindanao Eddy and Halmahera Eddy, the Philippines Current (PC) and the New Guinea Coastal Current (NGCC) in the Pacific Ocean; the Sibutu Passage Throughflow (SPTF) and the South China Sea Throughflow (SCSTF) in the South China Sea; the Indonesian Throughflow (ITF) in red in the Indonesian Seas; the South Equatorial Countercurrent (SECC), the Northeast Monsoon Current (NMC) and Southwest Monsoon Current (SMC), the South Java Current (SJC) and the ITF forming the South Equatorial Current (SEC) in the Indian Ocean. The maps were created by using GeoMapApp.

The South Equatorial Countercurrent (SECC) originates off the East African coast flowing eastward just south of the equator (Schott et al., 2009). This current splits up off Sumatra in the South Java Current (SJC) which flows eastward along the coast of Java while the other part is reflected by the fore-arc islands of Sumatra in northwestward direction forming the Northeast Monsoon Current (NMC, Fig. 3, Schott et al., 2009).

During austral winter, the NGCC flows westward feeding the Halmahera Eddy (Fig. 3, Tomczak and Godfrey, 1994). After passing the coast of Papua New Guinea, surface waters flow southward and split up in the Banda Sea into a westward component flowing through the Flores Sea and a southward component entering the Indian Ocean via the Ombai Strait and the Timor Passage (Fig. 3, Wyrtki, 1961; Gordon, 2005). Surface water circulating in the Mindanao Eddy form the ITF flowing partly westward through the Sulawesi Sea and the Sulu Sea into the South China Sea (Wyrtki, 1961). The major part of the ITF passes the Makassar Strait and splits up into a southward component which enters the Indian Ocean via the Lombok Strait and a westward component which flows through the Java Sea and enters the South China Sea by passing the Karimata Strait (Fig.3, Wyrtki, 1961). In the Indian Ocean, the monsoon winds produce strong Ekman transport away from the western coastline of Indonesia resulting in the upwelling off Java, Sumatra (Schott et al., 2009) and Lesser Sunda Islands (Hendiarti et al., 2004; Susanto et al., 2006; Ningsih et al., 2013). The Southwest Monsoon Current (SMC) flows eastward just north of the equator (Fig. 3). After passing the coast of Sri Lanka it splits up in a northward component and an eastward component which flows southward along the coast of Sumatra (Fig. 3, Schott et al., 2009).

2.3. Climate of the Maritime Continent

The tropical climate of the Maritime Continent is controlled by the seasonal migration of the ITCZ and the Australian-Indonesian monsoon system on a seasonal scale (Robertson et al., 2011), and ENSO (Dai and Wigley, 2000) and the IOD (Saji et al., 1999; Webster et al., 1999) on an interannual scale. Furthermore, the Madden Julian Oscillation (MJO, Madden and Julian, 1971), an intraseasonal atmospheric oscillation system characterized by a strong deep convection cell crossing the Indian Ocean (60-90 days) influences the underlying weather and climate systems (Zhang, 2005). The Maritime Continent lies within the IPWP described as the largest area of warm SST and highest rainfall (Weller et al., 2016). More precise, it is located at the western edge of the Western Pacific Warm Pool (WPWP). The WPWP is characterized by the warmest SST of the global ocean with values higher than 28.5 °C (Cravatte et al., 2009)

and known the largest heat reservoir on earth providing water vapor and latent heat to the atmosphere (Chen et al., 2004; Cravatte et al., 2009) influencing the global climate system. The mean annual SST in the Indonesian Seas is above 28.5 °C (Fig. 4). During austral summer, SST in the north western Pacific and in the South China Sea are cooler with ~27 °C while SST within the eastern and southern Indonesian Seas are warmer with SST above 28.5 °C (Fig. 4). During austral winter, the northwestern Pacific is characterized by SST warmer than 28.5 °C while the southern Indonesian Seas are cooler with ~27 °C (Fig. 4). Sea surface salinity (SSS) is above 34 psu in the open Indian and Pacific Oceans during austral summer and winter (Fig. 4).

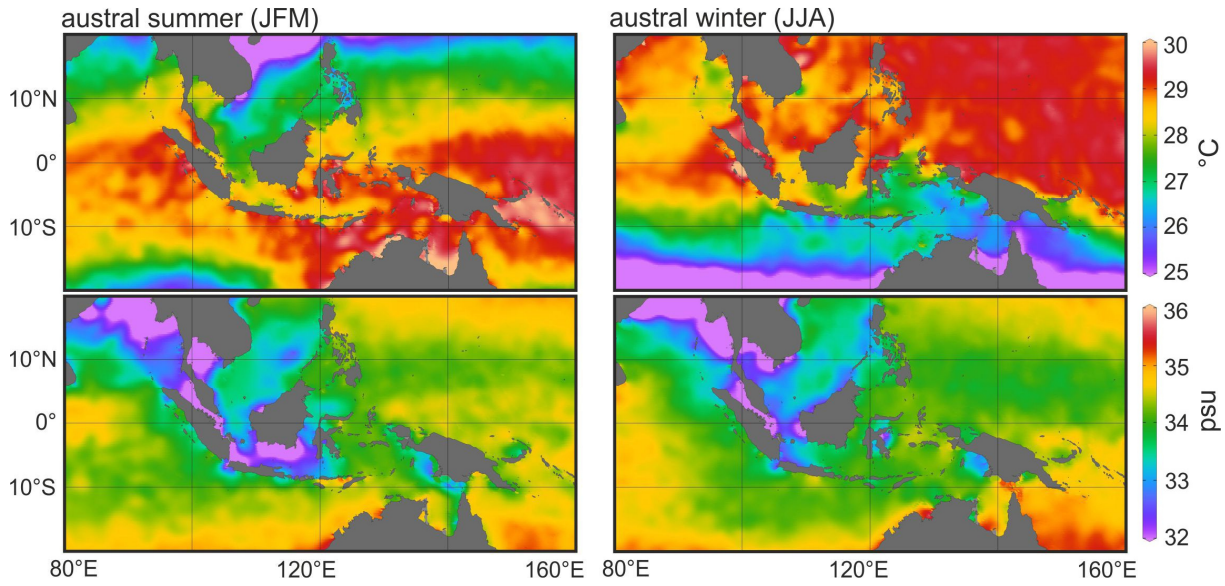

Figure 4: Maps of the Maritime Continent indicating sea surface temperatures (SST, upper panel) and sea surface salinity (lower panel) during austral summer (left) and during austral winter (right). Maps were created by using World Ocean Atlas 2013 (Levitus et al., 2013) and Ocean Data View (1990 – 2016; Reiner Schlitzer, Alfred Wegener Institute, Columbusstrasse, 27568 Bremerhaven, Germany. E-mail: Reiner.Schlitzer@awi.de).

Within the Indonesian Seas, SSS varies with season being fresher with only 32 psu along the eastern coast of Sumatra and in the Java Sea and 34 psu in the Molucca and Banda Sea during austral summer and more saline with 34 psu in the Makassar Strait and 34.5 psu in the Banda Sea during austral winter (Fig. 4). Due to the location around the equator, air temperatures show no seasonal cycle with temperatures between 23 and 27 °C varying with altitude (New et al., 1999). Precipitation over the Indonesian Archipelago shows a less pronounced seasonal cycle with year-round humid climate in northern Indonesia and a monsoon-related seasonal cycle in southern Indonesia with a dry season during austral winter and a wet season during austral summer (Wyrtki, 1961; Aldrian and Susanto, 2003; Robertson et al., 2011). Monthly mean

rainfall for the Maritime Continent varies between 0 to 500 mm/month depending on the season and location (Chang et al., 2005).

2.3.1. The Intertropical Convergence Zone (ITCZ)

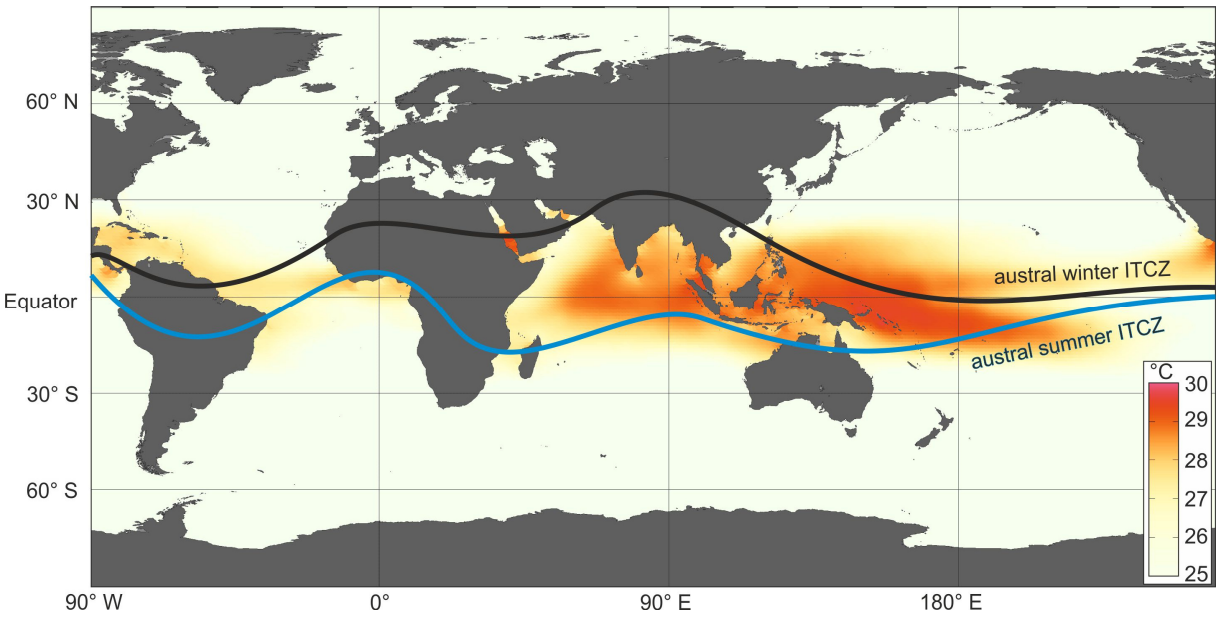

Figure 5: Global Map indicating the Indo-Pacific Warm Pool with SST above 28.5 °C (red; created by using data from World Ocean Atlas 2013 (Levitus et al., 2013) and Ocean Data View (1990 – 2016; Reiner Schlitzer, Alfred Wegener Institute, Columbusstrasse, 27568 Bremerhaven, Germany. E-mail: Reiner.Schlitzer@awi.de) and the southernmost position of the ITCZ during austral summer (blue) and the northernmost position of the ITCZ during austral winter (black; position was estimated on the basis of CPC CMAP monthly precipitation between 1985 and 2010 (http://iridl.ldeo.columbia.edu/maproom/IFRC/FIC/CMAP).

Following the zenith point of the sun on land (Mohtadi et al., 2016), the ITCZ is a narrow zonal belt of clouds providing the most intense rainfall on Earth (Schneider et al., 2014). The ITCZ is the rising branch of the meridional atmospheric overturning Hadley circulation which is fed by warm and moist trade winds (Schneider et al., 2014). The trade winds converge, rise and diverge as colder and drier air masses poleward exporting energy to the extratropics (Schneider et al., 2014). Thus, the position of the ITCZ varies with the atmospheric circulation which is itself tightly coupled to the ocean circulation (Schneider et al., 2014). Thus, the position of the ITCZ is strongly modified by the thermal conditions at the surface which are controlled by various factors such as insolation (Wanner et al., 2008) and oceanic energy transport (Broccoli et al., 2006) affecting the interhemispheric temperature contrast (Chiang and Friedman, 2012). The position of the ITCZ is also tightly coupled to large–scale phenomena such as the

monsoonal system (e.g. Gadgil, 2003; Wang, 2009) and ENSO (Philander, 1985). The migration of the ITCZ influences the onset, duration and termination of the rainy season in the tropics and subtropics and hence, exert a strong control on the regional monsoon systems (Gadgil, 2003). Due to the change in ocean energy in the Pacific (Schneider et al., 2014) and the zonal rearrangement of atmospheric deep convection (Dai and Wigley, 2000) ENSO exert as significant control on the position of the ITCZ being located father south during El Niño and farther north during La Niña (Philander, 1985; Schneider et al., 2014).

In general, the ITCZ migrates seasonally towards the warming Hemisphere (Fig. 5, Schneider et al., 2014). Today, the ITCZ mean position over the Atlantic and Pacific Ocean is located in the Northern Hemisphere as a consequence of northward oceanic energy transport (Marshall et al., 2014). Over the Indian Ocean region, the annual mean position is located in the southern Hemisphere likely caused by a secondary precipitation maximum south of the equator related to the monsoon system (Schneider et al., 2014). The ITCZ over the Indian Ocean region also shows the largest seasonal shifts passing Indonesia twice a year during austral spring and fall (Fig. 5). Changes in precipitation in response to shifts in ITCZ are documented on seasonal to geological time scales (Schneider et al., 2014).

Proxy records as well as model simulations imply that the expansion as well as the annual mean position of the ITCZ shifted on centennial to orbital time scales mainly controlled by changes in orbital forced insolation (Wang et al., 2005) as well as solar activity (Yan et al., 2015), variations in the Atlantic Overturning circulation (Zhang and Delworth, 2005), and climatic shifts in the northern high latitudes (Haug et al., 2001; Knudsen et al., 2011).

2.3.2. The Australian-Indonesian monsoon system

The Australian-Indonesian monsoon system, also often named as the Maritime Continent monsoon, leads to strong seasonal variations in wind and rainfall of the Maritime Continent (Fig. 6). The dry season peaks in July-August (austral winter) and is characterized by prevailing easterly winds (Aldrian and Susanto, 2003; Chang et al., 2004). The wet season culminates in December-February and is marked by prevailing westerly winds (Aldrian and Susanto, 2003; Chang et al., 2004). Austral spring (September-October-November, SON) and austral fall (March-April-May, MAM) are the monsoonal transition seasons (Aldrian and Susanto, 2003).

The Australian-Indonesian monsoon is characterized by two distinct asymmetries between austral winter and summer and austral fall and spring related to interactions between monsoonal surface winds and the complex topography of the Maritime Continent (Chang et al., 2005;

Robertson et al., 2011). The Australian-Indonesian summer monsoon (AISM) extends far northward crossing the Equator and causes monsoonal rainfall on the eastern coast of Malaysia and the Philippines while the boreal summer monsoons are restricted to the northern hemisphere (Chang et al., 2005). This asymmetry is caused by the strong baroclinicity over the cold Asian continent in austral summer producing strong East Asian winter monsoon surface winds being fed by AISM air masses (Chang et al., 2005; Robertson et al., 2011).

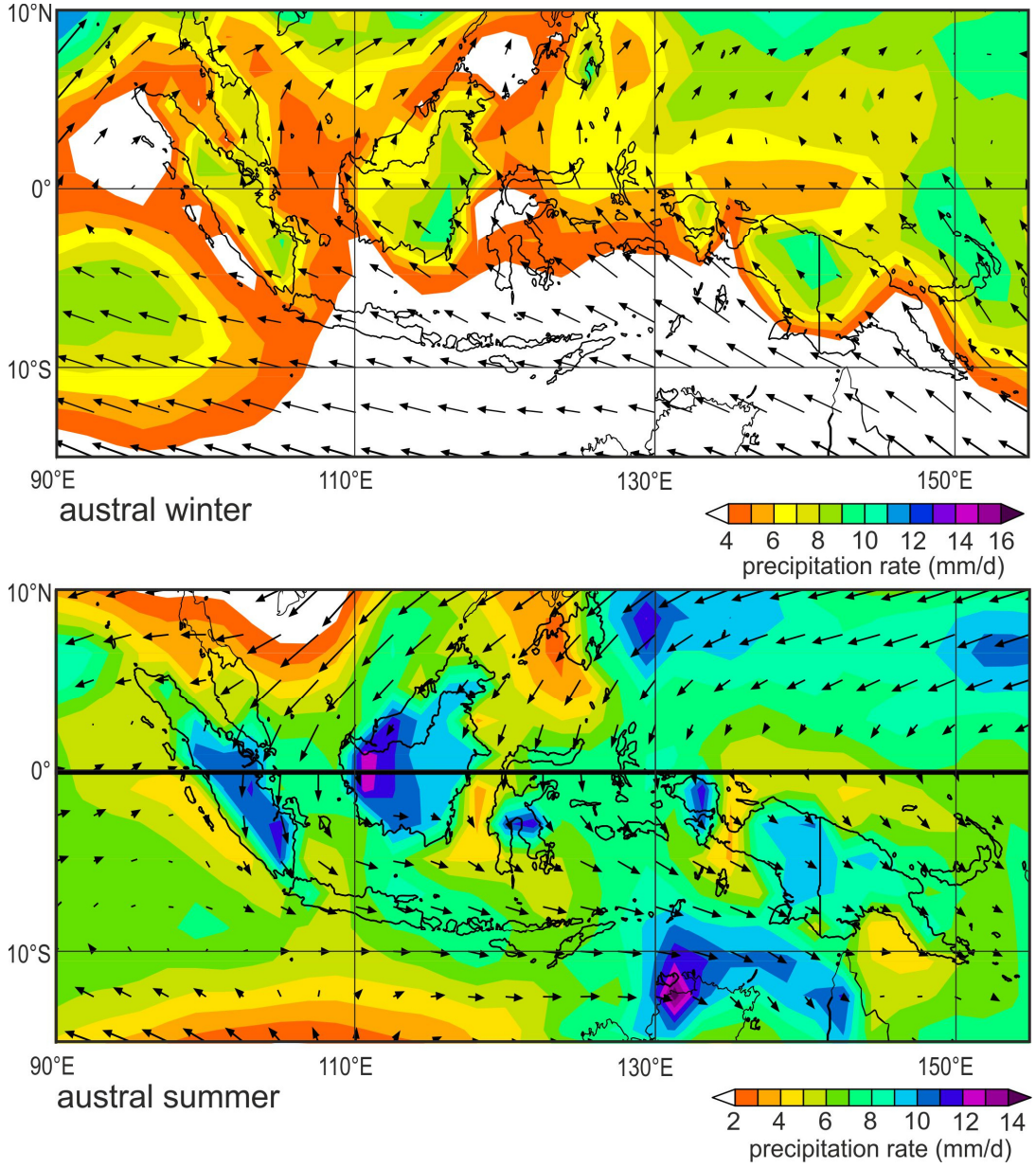

Figure 6: Map representing monsoonal precipitation (color shaping) and wind (vectors) over the Maritime Continent. Seasonal precipitation during JJA with July wind vectors indicate AIWM conditions during austral winter (top) while seasonal precipitation during DJF with January wind vectors represent AISM conditions during austral summer (bottom). Seasonal precipitation data (Kalnay et al., 1996) derived Climatological wind vectors for the 925 hPa pressure level indicate wind direction with speed proportional to the length of the vectors provided by NCEP, Climate Prediction Center USA (data from 1961 –1990, http://iridl.ldeo.columbia.edu/maproom/.Regional/.Asia_Indonesia/.Climatologies/.Precip_Loop.html).

The asymmetry between austral spring and fall results in a slow transition during austral spring but a sharp transition during austral fall. During austral spring monsoonal rainfall dominates westerly areas north of the equator, e.g. northwestern Sumatra while during austral fall monsoonal rainfall dominates easterly areas south of the Equator, e.g. Papua New Guinea (Chang et al., 2005). During austral spring, maximum convection follows the land masses from India over Southeast Asia to northern Australia while during austral fall the maximum convection remains mostly south of the Equator and jumps northward in response to the reversal of the meridional temperature gradient to mark the onset of the East Asian summer monsoon (Chang et al., 2005). This asymmetry might be caused by complex wind-terrain interactions in relation to the different strength in Walker circulations over the western Pacific and the eastern Indian Ocean (Chang et al., 2005), the different strength of cold surges from Asia and Australia affecting deep convection (Matsumoto and Murakami, 2000), or different oceanic flows in the equatorial western Pacific and eastern Indian Oceans promoting convection and the migration of convection cells (Matsumoto and Murakami, 2002). Thus, the monsoonal system over the Maritime Continent is obviously influenced by interannual climate modes operating in the Indian and Pacific Oceans in terms of wind strength, precipitation intensity and the onset of monsoonal rainy season.

In general, monsoon dynamics are related to meridional temperature gradients and the associated position of the ITCZ and thus, are very sensitive to various forcing mechanisms from tectonic to seasonal time scales (Donohoe et al., 2012; Mohtadi et al., 2016). By controlling surface albedo and moisture fluxes, land cover influences the evolution of monsoonal precipitation (Mohtadi et al., 2016). On interannual time scales, climate oscillations such as ENSO are interpreted to affect global atmospheric circulation and moisture content and hence, influences monsoonal rainfall in the Northern (Wang et al., 2013) and Southern Hemisphere (McBride and Nicholls, 1983; Jourdain et al., 2013). Considering the last glacial-interglacial cycle, orbital parameters like obliquity and precession affected the intrahemispheric and the interhemispheric insolation gradient (Mantsis et al., 2014) resulting in changes in monsoon strength (e.g. Clemens et al., 2010) as well as the hemispheric distribution of insolation resulting in a land-ocean shifts of precipitation (Battisti et al., 2014). Proxy records have shown that monsoonal evolution might be controlled by northern Hemisphere climate (e.g. Mohtadi et al., 2011) or southern Hemisphere climate (Kuhnt et al., 2015) shifting the ITCZ in response to changes in the meridional temperature gradient. Also solar and volcanic activity influences monsoon dynamics by affecting the distribution of energy (Gray et al., 2010; Steinke et al., 2014).

2.3.3. El Niño – Southern Oscillation (ENSO)

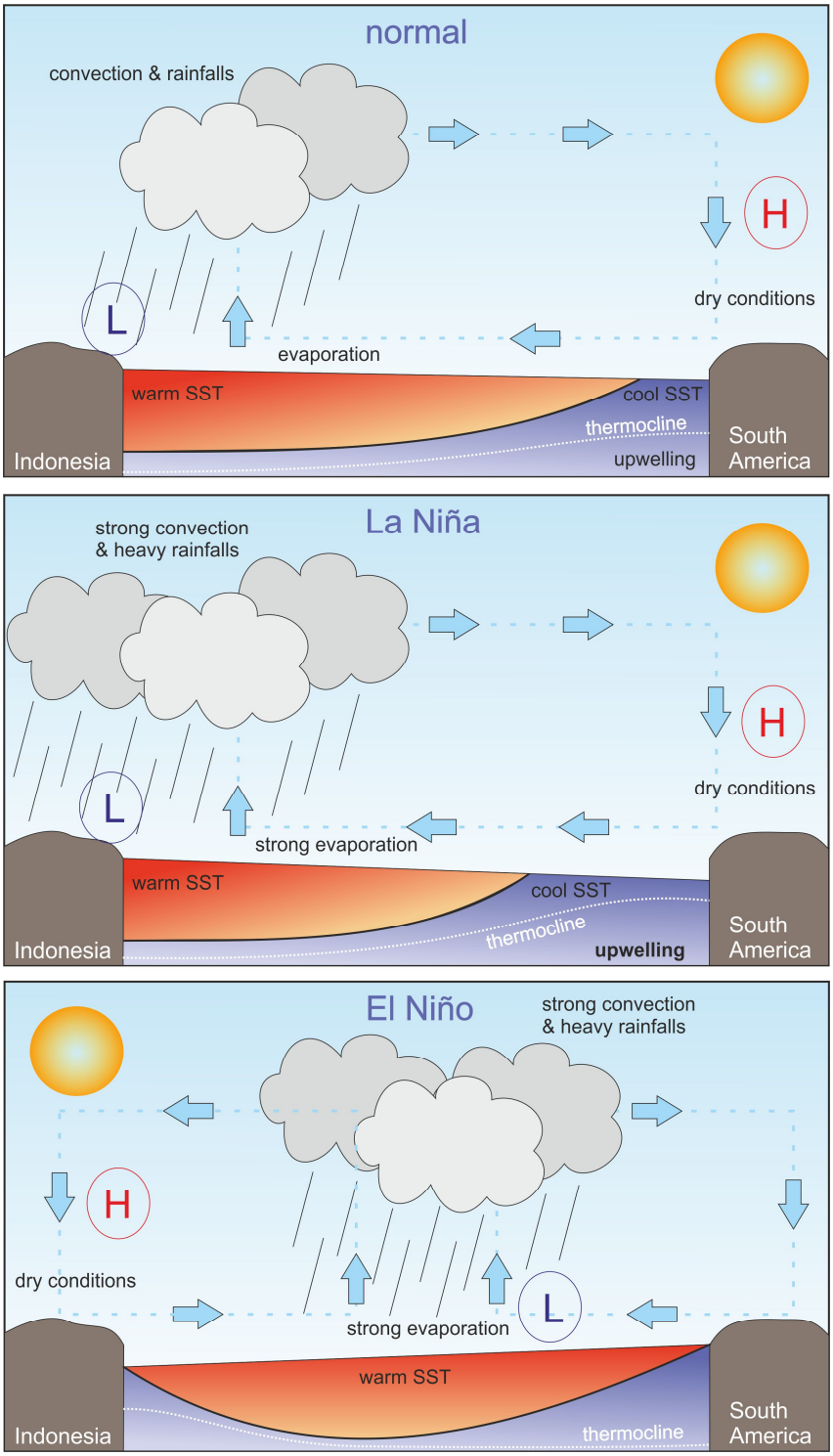

Figure 7: Schematic drawing of normal, La Niña, and El Niño conditions in the equatorial Pacific Ocean. During normal conditions upwelling of cold subsurface water in the eastern Pacific and warm SST in the western Pacific result in dry conditions over eastern South America and rainfall over the Maritime Continent (top). La Niña conditions (middle) are expressed as an extreme of normal conditions with enhanced rainfall over the Maritime Continent and enhanced upwelling in the eastern Pacific Ocean. During El Niño conditions (bottom), upwelling in the eastern Pacific is suppressed, the convection cell over the Maritime Continent is shifted eastward resulting in dry conditions in the western Pacific and heavy rainfall in the central and eastern Pacific Ocean. Blue arrows represent the Pacific Walker Circulation. H is indicative for an atmospheric high pressure cell while L stands for an atmospheric low pressure cell.

ENSO is an intrinsically coupled ocean-atmosphere process irregularly evolving in the Pacific Ocean in intervals of a few years (Clarke, 2008; Sarachik and Cane, 2010). The atmospheric component, the Southern Oscillation, is associated with fluctuations in rainfall, variations in SST, and the intensity of trade winds in the Pacific region closely engaged to variations in upper ocean stratification in response to El Niño (Philander, 1983). ENSO is an interannual oscillatory mode phase-locked in the annual cycle which starts to evolve in early boreal spring, grows through boreal summer, peaks in boreal winter and returns to normal conditions in the following months (Rasmusson and Carpenter, 1982). During the past decade various forms of ENSO events such as the El Niño-Modoki (Ashok et al., 2007) are described which are mainly characterized by different locations of the SST anomaly. In the following, only the classical El Niño and La Niña modes are described.

Normal (ENSO neutral) years are characterized by warm SST in the western equatorial Pacific promoting intense convection and rainfall over the Maritime Continent, coastal upwelling of cold subsurface water in the eastern equatorial Pacific Ocean, and dry conditions over western South America (Fig. 7). The upwelling along the coast of South America is caused by southerly winds producing an effective Ekman transport (Tomczak and Godfrey, 1994). An atmospheric low pressure cell is located in the West while an atmospheric high pressure cell is established over the East driving the Pacific Walker circulation with a rising branch over the western equatorial Pacific Ocean and a sinking branch over the eastern equatorial Pacific Ocean. Easterly surface winds over the central Pacific Ocean carry warm surface water towards the Maritime Continent allowing the deepening of the thermocline in the West.

La Niña (or ENSO cold event) is the extreme of the ENSO neutral mode in the Pacific Ocean and the complement of El Niño. La Niña is characterized by an intensified Walker circulation and colder than normal conditions owing to enhanced coastal upwelling of cool subsurface water off South America (Fig. 7, Philander, 1985).

El Niño (or ENSO warm event) is characterized by the reversed configuration with a decrease in SST in the western equatorial Pacific Ocean and a suppressed upwelling associated with surface warming in the eastern equatorial Pacific Ocean resulting in a weaker SST gradient across the Pacific Ocean and hence a weaker Pacific Walker circulation (Fig. 7, McPhaden, 1999). Weak southerly winds in the eastern equatorial Pacific Ocean result in a southward displacement of the ITCZ close to or even south of the equator during early months of El Niño years (Philander, 1983). The weaker southerly winds weaken the upwelling along the coast of South America due to less effective Ekman transport. In the western Pacific Ocean, the rising branch of the Walker circulation is shifted eastward resulting in dry conditions over the

Maritime Continent, anomalous westerly winds over the western Pacific Ocean, and a weakening of the easterly trade winds over the central and eastern Pacific Ocean (Philander, 1983; McPhaden, 1999). Westerly winds push the warm surface water and hence the convection cell even further to the East (Clarke, 2008). In response to the weaker trade winds, the upper ocean adjusts by equatorial Kelvin and Rossby wave dynamics shallowing the thermocline in the western Pacific Ocean and deepening the thermocline in the eastern Pacific Ocean (Boulanger and Menkes, 1999; McPhaden, 1999; Clarke, 2008). The warm SST promote a strong convection cell which causes heavy rainfall over the central and eastern Pacific (Philander, 1983).

The positive Bjerknes feedback contributes fundamentally to the evolution of ENSO events (Bjerknes, 1969): Warm SST in the eastern Pacific Ocean promote a weakening of the temperature gradient across the Pacific Ocean resulting in a weakening of easterly trade winds. In response to weaker trade winds, more warm surface water flows eastward deepening the thermocline further. Equatorial upwelling generates the upward motion of warmer subsurface water resulting in warmer SST in the central and eastern Pacific Ocean. Although the Bjerknes feedback implies that eastern SST drives the oscillation, western Pacific SST are much more important because warm pool surface waters are warm enough to generate deep atmospheric convection in contrast to surface water in the eastern Pacific Ocean (Clarke, 2008). Thermocline depth in the equatorial Pacific Ocean, ocean dynamics and the atmospheric-ocean interactions in the western equatorial Pacific Ocean are supposed to be the main drivers of ENSO (Jin, 1997; Cane, 2005).

ENSO has a strong impact on the Australian-Indonesian monsoon system causing reduced monsoon rainfall over Australia during El Niño years as indicated by model simulations (Jourdain et al., 2013). Studies based on observational data have shown that the onset of the monsoonal rainy season is delayed in response to the growing phase of El Niño and pre-matured in La Niña years (Hamada et al., 2002). Furthermore the dry season tends to be drier (wetter) in response to the cold (warm) SST anomaly around Indonesia caused by El Niño (La Niña, Hendon, 2003). However, climate models focusing on precipitation over the Maritime Continent are contradictory in reproducing changes in monsoonal rainfall in response to ENSO (Jourdain et al., 2013). On a local scale, weather-type analyses indicate enhanced rainfall over island orography and southern and western coasts and a decrease in rainfall over flat land and sea areas during austral summer associated with enhanced diurnal sea-land breeze circulation during El Niño (Moron et al., 2010; Qian et al., 2010; Qian et al., 2013). This is consistent with model simulations indicating a more negative correlation of rainfall over sea than over land

during austral summer (Jourdain et al., 2013; Moron et al., 2015). Supporting these model simulations, the amount of precipitation seems to be unaffected by ENSO during the peak rainy season (Hamada et al., 2002) probably caused by opposing or even canceling effects of local SST warming (Hendon, 2003). Thus, the inconsistency of modeled interaction between ENSO and the Australian-Indonesian monsoon system and very local air-sea interactions complicates the proxy interpretation for that region. Furthermore, ENSO influences the upper water column stratification and wind pattern in the equatorial Indian Ocean region via the atmospheric as well as the oceanic pathway (Susanto et al., 2001) and hence, interacts with the IOD.

2.3.4. The Indian Ocean Dipole (IOD)

The Indian Ocean Dipole is a mode of coupled ocean-atmosphere interaction internal to the Indian Ocean which evolves during austral winter and peaks in September-October-November (Saji et al., 1999; Webster et al., 1999). The negative phase is characterized by cool SST off East Africa caused by southerly monsoonal surface winds that produce upwelling along the coast (Fig. 8, Tomczak and Godfrey, 1994). Cool SST in the western Indian Ocean and the suppressed convection promote dry conditions over East Africa, Arabia and India. Inter-monsoonal westerly winds, known as Wyrtki Jets, carry warm surface water eastward causing a rise in sea level and an increase in mixed layer thickness in the eastern Indian Ocean further strengthening the upwelling off East Africa (Wyrtki, 1973; Schott et al., 2009; McPhaden et al., 2015). Potential upwelling-related cooling along the coast of Indonesia is counter-balanced by warm water advection through the ITF (Murtugudde and Busalacchi, 1999; Du et al., 2005; 2008). Additionally, monsoonal precipitation during austral summer results in enhanced freshwater input which forms a thick barrier layer. This barrier layer separates the thermocline from the mixed layer and hence, impedes the upward movement of cold subsurface water masses to enter the mixed layer (Spintall and Tomczak, 1992; Du et al., 2005; Qu and Meyers, 2005). Warm SST in the eastern Indian Ocean generates strong convection and hence heavy rainfalls over Indonesia further stabilizing the upper water column in the eastern Indian Ocean. Forced by the SST gradient across the Indian Ocean, the westerly winds speed up and become more effective in transporting warm surface water from the western to the eastern Indian Ocean (Saji et al., 1999).

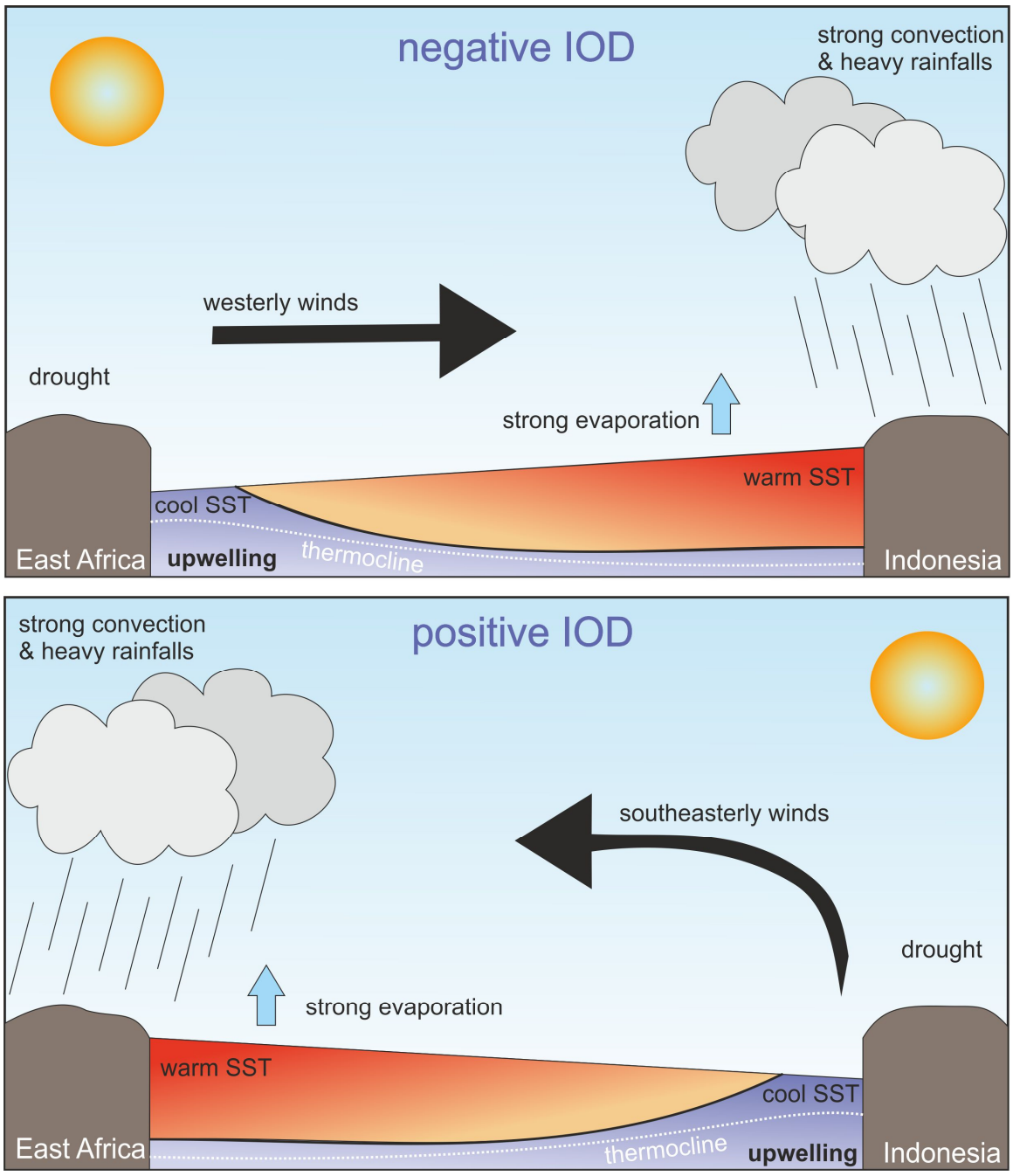

Figure 8: Schematic drawing of a positive and negative Indian Ocean Dipole (IOD) event in the equatorial Indian Ocean. During positive IOD events, southeasterly winds promote upwelling conditions in the eastern Indian Ocean while warm surface water advects off East Africa resulting in strong convection over the western Indian Ocean and heavy rainfall over East Africa. During negative IOD events, westerly winds result in warm surface water in the eastern Indian Ocean causing strong convection and heavy rainfall over Indonesia while upwelling of cool subsurface water in the western Indian Ocean trigger dry conditions in East Africa.

Episodically occurring positive IOD events are mainly characterized by strong upwelling of cold subsurface water cooling the ocean surface in the eastern Indian Ocean with the strongest signal off Sumatra (Fig. 8, Webster et al., 1999). Extreme events can result in a SST cooling of > 2 °C (Webster et al., 1999; Du et al., 2008) while changes in SST during moderate or weak

positive IOD events are relatively small (< 1 °C) compared to changes in the subsurface (~3 °C, Qiu et al., 2012). Thus, positive IOD events are most obvious in the subsurface (Rao et al., 2002; Saji and Yamagata, 2003; Zhao and Nigam, 2015). Stronger southeasterly surface winds produce an effective Ekman transport resulting in enhanced coastal upwelling in the eastern Indian Ocean while weaker northeasterly winds alongshore East Africa result in a reversal of the usually westerly winds over the central Indian Ocean (Saji et al., 1999; Webster et al., 1999). The decrease in warm water advection (Murtugudde et al., 2000) in addition to the reduction of the barrier layer as a result of the decrease in rainfall promotes cold subsurface water to enter the mixed-layer (Murtugudde et al., 2000; Du et al., 2008). The cold SST weaken or even suppress the convection over Indonesia leading to droughts in Indonesia and a surface pressure modification which generates extended southeast trade winds (Saji et al., 1999). The easterly winds result in adjustment dynamics of the surface height along the equator further shallowing the thermocline in the East and deepening the thermocline in the West (Webster et al., 1999). The upwelling is impeded off East Africa resulting in warm SST and a strong convection in the western Indian Ocean. The warm SST in the western Indian Ocean lead to the development of a strong convection cell over East Africa generating strong rainfalls in East Africa and India. The enhanced freshwater input further stabilizes the upper water column in the western Indian Ocean (Murtugudde et al., 2000). The convection over East Africa causes a pressure modification which enhances the equatorial easterly winds. The wind-induced Ekman transport produces an Ekman ridge just south of the Equator which is caused to propagate westward and further deepen the thermocline via Rossby waves resulting from internal adjustment dynamics of the Indian Ocean (Webster et al., 1999). Various feedback mechanisms like the Bjerknes feedback (Bjerknes, 1969) which also operates in the Indian Ocean, and a seasonal thermodynamic Air-Sea-Feedback off the coast of Sumatra may be involved in the evolution of positive IOD events (Fig. 9, Li et al., 2003).

Positive IOD events may occur in response to zonal wind anomalies along the equator associated with the eastward propagating intra-seasonal MJO (Iskandar et al., 2006) forcing intra-seasonal Kelvin waves which result in sea surface height variabilities off Sumatra and Java (Schott et al., 2009). Furthermore, the SST anomalies of about 0.35 °C in the Indonesian region associated with the MJO affect the surface moisture and heat flux and hence, convection processes over the eastern Indian Ocean (Shinoda et al., 1998).

The IOD is also tightly coupled to the regional monsoonal systems. On the one hand, the IOD is strongly phase-locked due to the annual cycle of the Indian and Australian-Indonesian monsoon systems. Since the strong upwelling off Sumatra is a major component of positive

IOD events forced by alongshore winds and equatorial and coastal Kelvin waves (Murtugudde et al., 2000), positive IOD events may be terminated by the monsoonal wind reversal inhibiting an effective Ekman transport and hence upwelling off Sumatra. In the northwestern Indian Ocean, warm surface waters lead to a strengthened Indian summer monsoon (Rao and Goswami, 1988) resulting in greater mixing during late austral winter and therewith a surface cooling in the western Indian Ocean (Webster et al., 1999). Furthermore, the IOD shows a biennial tendency probably caused by a negative feedback mechanism between the Indian monsoon and the IOD (Li et al., 2003). A positive IOD leads to an intensified Indian summer monsoon inducing anomalous east-west circulation which in turn results in warm SST in the eastern Indian Ocean (Li et al., 2003). This warming tends to affect the equatorial Indian Ocean through an intensified Indian Ocean Walker cell promoting a negative phase in the following year (Li et al., 2003). On the other hand, the anomalous anticyclonic atmospheric circulation over the Indian Ocean in response to the sea surface cooling during positive IOD events results in baroclinic changes in the atmosphere causing anomalous subsidence and therewith a weakening of the already low Australian Indonesia winter monsoon (AIWM) rainfall (Ashok et al., 2003). Furthermore, the Holocene reconstruction of single positive IOD events from tropical corals implies prolonged IOD events in response of a strong East Asian summer monsoon (Abram et al., 2007). Nevertheless, model simulations indicate only a weak influence of IOD on AISM strength during the rainy season (Jourdain et al., 2013).

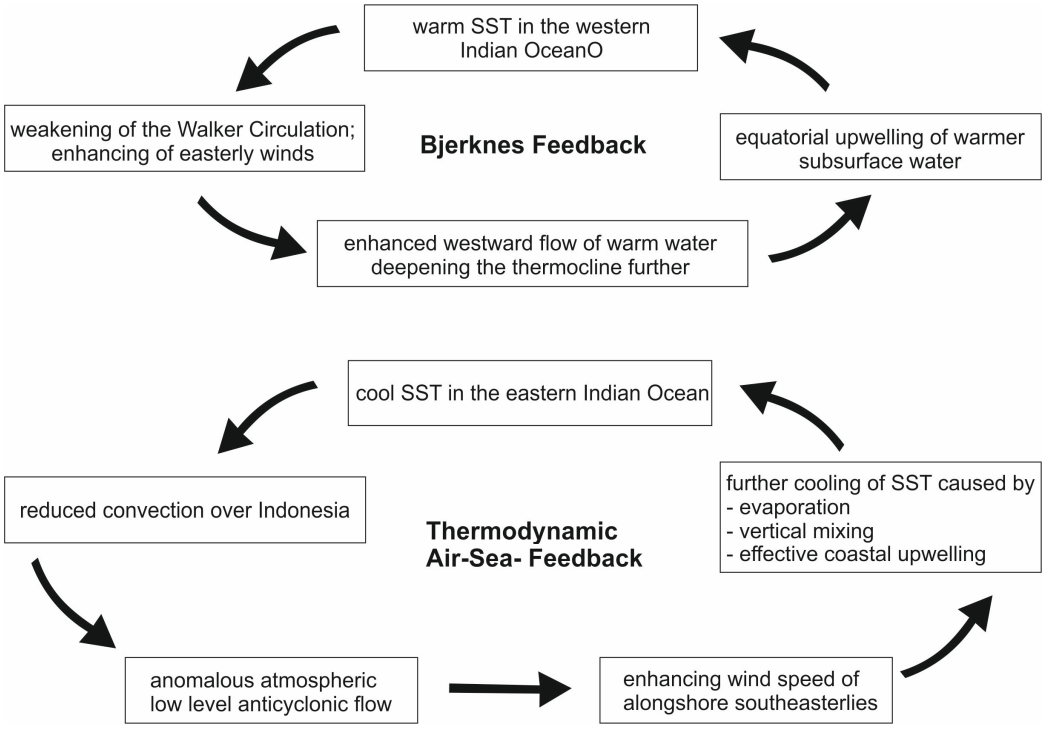

Figure 9: Feedback mechanisms involved in the Indian Ocean Dipole within the Indian Ocean.

As already mentioned, El Niño conditions are favorable for positive IOD events while La Niña conditions are unfavorable for triggering positive IOD events. An observed sea surface cooling of 0.5 °C in the eastern Indian Ocean is attributed to El Niño (Webster et al., 1999) promoting droughts over Indonesia owing to a reduced convection over Indonesia. Furthermore, El Niño forces anomalous easterly winds over the eastern Indian Ocean which suppresses coastally trapped Kelvin waves and monsoon transition and hence, results in spatial and temporal extension of effective upwelling (Susanto et al., 2001). The weakening of the pressure gradient between the Indian and the Pacific Ocean in years of co-occurrence causes a weakening of water mass transport through the ITF influencing the warm water advection in the eastern Indian Ocean (Gordon, 2005). Additionally, the ITF transports generally colder water shallowing the thermocline depth in the eastern Indian Ocean (Susanto et al., 2001). However, three consecutive positive IOD events (2006-2008) imply that subsurface variations internal to the Indian Ocean and anomalous upwelling Rossby waves may also trigger the IOD (Cai et al., 2009a; 2009b). In times of co-occurrence, a weakening El Niño contributes to the termination of a positive IOD event by relaxing the sea surface height gradient across the Indian Ocean forcing eastward propagating and downwelling Kelvin waves which deepen the eastern mixed layer in the eastern Indian Ocean (Webster et al., 1999). Also enhanced insolation in response to the absence of convective clouds (Saji et al., 1999) or enhanced latent heat flux from the atmosphere and short wave radiation (Du et al., 2008) may contribute to the termination by warming the SST in the eastern Indian Ocean.

3. Holocene climate reconstructions from Indonesia

The Holocene as the current interglacial began at 11.7 ka (e.g. Walker et al., 2009). As indicated e.g. by the Bond cycles in the north Atlantic (Bond et al., 1997), the Holocene climate appeared to be more variable as previously thought. Also in the Indo-Pacific region, Holocene climate reconstructions reveal large shifts in the seasonal and annual mean position of the ITCZ and associated variations in the Australian-Indonesian monsoon system (Griffiths et al., 2009; 2010; Mohtadi et al., 2011; Kuhnt et al., 2015), the ENSO-state of the Pacific Ocean (Moy et al., 2002; Conroy et al., 2008; Koutavas and Joanides, 2012) or the IOD-state in the Indian Ocean (Abram et al., 2007; 2009; Niedermeyer et al., 2014) . Proxy time series from different climate archives of the Indo-Pacific region have been studied in order to reconstruct past climate variations (Fig. 10). Stable oxygen isotopes from speleothems as well as deuterium isotopes, and stable carbon isotopes from plant material from marine and lacustrine sediment cores reflect variations in rainfall while element compositions in marine and lacustrine sediment records can be interpreted as terrigenous runoff often interpreted as response to changes in precipitation. Furthermore, by using corals and marine sedimentary records, variations in surface water conditions and upper water column stratification can be reconstructed indicating changes in the controlling climate phenomena.

Global SST warming during the last deglaciation (Clark et al., 2012) is also observed in the IPWP (Rosenthal et al., 2003; Stott et al., 2004; Lückge et al., 2009; Linsley et al., 2010; Mohtadi et al., 2014). During the early Holocene, sea surface conditions indicate warmest SST. Sea surface cools by ~0.5°C during the course of the Holocene related to either an eastward shift of the WPWP (Linsley et al., 2010), an upward mixing of cold subsurface waters within the Indonesian Seas (Rosenthal et al., 2013), or intensified ENSO during the late Holocene (Linsley et al., 2010). Based on thermal and density gradients, Holocene surface ITF intensity along the Makassar Strait reflects generally El Niño-like conditions during the Holocene interrupted by short periods of La Niña-like conditions (Newton et al., 2011; Fan et al., 2013). However, the authors suggest a secondary influence of the seasonal migration of the ITCZ and the associated monsoonal precipitation (Fan et al., 2013) probably complicating a straight forward interpretation. Coral-based SST reconstructions from the IPWP reveal cooler SST and a contraction of the southeastern and southwestern margins of the IPWP related to a more northerly position of the ITCZ and a strong Asian summer monsoon corresponding to a more positive IOD-like mean state of the Indian Ocean (Abram et al., 2009). Intervals of abrupt warming are associated with a weakening of the Asian summer monsoon and a more southerly displaced ITCZ and probably reflect negative-IOD-like mean states (Abram et al., 2009).

Sea surface $\delta^{18}O_{sw}$ within the Indonesian Seas indicate a sea surface freshening during the past 15 ka (Rosenthal et al., 2003; Stott et al., 2004; Linsley et al., 2010) probably related to the intrusion of low-saline surface waters from the South China Sea after the flooding of the Sunda shelf in the early Holocene (Linsley et al., 2010) or a basin-wide freshening of the Pacific Ocean (Stott et al., 2004) and might be additionally affected by changes in regional rainfall (e.g. during the mid-Holocene, Linsley et al., 2010). In the eastern Indian Ocean, $\delta^{18}O_{sw}$ shows no change between the LGM and the Holocene but a strong response during North Atlantic cold spells (Younger Dryas and Heinrich stadials, Mohtadi et al., 2014). Those changes in $\delta^{18}O$ of seawater point to a decrease in rainfall due to changes of the Hadley circulation including a southward shift of the ITCZ in response to a slowdown of the Atlantic Meridional Overturning Circulation (Mohtadi et al., 2014). This is supported by sea surface $\delta^{18}O_{sw}$ from the IPWP following the interhemispheric temperature gradient implying a direct control on the tropical hydrologic cycle (Gibbons et al., 2014).

Rainfall during the last deglaciation reveal an inconsistent precipitation history within the IPWP reflecting relatively unchanged rainfall with signinficant excursions associated with North Atlantic cold spells in the eastern Indian Ocean (Mohtadi et al., 2011; Niedermeyer et al., 2014) or intensified precipitation over Borneo and Sulawesi (Partin et al., 2007; Russell et al., 2014). Global sea level rise and hence, the early Holocene Sunda shelf flooding most likely provided a new, close moisture source which likely contributes to intensified rainfall over the Maritime Continent in the Holocene compared to the LGM (Griffiths et al., 2009).

The early Holocene is characterized by high precipitation over central Sulawesi (Russell et al., 2014) and the Timor Sea (Kuhnt et al., 2015) while speleothem $\delta^{18}O$ records from northern Australia (Denniston et al., 2013) and Flores (Griffiths et al., 2009) indicate a strong increase in precipitation reaching peak rainfall between 8 ka and 4 ka and between 8 ka and 6 ka, respectively. Intensified monsoonal rainfall between 8 and 6 ka is also supported by stable carbon isotopes of plant material from a marine record off Sumba Island (Dubois et al., 2014). Intensified monsoonal rainfall during the early Holocene might be caused by a southernmost located austral summer ITCZ during this period in response to southern Hemisphere forcing (Kuhnt et al., 2015) or northern high latitude forcing (Russell et al., 2014). In contrast to intensified monsoonal rainfall during the early Holocene, AISM rainfall appeared relatively constant over Java throughout the early to mid-Holocene (Mohtadi et al., 2011).

Northern Borneo experienced highest rainfall during the mid-Holocene which is most likely associated with an insolation-driven southward shift of the annual mean ITCZ or a stronger Pacific Walker circulation (Partin et al., 2007). Speleothem records suggest high rainfall over

northern Australia during the mid-Holocene which is probably related to ENSO dynamics (Denniston et al., 2013) whereas speleothems indicate decreased rainfall over Flores between 6 and 4 ka (Griffiths et al., 2009; 2010). Drier conditions and thus a weaker AISM during the mid-Holocene are supported by a decrease in terrigenous supply recorded in marine records off Timor and off northern Australia (Kuhnt et al., 2015), off Sumba Island (Steinke et al., 2014) and in lacustrine sediments from Lake Towuti in Sulawesi (Russell et al., 2014). Drier conditions are recorded in a marine sediment core collected off northwestern Sumatra between 6.5 ka and 4.5 ka due to a positive IOD-like mean state of the Indian Ocean (Niedermeyer et al., 2014). Positive IOD conditions are supported by sea surface cooling recorded in corals from the eastern Indian Ocean (Abram et al., 2009). In contrast to drier conditions during the mid-Holocene, the area around Sumba Islands experienced higher rainfall during the late dry season (Dubois et al., 2014). Deuterium isotopes from marine sediments off southern Sulawesi indicate relatively constant precipitation during the past 8 ka with slightly enhanced rainfall around ~4 ka and during the past 1 kyr (Tierney et al., 2012).

During the late Holocene, more frequent and/or intensified El Niño conditions might be responsible for drier conditions over northern Borneo (Partin et al., 2007). Decreased pre-monsoonal rainfall observed in northern Australia around ~2 ka point to intensified El Niño (Denniston et al., 2013). In contrast, Dubois et al. (2014) suggest that prolonged dry periods in response to enhance rainfall seasonality and a weaker AISM resulted in drier conditions around 2 ka (Dubois et al., 2014). On the other hand, speleothem stable oxygen isotope records from Flores indicate a Holocene maximum in rainfall between 3 and 2 ka and a slight decrease in rainfall thereafter (Griffiths et al., 2009; 2010). Overall, monsoonal rainfall reconstructions reveal a strengthening of the AISM over southern Indonesia during the late Holocene either related to shifts in the ITCZ (Tierney et al., 2010; Mohtadi et al., 2011; Russell et al., 2014; Kuhnt et al., 2015) or solar activity (Steinke et al., 2014). In contrast to an intensified AISM, upwelling off Java and thus AIWM winds were weaker during the late Holocene compared to the early Holocene, which is most likely associated with a weaker northern Hemisphere summer insolation during the late Holocene (Mohtadi et al., 2011). In line with slightly positive SST anomalies as deduced from corals of the eastern Indian Ocean (Abram et al., 2009), increased rainfall between 2 ka and 1 ka in Sumatra suggests a more negative IOD-like mean state of the Indian Ocean (Niedermeyer et al., 2014).

Environmental and climatic reconstructions in Indonesia illustrate the strong influence of the ITCZ, the Australian-Indonesian monsoon system, ENSO and IOD on the climate of the Maritime Continent and sea surface conditions within the Indonesian Seas. By using different

proxies, these reconstructions draw a picture of Holocene climate evolution in the Maritime Continent which is, however, partly contradictory. As we know from present-day data, the influence of climate phenomena varies across the region in response to topography and/or ocean–atmosphere fluxes, which are imposed by local air-sea interactions (Aldrian and Susanto, 2003). Furthermore, these climate phenomena interact with each other e.g. via changes in SST or shifts in atmospheric pressure cells, and exert a significant control on the initiation and/or termination but also on the strength of the climatic events which further complicates the proxy interpretation from the IPWP. To understand the complexity of the climate variability in Indonesia during the past, it is crucial to reconstruct climate variations from various regions in Indonesia on centennial to millennial time scales.

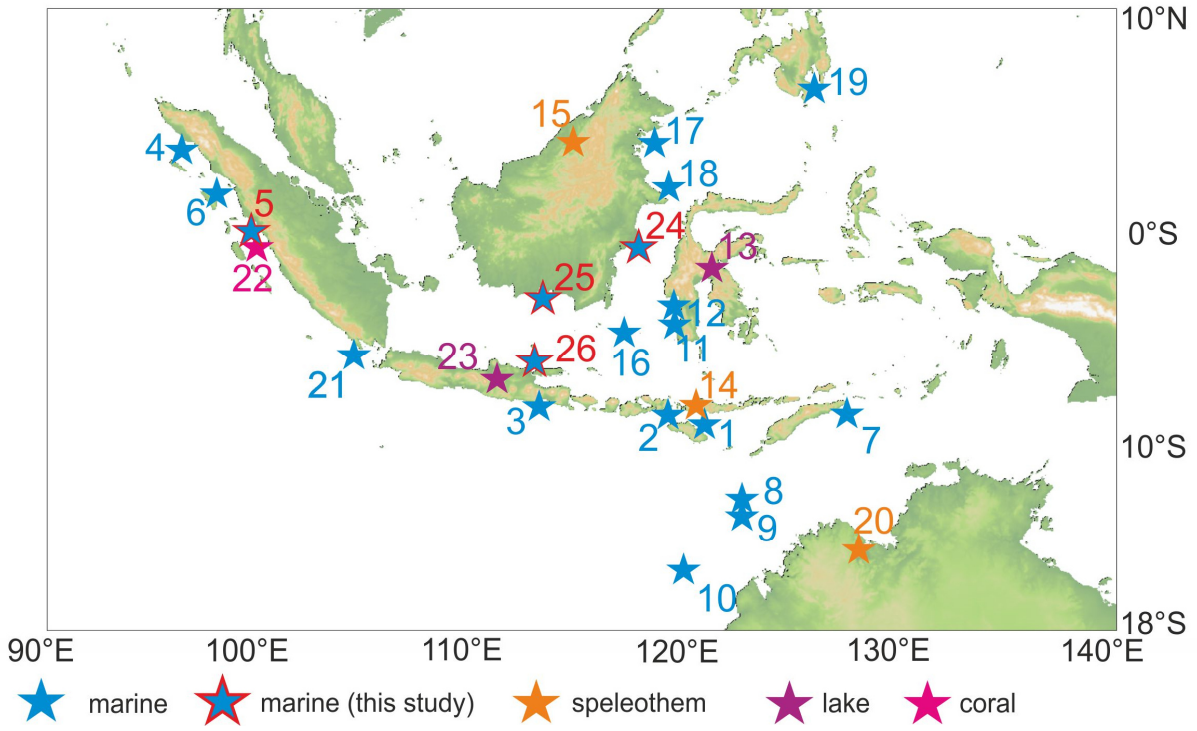

Figure 10: Study sites of environmental reconstructions from the Maritime Continent. Core names, exact positions, used proxies and investigators are listed in table 2. The map was created by using GeoMapApp.

Table 2: Study sites with the exact position, the used proxies, the time span of reconstruction and the investigator.

Map ID	Core ID	Position	Proxy	age	published by
1	GeoB 10069-3	9° 35.69' S; 120° 55.02' E	stable isotopes of fatty acids in plant material	25 ka	Dubois et al. 2014
2	GeoB 10065-7	9° 13.39' S; 118° 53.58' E	Trace elements in bulk sediment	6 ka	Steinke et al. 2014
3	GeoB 10053-7	8° 41' S; 112° 52' E	trace elements in bulk sediments, stable isotopes of planktic foraminifera, *G. bulliodes* counts	22 ka	Mohtadi et al. 2011
4	SO 189-119KL	3° 31' N; 96° 19' E	stable isotopes and trace elements of planktic foraminifera	45 ka	Mohtadi et al. 2014
5	SO 189-39KL	0° 47' S; 99° 54' E			
6	SO 189-144KL	1° 09' N; 98° 04' E	Deuterium isotopes in plant material	24 ka	Niedermeyer et al. 2014
7	SO 185-18460	8° 47.386' S; 128° 38.485' E	Trace elements in bulk sediment	25 ka	Kuhnt et al. 2015
8	SO 185-18479	12° 27.159' S; 121° 22.395' E			
9	MD 01-2378	13° 4.95' S; 121° 47.27' E			
10	SO 185-18506	15° 18.656' S; 119° 30.052' E			
11	BJ8-03-34 GGC	3° 52.8' S; 119° 26.76' E	Deuterium isotopes in plant material	2 ka	Tierney et al. 2010
12	BJ8-03-70GGC	3° 33.96' S; 119° 22.98' E	Deuterium isotopes in plant material	15 ka	Tierney et al. 2012
13	IDLE-TOW10-9B	2° 30' S; 121° 30' E	trace elements of bulk sediments and stable isotopes in plant waxes	60 ka	Russell et al. 2014
14	LR06-B1	8° 32' S; 120° 26' E	stable oxygen isotopes in speleothems	12 ka	Griffiths et al. 2009, 2010, 2016
	LR06-B3				
15	SCH02	4° N; 114° E	stable oxygen isotopes in speleothems	27 ka	Partin et al. 2007
	SSC01				
	BA04				
16	MD 98-2161	05° 12.6' S, 117° 28.8' E	stable isotopes and trace elements of planktic foraminifera	2 ka	Oppo et al. 2009
17	MD 98-2178	3° 37.2' N, 118° 42' E	stable isotopes and trace elements of planktic foraminifera	12 ka	Fan et al. 2013
18	MD 98-2177	1° 24.18 N; 119° 4.68' E	stable isotopes and trace elements of planktic foraminifera	2 ka	Newton et al. 2011
16	MD98-2160	5° 12' S, 117° 29' E			
19	MD 98-2181	6° 18' N; 125° 49.8' E	stable isotopes and trace elements of planktic foraminifera	15 ka	Stott et al. 2004
20	KN-51-10	15° 18' S; 128° 37' E	stable oxygen isotopes in speleothems	9 ka	Denniston et al. 2013
21	SO 139-74KL	6° 32.6' S; 103° 50.0' E	Stable isotopes, alkenones, biogenic sediment components, trace elements of bulk sediments	300 ka	Lückge et al. 2009
22	corals	0–5° S; 99-102° E	Sr/Ca SST	7.5 ka	Abram et al., 2009
23	LAD08-2P LAD08-3P	8° S; 113° E	stable isotopes in plant waxes	1 ka	Konecky et al. 2013
5	SO 189-39KL	0° 47' S; 99° 54' E	trace elements of planktic foraminifera	8 ka	this study
24	SO 217-18517	1° 32.199' S; 117° 33.756' E	stable isotopes and trace elements of planktic foraminifera, elemental composition of bulk sediments	5ka	
25	1612-23	3° 35.36' S, 112° 44.23' E	grain size and elemental composition	3 ka	
26	1609-05	6° 43.15' S, 112° 44.84' E		5.5 ka	

4. Material and Methods

4.1. Material

Two high-resolution piston and two gravity cores from different regions of Indonesia have been investigated in order to explore the influence of different controlling mechanism on the local climate (Fig. 2, Tab. 2). Piston core SO 189-39KL was taken in the northern Mentawai Basin between the fore-arc islands and mainland of Sumatra in the eastern Indian Ocean from a water depth of 517 m (Wiedicke-Hombach et al., 2007) providing a continuous sedimentary sequence. The core length is 1354 cm (Wiedicke-Hombach et al., 2007) while only the uppermost 270 cm are used for environmental reconstruction in this thesis. The sediment consist of olive-green foram-bearing silty clay which is slightly mottled (Wiedicke-Hombach et al., 2007). A gray volcanic ash layer as well as a layer of coarse-grained sand indicative for a turbidite layer were found in 60-62.5 cm and 174-179 cm core depth, respectively (Wiedicke-Hombach et al., 2007). Samples from these layers were not used for environmental reconstruction.

Piston core SO 217-18517 was taken ~ 60 km southeast off the Mahakam Delta in the Makassar Strait, central Indonesia from a water depth of 699 m (Kuhnt et al., 2011). The total length is 1,427 cm (Kuhnt et al., 2011) while only the uppermost 400 cm are investigated in this thesis. Beside a slight sediment loss at the core top, the core provides a continuous sedimentary sequence of olive-green and brownish, foram- and mollusc-bearing silty clay (Kuhnt et al., 2011).

The gravity cores 1612-23 and 1609-05 were taken off the Solo Delta, eastern Java, and the Seruyan Delta, southern Borneo, within the Java Sea, southern Indonesia. The sediment core 1612-23 has a total length of 134 cm and was retrieved 24 km southeast off the Seruyan Delta from a water depth of ~20 m. The sediment consists of foram-bearing silty clay. The sediment core 1609-05 has a core length of 92 cm and was taken 35 km off the Solo Delta in a water depth of 47 m. The sediment can be described as foram-bearing silty clay. The sedimentary records dried out during the storage resulting in large cracks and very hard sediment. However, radiocarbon dating indicated continuous sedimentary sequences which were used for investigations of the regional paleo-environment in this thesis.

Multi-proxy reconstructions provide insights in environmental changes of these study sites during the mid- to late Holocene. The age models are based on radiocarbon dating on foraminiferal tests. Sedimentation rates in addition to the elemental composition and the grain size distribution of bulk sediment is used to characterize terrigenous input. Stable isotopes and trace elements from planktic foraminifera as well as assemblage counts on planktic foraminifera indicate surface water conditions.

4.2. Methods

4.2.1. Radiocarbon dating and age determination

A chronological age-depth relationship is probably the most important requirement to reconstruct the evolution of climatic or oceanographic conditions throughout the past. With a half-life of 5,7 ± 0.03 kyr (Mook, 1986), radiocarbon dating provides a good age control for samples younger than 45 ka (Lowe and Walker, 1997). Due to the detonation of thermonuclear devices, 1950 AD is the reference date for ^{14}C yrs BP and hence represents 0 ka (Stuiver and Polach, 1977; Lowe and Walker, 1997). Samples need to be corrected for isotopic fractionation ($\delta^{13}C$) and ages might be adjusted for potential reservoir effects separately (Stuiver and Polach, 1977).

Carbonate samples used in this study for dating contain either mono- or multi-species planktic or (epi)benthic foraminifera, or gastropods, respectively, depending on the availability of carbonate-producing organisms in the samples (see manuscripts for details). Samples for ^{14}C ages were measured at the National Ocean Sciences Accelerator Mass Spectrometry Facility (NOSAMS) in Woods Hole, USA, and Keck Carbon Cycle Accelerator Mass Spectrometry Facility at the University of California in Irvine, USA. The ages were corrected for $\delta^{13}C$ and converted to calendar years using the CALIB 7.0 program and the Marine13 calibration curve (Reimer et al., 2013) without a further adjustment for a regional ^{14}C reservoir age This age model was developed and published by Mohtadi et al. (2014).

The age models of all other records are based on ^{14}C ages analyzed at the Keck Carbon Cycle Accelerator Mass Spectrometry Facility at the University of California in Irvine, USA. Samples were corrected for $\delta^{13}C$ and the age models were generated by using Bayesian age modelling. In contrast to linear age models, Bayesian age modelling provides a more environmentally realistic age-depth relationship by reconstructing the sedimentation process in response to changes in environmental conditions (Blaauw and Christen, 2011). We used the Bacon R 2.2 software developed by Blaauw and Christen (2011) with the default settings and the calibration curve Marine 13 converting ^{14}C ages to calendar years (Reimer et al., 2013) without any local offsets (Southon et al., 2002).

4.2.2. Foraminiferal trace element analyses

During the past decade, foraminiferal Mg/Ca has become a common and reliable proxy for paleo water temperatures. The Mg incorporation in foraminiferal tests predominantly depends on temperature with higher Mg/Ca reflecting higher water temperatures (Elderfield and

Ganssen, 2000) and, to a much lesser extent, salinity and pH of the surrounding water during shell calcification as well as vital effects (Lea et al., 1999). A cleaning procedure prior to the analyses is crucial because clay and organic material trapped in the foraminiferal tests might contain additional Mg and and hence might alter the foraminiferal Mg/Ca ratios. Post-depositional processes might also elevate foraminiferal Mg/Ca. Post-depositional authigenic coatings like Mn-rich oxyhydroxide containing Mg (Martin and Lea, 2002; Pena et al., 2005) might require an additonal reductive cleaning step. Opposing to elevated Mg/Ca caused by post-depositional coatings, dissolution of the foraminiferal carbonate after deposition decreases foraminiferal Mg/Ca (Brown and Elderfield, 1996). Therefore, it is important to estimate the effect of dissolution e.g. by searching for aragonitic components in the sample. Post-depositional dissolution effects would dissolve these components first. Thus, the continuous occurrence of pteropods or pteropod fragments which was checked randomly implies a good preservation of carbonate allowing foraminiferal trace element analysis in the investigated records.

The planktic foraminifera *Globigerinoides ruber* s.s. (sensu stricto) as a mixed-layer dwelling species and *Pulleniatina obliquiloculata* as an upper-thermocline dwelling species were used to reconstruct SST and thermocline temperatures (TT, Mohtadi et al., 2011a). Selected foraminifera were gently crushed, homogenized and the shell fragments were splitted into aliquots for stable isotope (~5 individuals) and trace element analyses (>10 individuals) to ensure that the stable isotopes and trace element ratios reflect the same sample composition.

The cleaning protocol applied here was originally proposed by Barker et al. (2003): The samples were rinsed and ultra-sonicated using ultra-pure water and methanol to remove clay minerals trapped in the shell fragments. Thereafter, the samples were treated with 1%-NaOH-buffered H_2O_2 and placed in a warm water bath to oxidize organic material. After the transfer into new acid-cleaned vials, no weak acid leach was applied to avoid partial dissolution of the tests (Barker et al., 2003). The samples of SO 189-39KL which were dissolved using 0.075 M QD HNO_3 and centrifuged for 10 min. at 6,000 rpm.

Foraminiferal Ba/Ca represent the Ba concentration of sea water during calcification. Ba/Ca ratios are unaffected by temperature, salinity and/or pH (Lea and Spero, 1992; 1994; Hönisch et al., 2011). Continental runoff supplies high concentrations of Ba to the ocean and allows the reconstruction of variations in fresh water input close to rivers by using foraminiferal Ba/Ca (Hönisch et al., 2011). Previous studies highlighted that the removal of authigenic coatings and hence reductive cleaning is crucial for Ba/Ca determination (Boyle, 1981; Lea and Boyle, 1991). Therefore, samples of SO 217-18517 were additionally cleaned with an reductive

cleaning step after the oxidation using a hydrazine solution (basis solution Hydrazine Reagent 0.06%) buffered with a 0.25 M ammonium citrate solution and ammonium hydroxide (32%) according to Martin and Lea (2002). The samples, filled with 100 µl of the reagent, were placed in a 70 °C warm water bath for 30 minutes and rinsed with ultra-pure water to remove the reagent. After a weak acid leach using 0.001 M NHO_3, the samples were dissolved and centrifuged for 10 min. at 6,000 rpm.

After the cleaning, the solution was transferred into test tubes and diluted to the final volume dependent on the amount of calcite contained in each sample.

The trace element concentrations were measured with Inductively Coupled Plasma Optical Emission Spectrometry (Agilent Technologies 700 Series ICP-OES & Cetac ASX-520 autosampler) by using a multi-element approach at the MARUM, University of Bremen. The Mg/Ca values are reported as mmol mol^{-1} while the Ba/Ca values are reported as µmol mol^{-1}. The instrumental precision of the measurements was also monitored by using an external standard solution measured after every fifth sample as well as the ECRM 752-1 standard (Greaves et al., 2008) measured after every 50 sample (Tab. 3). Sample reproducibility was estimated by measuring replicate samples (Tab. 3).

Table 3: Analytical precession and sample reproducibility of trace element analyses.

Core	Species	Ext. Std.	ECRM 752-1	sample reproducibility
SO 189-39KL	*P. obliquiloculata*	0.005 mmol mol^{-1} (0.17%)	0.002 mmol mol^{-1} (0.06%)	0.2 mmol mol^{-1} (6.9%; n=10)
SO 217-18517	*G. ruber s.s.*	0.002 mmol mol^{-1} (0.06%)	0.002 mmol mol^{-1} (0.06%)	0.11 mmol mol^{-1} (2.31%; n=11)

Elements like aluminium (Al), iron (Fe) and manganese (Mn) and their ratio to calcium (Ca) were monitored in order to assess the influence of contamination on foraminiferal Mg/Ca after the cleaning treatment. Aluminum, which usually indicates a contamination by silicate minerals, in particular clays (Barker et al., 2003), was mostly under the detection limit in the investigated samples which is usually reflected by negative values (cf. Fig. 11). By evaluating cross plots of Al/Ca and Al in relationship to Mg/Ca, contamination by clay could be excluded (Fig. 11). Authigenic coatings or post-depositional Mn-rich oxyhydroxide coatings can be detected by foraminiferal Fe/Ca and Mn/Ca in relationship to Mg/Ca. Cross plots of Fe/Ca vs. Mg/Ca and Mn/Ca vs. Mg/Ca infer that the investigated samples are unaffected by contaminant phases (Fig. 11).

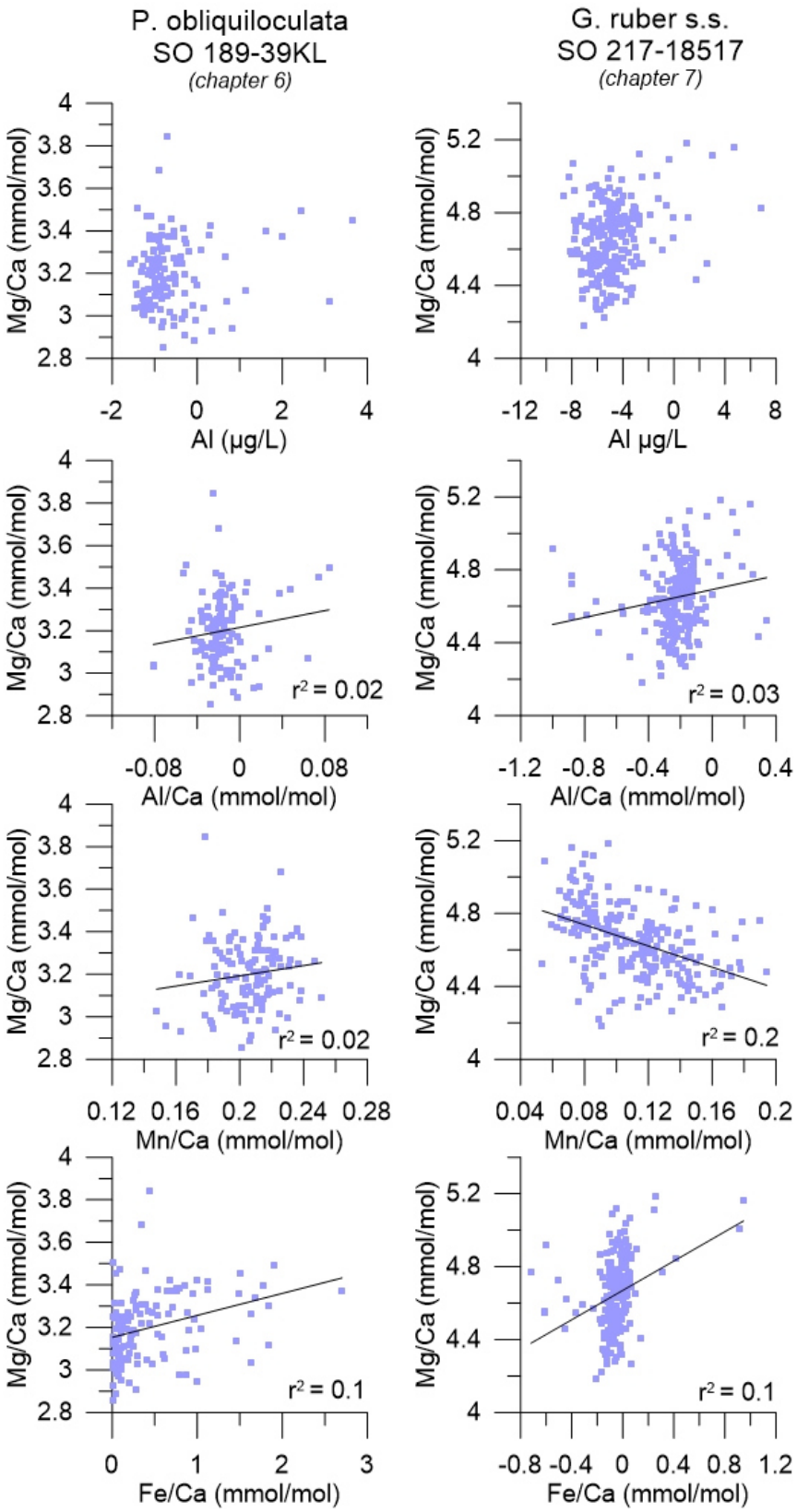

Figure 11: Cross plots of Mg/Ca of *P. obliquiloculata* (SO, 189-39KL; left) and *G. ruber* s.s. (SO 217-18517, right) to the corresponding Al concentrations, Al/Ca, Mn/Ca and Fe/Ca indicate no contamination of clay minerals or secondary phases.

Mg/Ca were converted into temperatures (T) using the species specific and the multi-species equations proposed by Anand et al. (2003):

$$Mg/Ca_{P.\ obliquiloculata} = 0.328 \exp(0.09\ T)$$
$$Mg/Ca_{multi\text{-}species.} = 0.38 \exp(0.09\ T).$$

The error of the temperature reconstructions was estimated by propagating the errors introduced by the Mg/Ca measurements and Mg/Ca-temperature calibration (see Mohtadi et al., 2014 for details) and is 1.2 °C for *P. obliquiloculata* (SO 189-39KL) and 1.1 °C for *G. ruber* s.s. (SO 217-18517).

4.2.3. Foraminiferal stable isotope analyses

Oxygen occurs in three stable isotopes: ^{16}O, ^{17}O, and ^{18}O in the relative proportions of 99.8%, 0.04%, and 0.2% (Böhlke et al., 2005). The oxygen isotopic composition in ocean surface waters is influenced by fractionation during evaporation and precipitation forced by thermodynamical processes. Lighter ^{16}O is preferred during evaporation while heavier ^{18}O is preferred during condensation (Pearson, 2012). Since planktic foraminifera tests are built close to equilibrium, test carbonate mainly reflects the isotopic composition of the surrounding sea water and can be used as a proxy for SST, ice volume, and salinity (Rostek et al., 1993). Combined stable oxygen isotope measurements and Mg/Ca temperature estimates allow the determination of sea water $\delta^{18}O$ ($\delta^{18}O_{sw}$) commonly used as an estimation of paleo-sea water salinity (Elderfield and Ganssen, 2000). More negative values indicate a freshening of the sea water while more positive values indicate an increase in salinity. Stable isotopes of crushed foraminiferal tests were measured with a Finnigan MAT 251 mass spectrometer at the Isotope Laboratory of MARUM, University of Bremen. The isotopic composition of foraminiferal calcium carbonate was analyzed on CO_2 emerged by treatment with phosphoric acid. The data are calibrated using a standard gas with an isotopic composition comparable to marine carbonates. The measurement of an internal standard (Solnhofen limestone) which was calibrated against Pee Dee Belemnite (PDB) by using the NBS 19 standard in order to ensure the detection of instrumental drifts and interlaboratory offsets. All foraminiferal isotopic data are reported relative to the PDB standard. The stable isotope analyses have a long-term standard deviation of 0.07‰ (Isotope Laboratory at Faculty of Geosciences, University of Bremen).

Sample reproducibility was determined by replicate measurements (0.18‰ (5.61%; n = 15 for *G. ruber* s.s. from SO 217-18517).

To estimate the $\delta^{18}O_{sw}$ the low light equation proposed by Bemis et al. (1998) was used:

$$T(°C) = 16.5\text{-}4.80*(\delta c - \delta w)$$

with δc representing $\delta^{18}O$ of the foraminiferal tests, T for the water temperature based on foraminiferal Mg/Ca, and δw representing $\delta^{18}O$ of sea water. Values were converted to Standard Mean Ocean Water (SMOW) by adding 0.27‰ to δc (Bemis et al., 1998). The error of the $\delta^{18}O_{sw}$ reconstructions is estimated by propagating the errors introduced by the SST, the error of SST, the $\delta^{18}O$ measurements, and $\delta^{18}O_{sw}$ calibration (0.25‰ SMOW, see Mohtadi et al., 2014 for calculation details).

4.2.4. Planktic foraminiferal assemblage analyses

Although the genetic diversity is much higher (Kucera and Darling, 2002; Darling and Wade, 2008) , approximately 50 morphospecies of planktic foraminifera live in the modern oceans (Kucera and Darling, 2002; Schiebel and Hemleben, 2005; Darling and Wade, 2008) while only 20 of them are sufficiently abundant in the larger sediment fractions to be used as a proxy for past oceanic environments (Kucera, 2007). Single index species can be used as an indicator for specific environmental conditions such as *Globigerina bulloides*. This species is commonly used as an upwelling indicator in the subtropics and tropics (as used in e.g. Gupta et al., 2003; Mohtadi et al., 2011b). In contrast to single species, indicator assemblages represent a more robust proxy to reconstruct paleo-environments (Kucera, 2007) e.g. subpolar species were used to reconstruct the extent of seasonally ice-free conditions in the Nordic Seas (Kucera et al., 2005), the planktic foraminiferal assemblage associated with the Agulhas leakage was used as a proxy for surface water exchange between the Indian and the Atlantic Ocean (Peeters et al., 2004) and planktic foraminiferal assemblage off Chile was used as an indicator for upwelling intensity (Marchant et al., 1999).

Assemblage counts in this study are used to assess the availability of nutrients in response to upwelling indicating the stratification of the upper water column in the eastern Indian Ocean. Previous studies highlight the energetic advantage for planktic foraminifera bearing symbionts to withstand periods of nutrient stress (Norris, 1996; Hallock, 1999). Symbionts provide nutrients to the hosting foraminifera therefore symbiont-bearing foraminifera might cope with unfavorable nutrient conditions in the water column while symbiont-barren foraminifera would

disappear (Hallock, 1999). Therefore, the abundance of mixed-layer dwelling, symbiont bearing foraminifera might indicate less nutrient availability related to a deep thermocline while mixed-layer and thermocline dwelling, symbiont-barren foraminifera might indicate abundant nutrients related to upwelling conditions off Sumatra. This allows an identification of periods with enhanced or less nutrient availability. The species *Orbunlina universa*, *Globigerinoides conglobatus*, *Globigerinoides ruber*, *Globigerinoides sacculifer*, *Globigerinella aequilateralis*, and *Globigerina falconensis* are counted among the mixed-layer dwelling, symbiont bearing foraminifera while the species *Globigerina bulloides*, *Neogloboquadrina dutertrei*, *Neogloboquadrina pachyderma*, *Pulleniatina obliquiloculata*, *Globigerinita glutinata*, *Globigerina calida*, *Globorotalia scitula*, *Globigerina quinqueloba*, and *Globorotalia tumida* belong to the mixed-layer and thermocline dwelling, symbiont-barren foraminifera (Hemleben et al., 1989). Samples were split and a minimum of 300 individuals of planktic foraminifera from the size fraction >125µm were counted. The abundance of single species relative to total planktic foraminifera was calculated. To obtain the statistical error the standard deviation was calculated on 3 replicate counts of 3 replicate splits, respectively giving a relative error of 3% for mixed-layer dwelling, symbiont-bearing and 5% for mixed-layer and thermocline dwelling symbiont-barren foraminifera.

4.2.5. X-Ray Fluorescence (XRF)

Elemental composition in marine sediments often reflects past climate variations (e.g. Lückge et al., 2009; Steinke et al., 2014). Temperature, rainfall, and vegetation cover control chemical weathering and physical erosion on land (Croudace and Rothwell, 2015). The weathering products are transported by wind and rivers to the marine environment being preserved in the geochemistry and mineralogy of the sediment (Croudace and Rothwell, 2015). Volcanic eruptions or changes in the source area are reflected by the elemental composition of the sediment. In the marine environments, the elemental composition might additionally be influenced by marine productivity and diagenesis (Croudace and Rothwell, 2015).

X-Ray Fluorescence can be measured non-destructively on the archive half of the sediment core using a core scanner technique as it was done on the sediment core SO 217-18517. The data were provided by A. Holbourn and W. Kuhnt (Institute of Geosciences, University Kiel). The sediment surface was covered by using a 4-mm-thin SPEXCerti Prep Ultralene1 foil to avoid contamination of the XRF measurement unit and desiccation of the sediment. By using the AVAATECH XRF core scanners at IfG, Kiel University with 10 and 50kV, a current of 0.25 and 1.0 mA and a sampling time of 30s, the elemental composition of an area of 1 cm^2 was

analyzed with a downcore interval of 1 cm. The data were detected by an Amptek XR-100CR detector and an Oxford Instruments 50W XTF5011 X-Ray tube with rhodium (Rh) target material. Raw data spectra were processed by the Iterative Least square software (WIN AXIL) package from Canberra Eurisys. Results are reported in counts s^{-1} giving semi-quantitative element amounts (see Kuhnt et al., 2015 for analytical details). These relative changes in the chemical composition are reflected by natural logarithmic ratios minimizing the risk of measurement artefacts from variable signal intensities and matrix effects (Weltje and Tjallingii, 2008).

Using an energy-dispersive X-Ray Fluorescence spectrometer provides the possibility of a quantitative measurement of the elemental composition on selected samples. This method was applied in 3 cm intervals of the sedimentary records from the Java Sea in order to investigate changes in elemental composition. Prior to the analyses, the sediment samples were freeze-dried and homogenized via micronization. The element composition was measured by using Panalytical Epsilon 3XL, an energy-dispersive X-Ray Fluorescence spectrometer with a high-resolution Si-drift detector at the Marum, University of Bremen. The X-Ray tube has a rhodium anode which is software controlled using generator settings of a max. voltage of 30kV, max. 1 A and a max. tube power of 9 W. The Si-detector operates with a main voltage of 90-264 V at a frequency of 47-63 Hz power consumption of 250 VA. The calibration is based on various certified and in-house standards giving a precision of < 1% and an accuracy of < 3% for all element concentrations. Values are given in mg/kg.

4.2.6. Particle Size Analysis

The grain size distribution of marine sediment allows assumptions about possible transport mechanisms or current dynamics. While hemipelagic sediment consists of relatively fine-grained sediment which is mainly associated with terrigenous fluvial runoff, wind is supposed to transport relatively coarse particles (> 6 µm) over long distances (Koopmann, 1981; Sarnthein et al., 1981; Sirocko, 1991). Therefore, grain size analysis might reflect variations in river-derived fine grained siliciclastics in response to changes in continental runoff, and thus, provides a proxy for continental humidity (Prins and Weltje, 1999).

Particle size analyses were obtained by using 1 g of sediment in ~5 cm intervals. The terrigenous sediment fraction was isolated by removing organic carbon (10 ml of 35% H_2O_2, until the reaction stopped), calcium carbonate (10 ml of 10% HCl; 1 min.) and biogenic opal (6 g NaOH pellets; 10 min). Samples were diluted after every preparation step to 1 l with deionized water (filter mesh size: 0.2 µm; dilution factor: > 25). Prior to the measurements, samples were boiled

with ~300 mg tetra-sodium diphosphate decahydrate ($Na_4P_2O_7$ * $10H_2O$, 3 min) to remove any remaining aggregates (see also McGregor et al., 2009). To prevent any disturbances by gas bubbles, deionized, filtered and degassed water was used during the measurement. Particle-size measurements were performed at the Particle-Size Laboratory of MARUM, University of Bremen with a Laser Diffraction Particle Size Analyzer (Beckman Coulter) LS 13320. Results show the particle-size distribution of a sample from 0.04 to 2000 µm divided in 116 size classes. Particle sizes are calculated on the basis of the Fraunhofer diffraction theory and the Polarization Intensity Differential Scattering (PIDS) for particles from 0.4 to 2000 µm and from 0.04 to 0.4 µm, respectively. Three internal glass-bead standards give a reproducibility of < 0.7 µm for the mean and < 0.6 µm for the median particle size. The average standard deviation of all size classes is < 4 vol% (the standard deviation of the individual size classes is not distributed uniformly). All provided statistic values are based on a geometric statistic.

5. Overview of own research

Scientific hypotheses outlined in this thesis are discussed within 3 individual studies and presented in Chapter 6 to 8. The main outcome of these studies and the contributions of all co-authors are summarized as follows:

The first Manuscript (Chapter 6)

Holocene variations of thermocline conditions in the eastern tropical Indian Ocean

C. Kwiatkowski, M. Prange, V. Varma, S. Steinke, D. Hebbeln, M. Mohtadi

Published in *Quaternary Sciences Reviews*, Vol. 114, pp. 33-42, 2015
http://dx.doi.org/10.1016/j.quascirev.2015.01.028

By using a multi-proxy approach, Holocene changes in thermocline temperatures and upper ocean structure (or stratification) in the eastern Indian Ocean are reconstructed from a sedimentary record (SO 189-39KL) off western Sumatra, a key area for studying the "Indian Ocean Dipole" (IOD) phenomenon. The early to mid (late) Holocene is mainly characterized by a more negative (positive) IOD-like mean state. This is supported by a state of the art model simulation allowing the interpretation of the underlying physical mechanisms.

Contribution: The study was designed by M. Mohtadi and D. Hebbeln. C. Kwiatkowski generated and analyzed the Mg/Ca data of *P. obliquiloculata* and counted planktic foraminiferal for the assemblage analysis. The age model and SST derived from *G. ruber* are published by Mohtadi et al. (2014). The model simulation was set up by M. Prange and V. Varma. C. Kwiatkowski wrote the paper with main contribution from the co-authors.

The second Manuscript (Chapter 7)

Late Holocene intensification of the Australian-Indonesian summer monsoon and ENSO recorded in a sediment core off the Mahakam Delta, Makassar Strait

C. Kwiatkowski, M. Mohtadi, A. Holbourn, W. Kuhnt, D. Hebbeln

to be submitted to *Quaternary International* soon

The multi-proxy reconstruction of late Holocene variations in surface water conditions in the Makassar Strait and changes in continental runoff from eastern Borneo are recorded in the sedimentary archive (SO 217-18517) off the Mahakam Delta. It is shown that the freshening and cooling trend of surface waters is related to an intensified AISM while the increase in precipitation might be additionally influenced by a strengthening El Niño Southern Oscillation with intensified La Niña and El Niño during the late Holocene.

Contribution: The study was designed by A. Holbourn, W. Kuhnt, M. Mohtadi and D. Hebbeln. The X-Ray Fluorescence data are provided by A. Holbourn and W. Kuhnt. The radiocarbon dating was performed at the Keck Carbon Cycle Accelerator Mass Spectrometry Facility at the University of California in Irvine, USA. C. Kwiatkowski established the age model by using Bayesian age modelling, generated and analyzed foraminiferal trace element and stable isotope data. C. Kwiatkowski interpreted the data and wrote the manuscript with contributions from all co-authors.

The third Manuscript (Chapter 8)

Late Holocene variations in precipitation pattern over the Java Sea in response to monsoon, ENSO and northern high latitude forcing

C. Kwiatkowski, M. Mohtadi, H. Permana, S. Susilohadi, Rina Zuraida, D. Hebbeln

to be submitted to *Quaternary Science Reviews* soon

Late Holocene changes in grain size and trace element distribution as deduced from sedimentary records retrieved from the Java Sea off the Seruyan Delta, southern Borneo and off the Solo Delta, northeastern Java are linked to variations in terrigenous runoff in the Java Sea. Changes in terrigenous runoff are mainly controlled by precipitation likely driven by an intensified ENSO and a strengthening Australian-Indonesian monsoon during the late Holocene. Based on present-day observations, the strengthening in monsoon might be related to changes in the Atlantic Multidecadal Oscillation in the northern Atlantic.

Contribution: The study is a collaboration between German and Indonesian scientists and was designed by D. Hebbeln, M. Mohtadi, S. Susilohadi and H. Permana. AMS ^{14}C dating was measured at the Keck Carbon Cycle Accelerator Mass Spectrometry Facility at the University of California in Irvine, USA. C. Kwiatkowski developed the Bayesian age model and generated the grain size and XRF analyses at the Marum, University Bremen. C. Kwiatkowski interpreted the data and wrote the manuscript with contributions from the co-authors.

6. Holocene variations of thermocline conditions in the eastern tropical Indian Ocean

Cornelia Kwiatkowski[1]*, Matthias Prange[1], Vidya Varma[1, 2], Stephan Steinke[1], Dierk Hebbeln[1], Mahyar Mohtadi[1]

[1] *MARUM – Center for Marine Environmental Sciences, University of Bremen, Bremen, Germany (*ckwiatkowski@marum.de)*

[2] *Dept. of Meteorology, Stockholm University, SE-10691 Stockholm, Sweden*

Abstract

Climate phenomena like the monsoon system, El Niño-Southern Oscillation (ENSO) and the Indian Ocean Dipole (IOD) are interconnected via various feedback mechanisms and control the climate of the Indian Ocean and its surrounding continents on various timescales. The eastern tropical Indian Ocean is a key area for the interplay of these phenomena and for reconstructing their past changes and forcing mechanisms. Here we present records of upper ocean thermal gradient, thermocline temperatures (TT) and relative abundances of planktic foraminifera in core SO 189-39KL taken off western Sumatra (0°47.400' S, 99°54.510' E) for the last 8 ka that we use as proxies for changes in upper ocean structure. The records suggest a deeper thermocline between 8 ka and ca. 3 ka compared to the late Holocene. We find a shoaling of the thermocline after 3 ka, most likely indicating an increased occurrence of upwelling during the late Holocene compared to the mid-Holocene which might represent changes in the IOD-like mean state of the Indian Ocean with a more negative IOD-like mean state during the mid-Holocene and a more positive IOD-like mean state during the past 3 ka. This interpretation is supported by a transient Holocene climate model simulation in which an IOD-like mode is identified that involves an insolation-forced long-term trend of increasing anomalous surface easterlies over the equatorial eastern Indian Ocean.

Key words: Indian Ocean, Sumatra, Indian Ocean Dipole, Mg/Ca, Thermocline, Holocene, Planktic foraminifera

6.1. Introduction

Presently, the Indonesian climate is mainly controlled by the seasonal migration of the Intertropical Convergence Zone (ITCZ), the Australian-Indonesian monsoon and the El Niño – Southern Oscillation (ENSO). The Indian Ocean Dipole (IOD) which is a coupled ocean-atmosphere phenomenon also exerts a significant control on the climate variability over western Indonesia (Saji et al., 1999; Webster et al., 1999; Abram et al., 2007). Negative IOD events are characterized by positive rainfall anomalies over western Indonesia accompanied by dry conditions over East Africa and eastward surface wind anomalies over the eastern Indian Ocean. On the other hand a positive IOD event is characterized by sea surface cooling (Fig. 1) and increased productivity off Sumatra due to enhanced upwelling in the eastern Indian Ocean accompanied by strong easterlies over the central Indian Ocean, dry conditions in western Indonesia and higher-than-normal rainfall over East Africa (Webster et al., 1999).

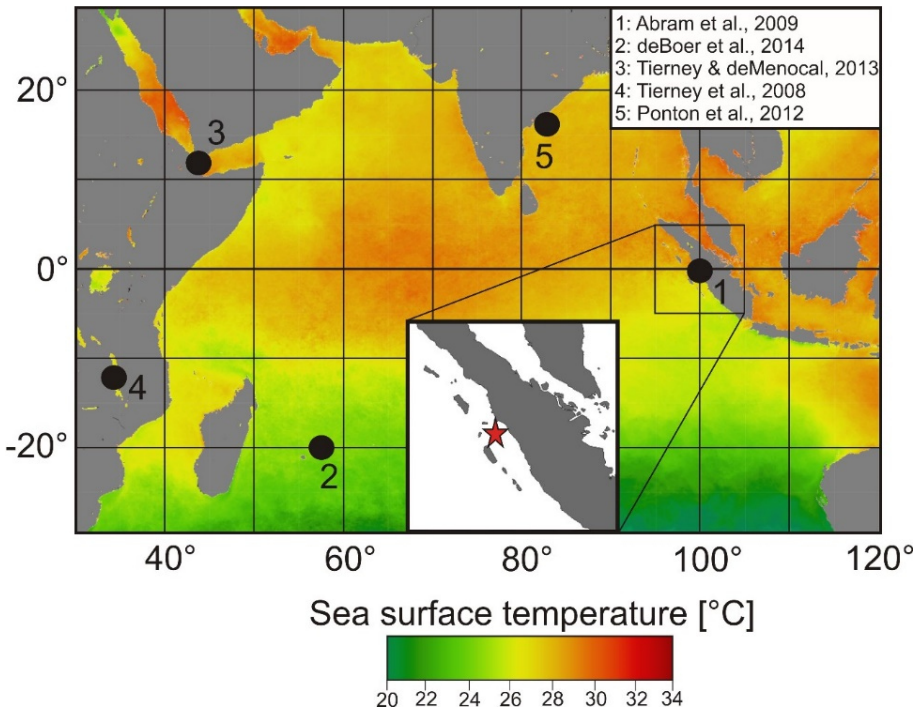

Figure 6.1: Map of SST in the Indian Ocean indicating the surface cooling caused by the upwelling of cold subsurface water in autumn 2006 during a positive IOD event (http://oceancolor.gsfc.nasa.gov). The red star indicates the core site of SO 189-39KL, sites from other studies relevant for this work are numbered serially.

Behera et al. (2006) suggest that the IOD is initiated by processes internal to the Indian Ocean and, might be additionally affected and amplified by other climatic phenomena as e.g. ENSO. Saji et al. (1999) suggested the IOD being independent of ENSO but

model simulations imply that ENSO has a strong influence on the periodicity, strength, and formation processes of the IOD in years of co-occurrences (Behera et al., 2006). However, since the occurrence of three positive IOD events in the years 2006 – 2008 it is obvious that ENSO is not the only triggering factor (Behera et al., 2006).

Previous studies on the IOD mainly focus on its present-day behavior, but only little is known about its past variability beyond the instrumental record. So far, there exist only three studies from the eastern Indian Ocean investigating the IOD variability during the Holocene; two are based on SST anomaly reconstructions from coraline Sr/Ca ratios off Sumatra (Abram et al., 2007; 2009) and one is based on precipitation changes derived from δD and $\delta^{13}C$ of plant waxes (Niedermeyer et al., 2014). Two studies investigate the IOD variability in the western Indian Ocean by using a multi-proxy reconstruction from the Mauritian lowlands (de Boer et al., 2014) and δD from Lake Tanganyika sediments (Tierney et al., 2008).

Abram et al. (2007) hypothesized that observed SST anomalies are related to IOD events and suggested the Asian monsoon and ENSO being capable of triggering positive IOD events. They stated a close relationship between the Asian monsoon system and IOD implied by a longer duration of positive IOD events during times of strong Asian summer monsoon and argue that sea surface cooling during a positive IOD event is constrained by the cross-equatorial wind reversal at the end of the Asian summer monsoon season resulting in an abrupt termination of Ekman upwelling along the coast of Sumatra (Abram et al., 2007). Furthermore, they assume that the monsoonal wind reversal controlling the timing of peak cooling during positive IOD events to be a consistent feature during the Holocene. The close relationship between the monsoon system and IOD is further supported by the study of Abram et al. (2009). Niedermeyer et al. (2014) investigated regional precipitation patterns over Sumatra in comparison to precipitation patterns from East Africa and Southeast India and found a general agreement with the reconstructed IOD variability by Abram et al. (2009).

The study of de Boer et al. (2014) suggests an anti-phased relationship of climate dynamics between the Mauritian lowlands and western tropical Australia during the middle Holocene reflecting a prolonged configuration of a negative mode of the IOD, which is partly inconsistent with the findings of Abram et al. (2009).

In order to understand the underlying mechanisms and the interaction between the IOD and other climate phenomena, e.g. the

monsoon or ENSO continuous long-term data series are essential.

In this study we use a continuous sediment archive recovered from the northern Mentawai Basin off western Sumatra, close to the site published by Abram et al. (2009), in order to estimate variations in upper water column temperature and thermal gradient (i.e. depth of thermocline), and investigate the planktic foraminiferal assemblage to reconstruct the upper water column structure during the past 8 ka. We compare our results to orbital-forced model simulations and other climatic records from the Indian Ocean region in order to better assess possible forcing mechanisms of the upper water column variations off western Sumatra.

6.2. Study Area

Aldrian and Susanto (2003) show that under modern conditions, SST and precipitation off western Sumatra are neither controlled by ENSO nor by the monsoonal system but by the seasonal migration of the ITCZ. At present, upper water column temperature and sea surface salinity anomalies in the study area are mainly controlled by the IOD (Yu et al., 2005; Qiu et al., 2012). This is also evident from several SST and TT datasets (e.g. SODA 2.2.4) in comparison to the Dipole Mode Index (DMI) introduced by Saji et al. (1999). Previous studies have shown that the western coast of Sumatra is one of the most sensitive areas for the development of the IOD (e.g. Abram et al., 2007). During positive IOD events, observational data of the last decades have shown that a decrease in SST is accompanied by a decrease in precipitation off Sumatra (Webster et al., 1999). Oceanic thermocline variations associated with IOD are confined to the region north of 6°S (Yu et al., 2005). Large-scale surface and subsurface circulation of the Indian Ocean might not affect the hydrography of the Mentawai Basin due to the topographic situation in which the fore-arc islands impede a direct influence of the open ocean (Mohtadi et al., 2014). Thus, paleoenvironmental archives from this area might record changes related to IOD variability. Seasonal changes are weak in the study area (Mohtadi et al., 2014) except for variations related to the IOD, which peaks in the September-October-November (SON) season (Saji et al., 1999). During extreme positive IOD events a SON SST decrease of > 2 °C off Sumatra is one of the most significant signals observed presently (Webster et al., 1999; Abram et al., 2007; Du et al., 2008). This surface cooling in the eastern basin of the Indian Ocean is caused by unusually strong upwelling along the equator and off Sumatra. Furthermore, strong precipitation in the eastern Indian Ocean during normal years results in the development of a barrier layer, a layer

separating the thermocline and the mixed layer, which impedes the upward movement of subsurface water masses (Spintall and Tomczak, 1992; Du et al., 2005; Qu and Meyers, 2005). During positive IOD events, the reduced warm water advection to the eastern equatorial Indian Ocean (Murtugudde et al., 2000) and the missing barrier layer in the water column due to decreased precipitation allow upwelling of cooler, nutrient-rich subsurface waters to the sea surface (Murtugudde et al., 2000; Du et al., 2008). However, Qiu et al. (2012) and Saji and Yamagata (2003) showed that changes in SON SST are relatively small (< 1 °C) during most positive IOD events and that temperature changes at the thermocline are much more prominent than changes at the sea surface (cf. Fig. 2).

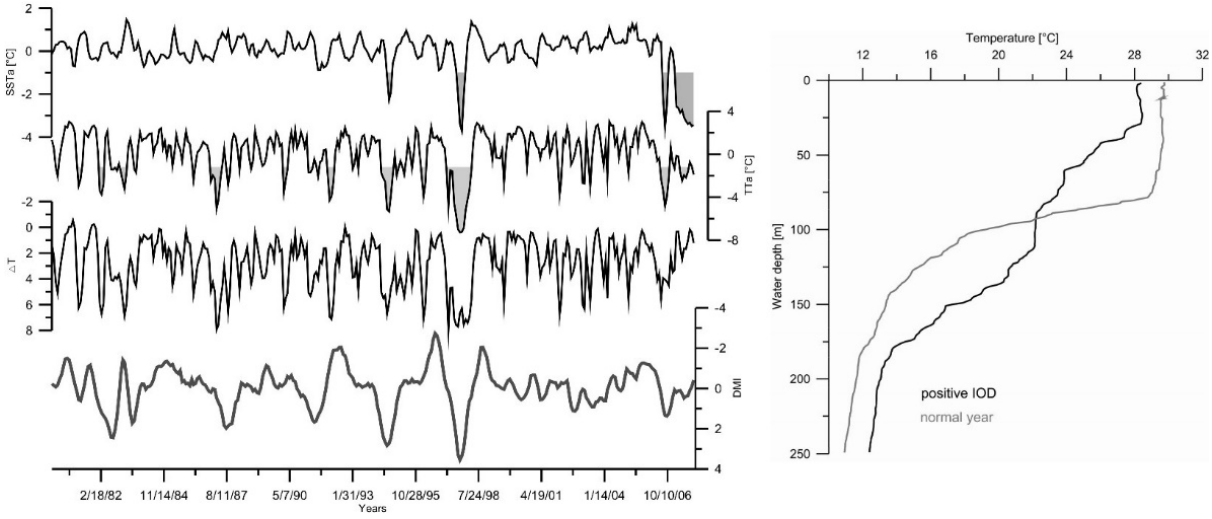

Figure 6.2: Monthly SST (5 m) and TT (70 m) anomalies relative to the mean SST and TT during Jan. 1980 to Dec. 2007 and ΔT_{SST-TT} calculated from SODA 2.2.4 time series from 0.75S 99.75E (http://iridl.ldeo.columbia.edu; Carton et al., 2005) during the years 1980 to 2007 compared to the Dipole Mode Index (Saji et al. 1999). The grey filling in the SST and TT records indicate anomalies exceeding the error of 1°C for SST and 1.2°C for TT reconstructions, respectively. Additionally, a comparison of water temperature profiles measured during August 2005 (normal year, Mohtadi et al. 2007) and September 2006 (positive IOD year, Mohtadi et al. 2007) in the Mentawai Basin indicates an uplift of the thermocline and a SST cooling of 1°C during a positive IOD event.

Zhao and Nigam (2015) show that the temperature dipole structure of the IOD occurs at the subsurface whereas the SST field shows a monopole structure over the Indian Ocean. Hence, when using foraminiferal Mg/Ca for the reconstruction of past IOD variations, the depth of thermocline and TT in the eastern Indian Ocean appear to be most suitable to characterize a possible IOD-like mean state – periods characterized either by stronger and/or more frequent positive IOD events (positive IOD-like mean state; upwelling; shallowing of the thermocline) or by

weaker and/or less frequent positive IOD events (negative IOD-like mean state; deepening of the thermocline).

6.3. Material and Methods

6.3.1. Sample material

Piston core SO189-39KL was recovered from the northern Mentawai Basin off western Sumatra (0°47.400' S, 99°54.510' E, 1,350 cm core length, 517 m water depth) during the R/V Sonne 189 – SUMATRA expedition in 2006 (Wiedicke-Hombach et al., 2007; Fig. 1). Here we study the upper 2.7 m of this core representing the past 8 kyr. The continuous occurrence of pteropods throughout the core implies good preservation of carbonate. The age model for this period is based on 20 AMS radiocarbon dates (Mohtadi et al., 2014).

6.3.2. Planktic foraminiferal trace element analysis

SST anomaly (a), TTa and, ΔT between 1980 and 2007 calculated from the SODA 2.2.4 dataset in comparison to the Dipole Mode Index (DMI) introduced by Saji et al. (1999) illustrate the relationship of upper water column characteristics to the IOD (Fig. 2). SODA 2.2.4 dataset represents realistic changes in timing and magnitude of SST variations therefore changes of TT might be also reliable. Large variations, especially in TT, correspond to variations in the IOD (correlation coefficient of -0.52 between TTa and DMI and 0.43 between ΔT and DMI; Fig. 2), thus, highlighting the suitability of TT off western Sumatra as a proxy to track past IOD changes.

The core was sampled at 2 cm intervals (sample resolution of ~60 years) for trace element analyses on thermocline dwelling planktic foraminifera *Pulleniatina obliquiloculata* with a calcification depth of ~75 m (Mohtadi et al., 2011a). Due to weak seasonal changes in the study area, we suggest an annual occurrence of *P. obliquiloculata.* Since upwelling and hence substantial shifts in thermocline depth can only occur during the IOD peak season, variations in the thermocline record should mainly reflect changes in the SON season.

For Mg/Ca analyses ~25 individuals of *P. obliquiloculata* from the size-fraction 355-500 µm were picked. For the selected foraminifera we applied the cleaning protocol originally proposed by Barker et al. (2003) consisting of a clay-removal step using ultra-pure water and methanol, followed by the oxidation of organic matter using 1% NaOH-buffered H_2O_2. The samples were dissolved into 0.075M QD HNO_3 and centrifuged for 10 min. at 6,000 rpm. The solution was transferred into test tubes and diluted to the final volume dependent on the amount of calcite contained in each sample. The trace element concentrations were measured with

Inductively Coupled Plasma Optical Emission Spectrometry (Agilent Technologies 700 Series ICP-OES & Cetac ASX-520 autosampler) by using a multi-element approach at the MARUM, University of Bremen. The Mg/Ca values are reported as mmol mol^{-1}. The instrumental precision of the measurements was also monitored by using an external standard solution (Mg/Ca=2.97 mmol mol^{-1}) measured after every fifth sample as well as the ECRM 752-1 standard measured after every 50 sample, providing a standard deviation of 0.005 mmol mol^{-1} (0.17%) for the external standard and 0.002 mmol mol^{-1} (0.06%) for the ECRM 752-1 standard, respectively. The reproducibility of the samples was 6.9% (n=10) corresponding to a standard deviation of 0.2 mmol mol^{-1} (Fig. 3b, error bar). Aluminum, which usually indicates a contamination by silicate minerals (Barker et al., 2003), is under the detection limit. Post-depositional Mn-rich carbonate/oxyhydroxides coatings can bias foraminiferal Mg/Ca ratios (Pena et al., 2005), and can be detected by foraminiferal Fe/Ca and Mn/Ca ratios. Due to relatively high Fe/Ca and Mn/Ca ratios, the influence of contaminant phases on Mg/Ca temperature estimates was determined via cross plots. No covariance between Mn/Ca and Mg/Ca ratios (r^2 = 0.02) or between Fe/Ca and Mg/Ca ratios (r^2 = 0.11) could be observed. Consequently, we infer the Mg/Ca values of the Holocene section of SO 189-39KL to be unaffected by contaminant phases.

P. obliquiloculata Mg/Ca ratios were converted into temperatures (T) using the species specific equations proposed by Anand et al. (2003):

$$Mg/Ca_{P.\ obliquiloculata} = 0.328 \exp(0.09\ T)$$

The error of the temperature reconstructions based on *P. obliquiloculata* Mg/Ca is estimated by propagating the errors introduced by the Mg/Ca measurements and Mg/Ca-temperature calibration (see Mohtadi et al., 2014 for details). The resulting error is on average 1.2°C (Fig. 3c). The upper water vertical temperature gradient (ΔT °C) has been estimated by subtracting thermocline temperatures (TT, based on $Mg/Ca_{P.\ obliquiloculata}$) from SST (based on $Mg/Ca_{G.\ ruber\ s.s.}$, published in Mohtadi et al., 2014). *G. ruber* s.s. has a calcification depth of 0-30 m (Mohtadi et al., 2011a). The error of the ΔT (°C) estimates was calculated by using the errors of the SST and TT (± ~1.6 °C, Fig. 3d). A smaller difference in ΔT indicates a lower temperature gradient and hence a deeper thermocline. A greater difference in ΔT indicates a larger temperature gradient and consequently, a shoaling of the thermocline typical for upwelling conditions (Mohtadi et al., 2010; Steinke et al., 2011).

6.3.3. Planktic foraminiferal assemblage

At every 10 cm a minimum of 300 individuals of planktic foraminifera from the size fraction >125 µm were counted. The abundance of single species relative to total planktic foraminifera was calculated. The abundance of mixed-layer (ML) dwelling, symbiont bearing foraminifera and ML and thermocline dwelling, symbiont-barren foraminifera was used to assess the nutrient availability related to upwelling conditions in the study area. ML dwelling, symbiont-bearing foraminifera are able to cope with the disadvantages of a deep mixed layer (e.g. during a more negative IOD-like mean state), while ML and thermocline dwelling, symbiont-barren foraminifera prefer nutrient-rich waters (e.g. during a positive IOD-like mean state). To obtain the statistical error the standard deviation was calculated on 3 replicate counts of 3 replicate splits, respectively. The counts have a relative error of 3% for ML dwelling, symbiont bearing foraminifera (*O. universa*, *G. conglobatus*, *G. ruber*, *G. sacculifer*, *G. aequilateralis*, *G. falconensis*) and 5% for ML and thermocline dwelling, symbiont-barren foraminifera (*G. bulloides*, *N. dutertrei*, *N. pachyderma*, *P. obliquiloculata*, *G. glutinata*, *G. calida*, *G. scitula*, *G. quinqueloba*, *G. tumida*).

6.3.4. Climate modelling

Output from transient Holocene climate simulations (Varma et al., 2012) was analyzed to help interpreting the proxy records. The simulations were performed using the low-resolution (T31 or 3.75° atmosphere) version of the comprehensive climate model CCSM3 (Yeager et al., 2006), which is a fully-coupled atmosphere-ocean general circulation model (Collins et al., 2006). From a pre-industrial equilibrium simulation, the model was integrated for 400 years with conditions representing 9 ka orbital forcing to reach a new quasi-equilibrium. After this spin-up, three transient Holocene (9-0 ka) simulations, which differ in their initial conditions, were carried out, where orbital forcing has been accelerated by a factor 10 (cf. Lorenz and Lohmann, 2004). While the first transient run was initialized with the quasi-equilibrated 9 ka state, the second and third runs used the 8.9 and 8.8 ka climates from the first transient run as initial conditions at 9 ka. Greenhouse gas concentrations, aerosol and ozone distributions have been kept constant at pre-industrial values in all Holocene experiments. Moreover, modern continental ice sheets were prescribed such that variations in the orbital parameters were the sole external forcing in the transient runs. The reader is referred to Varma et al.

(2012) for a detailed description of the model setup and experimental design.

Spatio-temporal patterns of low-level (850 hPa) zonal wind variability over the Indian Ocean were examined by means of empirical orthogonal function (EOF) analysis using the three-member ensemble average (averaging over the different runs reduces the influence of stochastical internal climate variability on the results).

The EOFs (or principal components) were found by computing the eigenvalues and eigenvectors of the wind-field covariance matrix (e.g. von Storch and Zwiers, 2004). The derived eigenvalues provide a measure of the percent variance explained by each mode (the first or leading mode provides the highest variance in the wind field). The time series of each mode were obtained by projecting the derived eigenvectors onto the spatially weighted anomalies.

6.4. Results

6.4.1. Mg/Ca Paleothermometry, upper water column structure and faunal analysis

The TT estimates fluctuate between 24 and 27.5 °C (2.8 and 3.8 mmol mol^{-1}) and are in good agreement with the SODA 2.2.4 dataset but also the CTD profiles which show a temperature at 70 m water depth of 23–24 °C during positive IOD events and 27-29 °C during normal years (Fig.2). TT estimates show a strong variability and discernable long-term variations with a general increase observable during the early Holocene, which peaks during the mid-Holocene (~26 °C at about 5 ka) and decreases thereafter towards the present (~24 °C, Fig. 3b, c). The SST estimates remain relatively constant during the Holocene (Fig. 3a, Mohtadi et al., 2014) and vary between 28.3 and 30.5 °C (4.9 and 5.9 mmol mol^{-1}). They show a slight decreasing trend between 8 and 6 ka followed by a period of strong SST fluctuations between 6 and 5.5 ka and a cooler and more stable period between 5.5 and 2.5 ka. The late Holocene is characterized by large variations and relatively high SST (~29.7 °C), interrupted by a period of slightly cooler SST between 1.9 and 1.2 ka.

Strong fluctuations in ΔT can be recognized throughout the Holocene with values ranging between 2 and 6 °C (Fig. 3d). The early to mid-Holocene is characterized by a lower ΔT (4 ± 0.7 °C). At around 3 ka, a shift from lower to higher values takes place, and ΔT remains high towards the present (4.6 ± 0.6 °C). This difference is highly significant ($p < 0.01$) according to the t-test. A decrease from 40% to 30% in the abundance of ML-dwelling, symbiont-bearing foraminifera coincides with an increase from 50% to 60% in the abundance of ML and thermocline dwelling, symbiont-barren foraminifera during the late

Holocene (Fig. 3e, f).

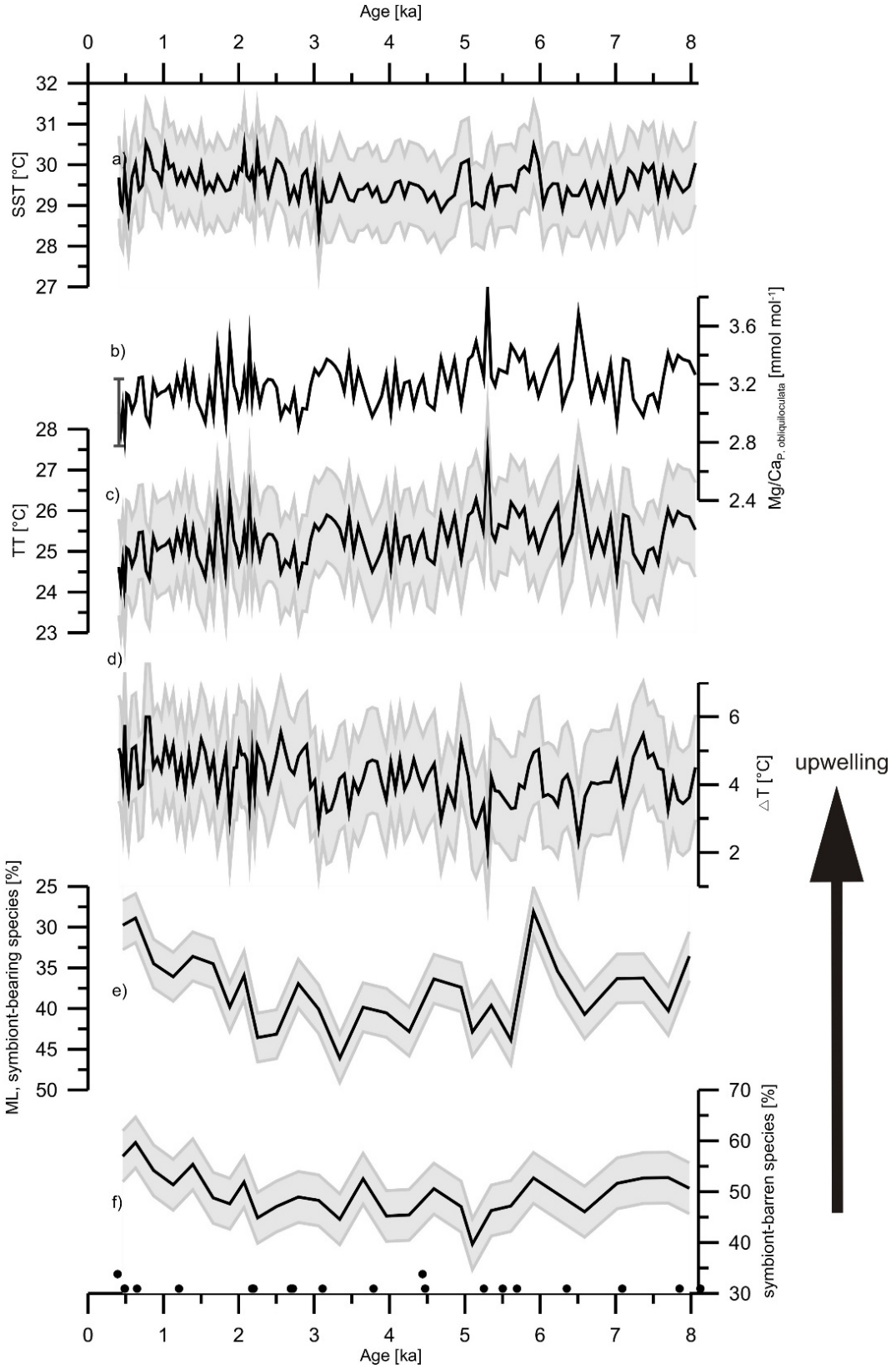

Figure 6.3: Analytical results of SO 189-39KL: **a)** SST estimates derived from Mg/Ca ratios of *G. ruber* s.s. (Mohtadi et al., 2014), **b)** Mg/Ca ratios of *P. obliquiloculata*, **c)** TT estimates derived from Mg/Ca ratios of *P. obliquiloculata,* **d)** temperature difference between SST and TT, **e)** abundance of planktic, ML dwelling, symbiont-bearing foraminifers, **f)** abundance of planktic, ML and thermocline dwelling, symbiont-barren foraminifers and AMS ^{14}C dates (dots; Mohtadi et al., 2014).

Power spectra (95% significance level) of SST, TT and ΔT indicate cycles centered at ~3,850, ~1,540 and ~1,290 years for SST, ~3,850, ~2,570, ~1,100, ~150 years for TT and, ~1,540 and ~150 years for ΔT.

6.4.2. Model results

The leading EOF of the annual mean zonal wind field (three-member ensemble average; see above) explains 23% of the variance and contains the long-term Holocene trend.

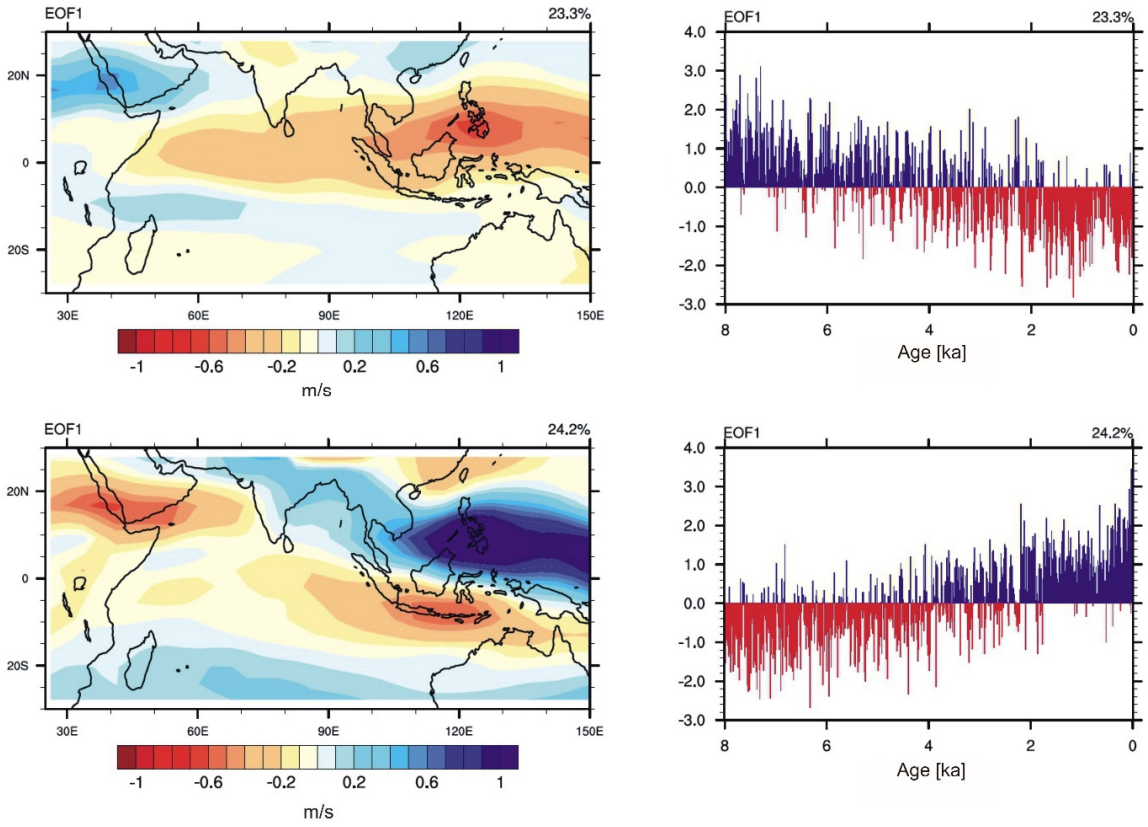

Figure 6.4: The spatial distribution and time-series of the first empirical orthogonal function (EOF) of annual-mean (top) and September-October-November (bottom) 850 hPa zonal wind simulated for the period 8 to 0 ka by CCSM3 using orbital acceleration with a factor of 10. The EOF analysis was performed on a three-member ensemble mean. The time-series are standardized and the EOF maps are obtained by regressing the wind data onto the corresponding standardized leading principal component time-series. Positive (negative) values in the maps correspond to westerly (easterly) wind anomalies. Multiplication of the values with the time-series provides the Holocene trends.

It shows a continuous increase of surface westerlies over the equatorial Indian Ocean and Southeast Asia (Fig. 4, upper panel; reddish region because the principal component time series has a negative trend) which is associated with the weakening of the Indian monsoon. The first EOF of the SON season (24% variance explained) shows an almost similar pattern over the West Pacific/Philippines region (Fig. 4, lower panel; bluish region because the corresponding principal component time

series has a positive trend). By contrast, an opposite trend is simulated over the tropical eastern Indian Ocean/Indonesian region with increasing easterly surface wind anomalies (reddish region). We note that qualitatively the same EOF patterns and time series were reproduced in all three individual Holocene runs.

6.5. Discussion

Our ΔT show a shift from lower to higher values at around 3 ka, indicating a shoaling of the thermocline off western Sumatra during the late Holocene. This is supported by the decrease in the relative abundance of ML dwelling, symbiont bearing planktic foraminifera and an increase in ML and thermocline dwelling, symbiont barren planktic foraminifera indicating a shift to an intensified upwelling (Fig. 3e, f). We suggest that changes in the IOD-like mean state might control the long-term variations in TT and ΔT. We interpret warmer TT and a smaller ΔT between 8 and 3 ka to reflect a more negative IOD-like mean state, whereas colder TT estimates and a greater ΔT after 3 ka are interpreted to reflect a more positive IOD-like mean state. Reconstructed Holocene TT variations are relatively small compared to the TT changes of the past three decades as indicated by the CTD or SODA 2.2.4 data at the calcification depth of *P. obliquiloculata* (~ 6 °C, Fig. 2). We attribute this discrepancy to a smoothing of the IOD-related temperature anomalies in our samples that encompass different seasons and several years.

Abram et al. (2007, 2009) observed a SST cooling of > 2 °C off Sumatra during the 1997 positive IOD event. Saji and Yamagata (2003) and Qiu et al. (2012) showed only a moderate SST cooling of < 1 °C during most of the 20th century positive IOD events. Deshpande et al. (2014) propose a difference between strong and weak positive IOD events: Strong IOD events driven by a thermocline–SST coupling are strongly interactive with the atmosphere, whereas weak IOD events are a response to surface winds without such dynamical coupling. The thermocline–SST coupling is primarily responsible for the enhanced SST gradient during strong IOD years leading to an anomalous Walker circulation within the Indian Ocean. Therefore, weaker positive IOD events have a weaker effect on SST in the eastern Indian Ocean than strong positive IOD events. Due to an error of ~1°C in our foraminiferal SST reconstruction, a more robust signal is expected from reconstructed variations in thermocline temperatures and upper water column structure. Moreover, in-situ observations indicate only a SST cooling of ~1°C between a normal year (August 2005) and a positive IOD year (September 2006), but a significant

shoaling of the thermocline during the positive IOD year in comparison to the normal year (Fig. 2, Mohtadi et al., 2007). This is corroborated by the comparison of the SODA 2.2.4 time series to the DMI (Fig. 2), further supporting the feasibility of using thermocline conditions as a sensitive proxy for IOD reconstructions. We therefore suggest that our approach of reconstructing the IOD-like mean state of the Indian Ocean during the Holocene is only capable of discriminating between periods characterized by more frequent and stronger positive or negative IOD events.

Our interpretation of the proxy data is corroborated by the results of the transient Holocene climate model simulation. The first EOF of the SON season shows an IOD-like pattern (cf. Saji et al., 1999; Qiu et al., 2012) with an increasing trend of surface easterly wind anomalies over the equatorial eastern Indian Ocean and Indonesian region, indicating a trend towards more positive IOD-like conditions during the late Holocene (Fig. 4). These anomalous easterly winds induce a shoaling of the tropical thermocline in the eastern Indian Ocean. The simulated interannual zonal surface wind and ΔT (temperature difference between surface and thermocline at 70 m depth) variations off the equatorial Sumatran coast are highly correlated for the SON season with ($r = -0.71$ at a model grid point nearest to the core location).

The reconstructions of Abram et al. (2009) show periods of a more positive IOD-like mean state e.g. during the mid-Holocene and periods of a more negative IOD-like mean state e.g. during the late Holocene and are partly anti-correlated to our ΔT record (Fig. 5b, c). This might be attributed to the different sample resolutions used in both studies: the reconstructions using corals allow the detection of single IOD events while our sedimentary record only allows the detection of long-term variability in the IOD-like mean states due to the general lower resolution of sedimentary archives. Considering that SST estimates derived from *G. ruber* are used to calculate ΔT, reconstructed upwelling intensity based on ΔT tends to be overestimated. *G. ruber* as a warm water species does not favor upwelling conditions and therefore might record annual mean temperatures with a stronger emphasis on non-upwelling seasons.

At present, another characteristic feature of the IOD is the contrasting rainfall pattern over the eastern and the western Indian Ocean. Sea surface salinity reconstructions shift from fresher to saltier conditions around ~3 ka as deduced from $\delta^{18}O_{sw}$ reconstructions (Fig. 5a, Mohtadi et al., 2014).

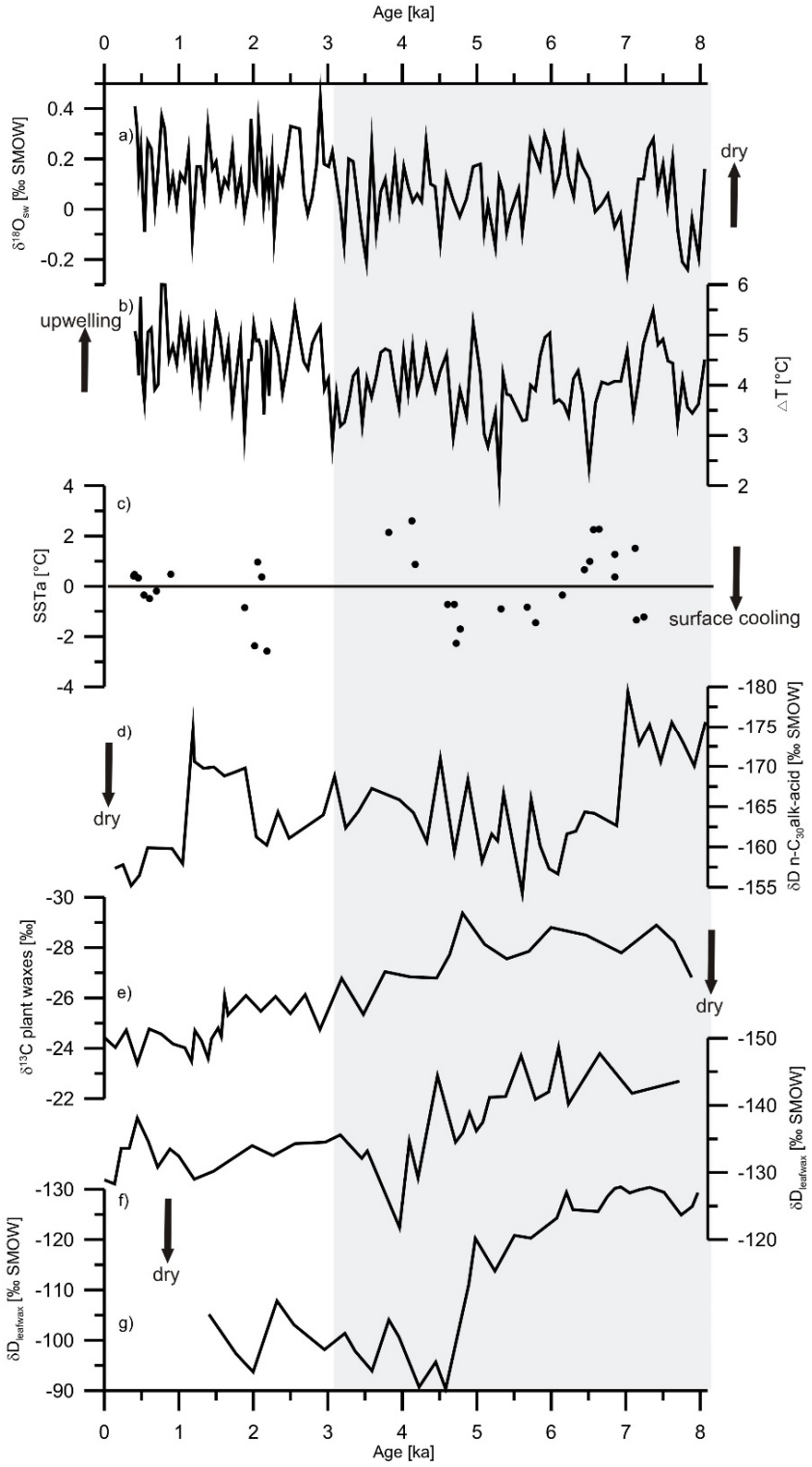

Figure 6.5: Comparison of a) $\delta^{18}O_{sw}$ indicating variations in sea surface salinity (Mohtadi et al., 2014), **b**) ΔT derived from SST estimates – TT estimates indicating the mixed layer thickness, **c**) coraline SST anomaly reconstructions (Abram et al., 2009), d) δD from SO189-144KL indicating rainfall variations off W Sumatra (Niedermeyer et al., 2014),, **e**) $\delta^{13}C$ from plant waxes from India indicating an aridification in India during the Holocene (Ponton et al., 2012), **f**) δD from leaf waxes from marine record P178-15P from the Gulf of Aden (Tierney and deMenocal, 2013) indicating an aridification in East Africa during the Holocene supported by **g**) δD from leaf waxes from Lake Tanganyika (Tierney et al., 2008). The grey box indicates a period of a more negative IOD-like mean state in the Indian Ocean.

However, the observed variations in $\delta^{18}O_{sw}$ are only minor and might not be a reliable indicator for precipitation changes during the Holocene. Rainfall reconstruction of western Sumatra based on δD of plant waxes show two distinct periods of enhanced precipitation and a supposably more negative IOD-like mean state between 6.5 to 8 ka and between 1 to 2 ka (Fig. 5d, Niedermeyer et al., 2014). This is partly in contrast to our reconstruction as well as to the reconstructions of Abram et al. (2009). Niedermeyer et al. (2014) suggest that the mid-Holocene decrease in precipitation off western Sumatra coeval with a decrease in East African rainfall and a warm SST anomaly off Sumatra (Abram et al., 2009) might be a result of a non-linear relationship between the eastern Indian Ocean SST and western Indian Ocean rainfall pattern. Alternatively, they argue that the core site of SO189-144KL might not be located within the center of precipitation changes during that time. Additional precipitation data from western Sumatra is necessary in order to better evaluate the IOD induced rainfall changes in the eastern Indian Ocean.

Tierney et al. (2013) reconstructs variations in precipitation over the western Indian Ocean on decadal timescales. Compared to Makassar Strait SST, this gives evidence that East African rainfall might be controlled by the Walker circulation over the Indian Ocean. Tierney et al. (2008) analyzed the δD of leaf waxes from Lake Tanganyika, which indicates a mayor shift to dry conditions around 4.7 ka (Fig. 5g) consistent with lake level reconstructions from Lake Turkana showing a water-level drop of ~50 m around 5.3 ka (Garcin et al., 2012). This is supported by the study of Tierney and deMenocal (2013) using δD of leaf waxes from a marine record in the Gulf of Aden (Fig. 5f). Comparison with other hydroclimate reconstructions shows a coherent picture of the development of the African Humid Period over northeast Africa, and suggests that the hydroclimate is mainly controlled by the African monsoonal system (Tierney and deMenocal, 2013). In comparison to our proxy data no correlation of climatic shifts can be identified and therefore we assume that the long-term IOD-like mean state signal is too weak in the western Indian Ocean. The IOD signal might be masked by the strong monsoon signal in the Holocene climate records from East Africa and the western Indian Ocean (de Boer et al., 2014) which further complicates a straightforward comparison of the eastern and the western Indian Ocean climate archives. This assumption is further supported by coherent changes in reconstructed Holocene SST anomalies off Tanzania (Kuhnert et al., 2014) and rainfall anomalies in Flores, Indonesia (Griffiths et al., 2009), with

positive SST anomalies off East Africa corresponding to positive rainfall anomalies over South Indonesia and vice versa. Kuhnert et al. (2014) therefore suggest that mid-Holocene climate was anomalous on a global scale and hypothesize that the unusual temperature pattern in the Indian Ocean reflects remote forcing rather than one of the climate modes internal to the Indian Ocean. Proxy-based reconstructions, including this study, might also incorporate other seasons and years which would hamper a direct comparison additionally.

Swapna and Krishnan (2008) suggest a strong pressure gradient along the equator producing an eastward equatorial undercurrent that leads to upwelling of cold subsurface waters in the eastern Indian Ocean during times of strong summer monsoon. During a weak summer monsoon, this pressure gradient is too weak to create an equatorial undercurrent and the resulting upward movement of subsurface waters in the eastern Indian Ocean (Swapna and Krishnan, 2008). This IOD-monsoon coupling has also been suggested for the past, with longer and stronger positive IOD events during the monsoon-dominated mid-Holocene (Abram et al., 2007). However, more positive IOD events during the last decades (Abram et al., 2008; Ihara et al., 2008; Cai et al., 2009) are associated with a weakening of the Indian summer monsoon (Naidu et al., 2009; Cai et al., 2013). Thus, observations suggest that both the sign and the phase of the IOD-monsoon relationship can change over decades, and it is likely that such changes also occurred in the past. Li et al. (2003) suggest a negative feedback mechanism between the Indian summer monsoon and the IOD leading to a contemporaneous decrease in precipitation over India and Indonesia. A positive IOD might strengthen the Indian monsoon whereas a strengthened Indian monsoon might weaken the IOD (Li et al., 2003). This relationship is also evident from our reconstruction when a positive IOD-like mean state during the late Holocene corresponds to a period of weaker Asian summer monsoon (Wang et al., 2005; Fleitmann et al., 2007; Mohtadi et al., 2011b), whereas a more negative IOD-like mean state during the mid-Holocene is accompanied by a stronger Asian summer monsoon (Wang et al., 2005; Fleitmann et al., 2007; Mohtadi et al., 2011b). Spectral analyses of our records from the eastern tropical Indian Ocean indicate an influence of solar activity with cycles of 2,500, 1,000 and, 150 years (Debret et al., 2007, Abreu et al., 2012) together with a 1.5 kyr cyclicity that might reflect the Bond cycles in the North Atlantic (Bond et al., 2001). It is suggested by previous studies that solar activity has a significant influence on monsoonal precipitation indicated by cycles centered at ~150 years (Fleitmann et al.,

2003; Wang et al., 2005). However, due to the relatively low temporal resolution of our records interpretations on a monsoon-IOD relationship on these frequencies would be speculative. Abram et al. (2007) propose a close relationship between the monsoonal system and the IOD because the monsoonal wind reversal at the onset of the Northwest monsoon terminates IOD events. However, IOD events also have a prominent influence on the moisture transport by monsoonal surface winds into areas surrounding the Indian Ocean. During the positive IOD event in 1994, when a positive IOD and an El Niño event co-occurred (Ding and Li, 2012), an enhanced convection over India resulted in heavy precipitation over Northern India, the Bay of Bengal, Indochina and Southern China (Behera et al., 1999; Guan and Yamagata, 2003). Large anomalies in Indian summer monsoon rainfall can be related to an additive influence of ENSO and the equatorial Indian Ocean Oscillation, the atmospheric component of the IOD (Gadgil et al., 2004) or strong IOD events (Deshpande et al. 2014). While during El Niño events an anomalous divergence over India cause anomalous subsidence and weakens the Indian summer monsoon rainfall, positive IOD-induced wind anomalies weaken the influence of ENSO and persuade a convergence over the Indian monsoon region (Ashok et al., 2004). Ponton et al. (2012) reconstructed the Holocene monsoon variability by using carbon isotopes of sedimentary leaf waxes in a marine record in the Bay of Bengal off the Godavari River. This record reflects a gradual increase in aridity-adapted flora indicating a decrease in precipitation during the Holocene (Fig. 5e). Climatic conditions in India became drier during the late Holocene whereas our ΔT reflects a more positive IOD-like mean state (Fig. 5b). The orbitally-forced weakening of the monsoon during the Holocene might have led to a shift to a more positive IOD-like mean state of the Indian Ocean, amplified by more frequent and intensive El Niño events (Li et al., 2003).

6.6. Summary

We present a continuous multi-proxy based reconstruction of the Holocene hydrography in the tropical eastern Indian Ocean, an area sensitive to IOD variability. Depth of thermocline and thermocline temperature reconstructions show a gradual decrease towards the late Holocene that might represent a shift to a more positive IOD-like mean state. Results from an orbital-forced climate model support our interpretation of long-term variations of the IOD-like mean state in the Indian Ocean. The gradual shift from a more negative IOD-like mean state to a more positive IOD-like mean state coincides with a shift

from a westerly-dominated wind regime to an easterly-dominated wind regime during the IOD season. Additional temperature and rainfall records from both sides of the tropical Indian Ocean realm less affected by the monsoon system are essential in order to better assess sign and spatial extent of climate change and their relationship to the IOD.

Acknowledgements

We acknowledge Silvana Pape, Monika Segl and, Birgit Meyer-Schack for technical assistance. CCSM3 simulations were performed on the SGI Altix supercomputer of the Norddeutscher Verbund für Hoch- und Höchstleistungsrechnen (HLRN). We are grateful to Jeroen Groeneveld, Andreas Lückge and Markus Kienast for helpful discussions. This study greatly benefited from three constructive reviews. This work was funded by the BMBF projects SUMATRA (03G0189A), CAFINDO (03F0645A) as part of the SPICE III cluster, and supported by the DFG-Research Center / Cluster of Excellence „The Ocean in the Earth System“.

7. Late Holocene intensification of the Australian-Indonesian summer monsoon and ENSO recorded off the Mahakam Delta, Makassar Strait

Cornelia Kwiatkowski[1], Mahyar Mohtadi[1], Ann Holbourn[2], Wolfgang Kuhnt[2], Dierk Hebbeln[1]

[1]MARUM – Center for Marine Environmental Sciences, University of Bremen, Bremen, Germany (ckwiatkowski@marum.de)

[2]Institute of Geosciences, Christian-Albrechts-University, Kiel, Germany

Abstract

The complex climate system of the Maritime Continent is characterized by interacting phenomena such as El Niño-Southern Oscillation (ENSO) and the Australian-Indonesian monsoon system. Model simulations struggle with these interactions and thus reveal an inconsistent picture of the monsoon-ENSO relationship. High resolution proxy records from the Maritime Continent are essential to validate these climate models and to contribute to reliable future climate predictions in times of a changing global climate. In order to disentangle their different influences on late Holocene climate in central Indonesia, we integrated multi-proxy data from sediment core SO 217-18517 collected off the Mahakam Delta and assessed changes in precipitation over central Borneo and variations in sea surface conditions in the Makassar Strait over the past 5 kyr. Using Mg/Ca in the planktic foraminifera *G. ruber* s.s. combined with stable isotopes, we reconstructed sea surface temperatures (SST) and seawater $\delta^{18}O$ ($\delta^{18}O_{sw}$). Sedimentation rates, Zr/Rb and foraminiferal Ba/Ca allow clues about changes in precipitation-related runoff.

Our proxy records suggest cooler and fresher sea surface waters in the Makassar Strait during the past ~2.7 kyr contemporaneous with sedimentation of finer sediment and the occurrence of fresh water pulses. Changes in SST, $\delta^{18}O_{sw}$ and terrigenous runoff follow the insolation gradient between 30°N and 20°S and imply stronger cross equatorial winds and hence, an intensified Australian-Indonesian summer monsoon. In addition to a late Holocene intensification of monsoonal rainfall during austral summer, precipitation over eastern Borneo was affected by an intensified ENSO activity. Periods of distinct freshwater pulses are interpreted to reflect ENSO conditions over the Pacific Ocean with intensified El Niño and La Niña.

Key words: Makassar Strait, Planktic foraminifera, sea surface $\delta^{18}O$, Mg/Ca, El Niño-Southern Oscillation, Australian-Indonesian monsoon, Holocene

7.1. Introduction

The Maritime Continent serves as a key location for climate research because its location between the Pacific and the Indian Oceans and between the Australian and Asian continents within the Indo Pacific Warm Pool (IPWP) results in a very complex climatic system, influenced by various large-scale climate phenomena. The Inter Tropical Convergence Zone (ITCZ) and the Australian-Indonesian monsoon system control the temporal and spatial distribution of rainfall. Additionally, Indonesia is located under the rising branches of the Indian and Pacific Walker circulation, which respond differently to global climate changes (DiNezio et al., 2011). Perturbations of the annual rainfall cycle by climate modes such as the Indian Ocean Dipole (IOD, Saji et al., 1999; Webster et al., 1999) or ENSO (Rasmusson and Carpenter, 1982) further complicate interpretations of past regional climate dynamics of the Maritime Continent.

The Makassar Strait between the islands Borneo and Sulawesi is the main pathway of water flowing from the Pacific into the Indian Ocean (Gordon and Fine, 1996). About 80% of the total Indonesian Throughflow (ITF) flows through the Makassar Strait (Gordon, 2005). Variations of the present-day and past ITF seem to be directly forced by changes in the main controlling climate phenomena such as ENSO and the Australian-Indonesian monsoon system. The monsoonal surface winds result in an intensified southward flow during austral winter (e.g. Gordon et al., 2003; Susanto et al., 2012) and a weakening of the ITF transport during El Niño events (e.g. Gordon et al., 2012; Susanto et al., 2012; Hu and Sprintall, 2016). By changes in SST which influences precipitation pattern over parts of the Maritime Continent (Aldrian and Susanto, 2003), these climate phenomena exert a strong control on sea surface conditions and over-land precipitation. Therefore, sedimentary archives from the Makassar Strait in the heart of the IPWP have the potential to record past local climate variability as well as remote climatic signals transported by atmospheric and ocean pathways to the Maritime Continent.

During El Niño years, cooler SST and westerly winds in the western Pacific region and an associated eastward shift of the convection cell, which is usually located over the Maritime continent, results in a decrease in rainfall over Indonesia (Rasmusson and Carpenter, 1982; Philander, 1983). During La Niña years, warm SST and strong eastward winds in the western Pacific region lead to a strong convection cell over the Maritime Continent with intensified precipitation (Philander, 1985). The ITCZ is shifted southward during El Niño years while it is

shifted northward during La Niña years (Philander, 1983, 1985; Schneider et al., 2014). Although only a few marine sedimentary records resolve the ENSO frequency, climatic shifts of the mean state in the Pacific Ocean are related to ENSO and interpreted either as an El Niño-like or La Niña-like state.

Previous paleo-environmental reconstructions from the eastern Pacific indicate intensified and more frequent El Niño during the late Holocene relative to the mid-Holocene (Moy et al., 2002; Conroy et al., 2008; Koutavas and Joanides, 2012). A general weakening of the Pacific Walker Circulation in response to El Niño is assumed to have caused a drying trend observed in northern Borneo speleothem records (Partin et al., 2007) and a cooling in Makassar Strait SST coincident with a reduced ITF flow velocity (Linsley et al., 2010). A reduced heat transport from the Pacific to the Indian Ocean has been inferred to reflect more frequent El Niño (e.g. 2 to 0.8 ka), whereas an enhanced heat transport has been related to more La Niña-like conditions (e.g. 0.8 to 0.3 ka, Newton et al., 2011).

A shift to more El Niño-like conditions should imply prolonged dry seasons and a decrease in monsoonal rainfall the Maritime Continent. Indeed, monsoon reconstructions based on $\delta^{18}O$ of speleothems from northwestern Australia indicate a decrease in pre-monsoonal rainfall in response to the El Niño-like state of the Pacific Ocean culminating in dry conditions around ~2 ka (Denniston et al., 2013). This is supported by a shift in vegetation owing to prolonged dry seasons recorded in Sumba around ~2 ka (Dubois et al., 2014). However, most reconstructions from the Maritime continent imply an increase in Australian-Indonesian summer monsoon (AISM) precipitation during the late Holocene. Such evidence is provided by speleothem $\delta^{18}O$ data from Flores (Griffiths et al., 2009; 2010) and by elemental compositions of Timor Sea sediments (Kuhnt et al. (2015). The latter authors interpreted an increase in AISM rainfall being a result of a southward shift of the austral summer ITCZ. In contrast, runoff proxies from the eastern Indian Ocean suggest that the increase in AISM precipitation during the late Holocene is forced by a northward shift of the austral summer ITCZ (Mohtadi et al., 2011) or by the orbital configuration and solar activity (Steinke et al., 2014). Other authors suggest that the response of land masses to changes in insolation seasonality is size-related and causes the inconsistent development of precipitation over Indonesia (Tierney et al., 2012).

So far the available proxy reconstructions of the late Holocene precipitation history over the Maritime Continent and its forcing factors are in part contradictory. By

providing data from a new site from the Makassar Strait, we explore variations in Makassar Strait sea surface conditions and terrigenous runoff from eastern Borneo during the past 5 kyr. These data allow to disentangle the different forcing factors and to highlight the overwhelming impact of an intensified AISM punctuated by an intensified ENSO on precipitation over eastern Borneo during the late Holocene.

7.2. Study Area

Precipitation over the catchment area of the Mahakam River that drains central Borneo indicates a year-round humid climate with minor seasonal variations (Fig. 1). Despite receiving rainfall all over the year, the seasonal distribution is influenced by the Australian-Indonesian monsoon system and ENSO (Aldrian and Susanto, 2003). It is slightly drier during May to September (Australian-Indonesian winter monsoon (AIWM)) and generally wetter during November to March (AISM). The ITCZ passes the study area twice a year resulting in enhanced rainfall in April and peak rainfall in October (Fig. 1, Aldrian and Susanto, 2003). The comparison of monthly precipitation anomalies between 1960 and 2011 to the Southern Oscillation Index, which represents the atmospheric component of ENSO, indicates that 23% of the rainfall variations are associated with ENSO (Fig.1).

Seasonal variations in surface waters off the Mahakam Delta are relatively small (Fig. 1). Sea surface is cooler during austral summer and winter and slightly warmer during austral spring and fall describing seasonal variations of ~1°C throughout the year (HadISST, Rayner et al., 2003). The comparison of monthly SST anomalies off the Mahakam Delta between 1960 and 2011 to the Nino 3.4 Index, which describes oceanic ENSO variations based on equatorial Pacific SST anomalies, indicates no correlation ($r = 0.02$, Fig. 1). Sea surface salinity (SSS) in the Makassar Strait and Java Sea is ~33 psu during austral fall, ~34 psu during the AIWM (Fig. 2) and ~33.5 during austral spring (World Ocean Atlas 2013). During austral summer and fall precipitation over Borneo results in fresher surface water around southeast Borneo. From there monsoonal surface winds carry this low-salinity surface water into the Makassar Strait, where it causes a lower surface salinity of ~32.5 psu off the Mahakam Delta (Fig. 2, World Ocean Atlas 2013). Therefore, salinity variations off the Mahakam Delta are influenced by low salinity water from the Java Sea entering the Makassar Strait from the South during the AISM season but also by changes in local precipitation due to seasonal migration of the ITCZ.

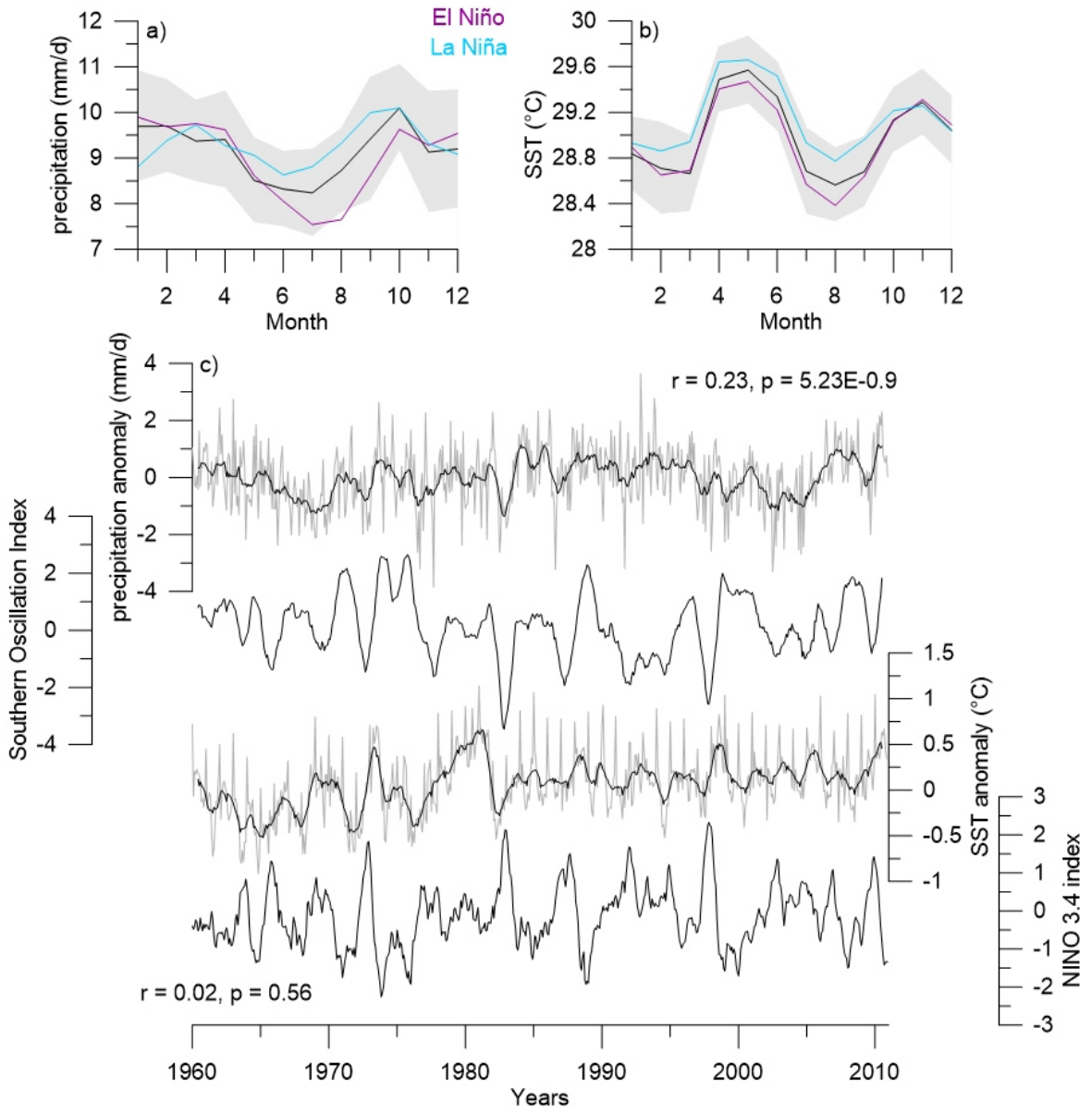

Figure 7.1: a) NCEP Reanalysis data provided by the NOAA/OAR/ESRL PSD, Boulder, Colorado, USA, indicate seasonal variations in precipitation over the Mahakam catchment area during normal years (black), El Niño years (purple) and La Niña years (blue, Kalnay et al., 1996). The gray shading indicates the standard deviation of variations in rainfall during normal years since 1960. **b)** HadISST data provided by the Met Office Hadley Centre indicate seasonal variations in SST at the core site during normal years (black), El Niño years (purple) and La Niña years (blue, Rayner et al., 2003). The gray shading indicates the standard deviation of SST variations during normal years since 1960. The definition of El Niño, La Niña and normal years is based on Ding and Li (2012) and Sprintall and Révelard (2014). **c)** Time series of precipitation anomaly (gray, Kalnay et al., 1996) and SST anomaly (gray, Rayner et al., 2003) with a 11-point running average (black) in comparison to the atmospheric SOI (11 point running average) and the oceanographic NINO3.4 index (11-point running average, http://www.cpc.ncep.noaa.gov/data/indices/). The top (bottom) r and p value describes the correlation between the Southern Oscillation Index (NINO3.4 index) and the precipitation anomalies (SST anomalies) in monthly resolution calculated by using Pearson

Variations in the ITF which transports relatively cool and fresh water in the thermocline (Gordon, 2005) but warm and saline water at the surface from the Pacific

to the Indian Ocean, additionally affect surface water conditions in the Makassar Strait.

The main transport in the Makassar Strait occurs in the upper 200 m with the highest southward velocities between 70 and 120 m water depth (Du and Qu, 2010). The relatively warm surface water (0–20 m) flows southward during austral fall, winter and spring but slightly northward during austral summer (Du and Qu, 2010). The deep ITF (> 400 m) flows southward with relatively low current velocities and periodically northward below 600 m (Gordon et al., 2003; Gordon et al., 2008; Shinoda et al., 2012). Low salinity Java Sea water carried by eastward zonal winds during the AISM acts as a 'freshwater plug' inhibiting the southward flow of Makassar Strait surface waters leading to a main ITF transport in cooler and deeper layers (Gordon et al., 2003). During austral winter, westward winds of the AIWM carry more saline surface waters from the Flores and Banda Sea towards the Java Sea enabling maximum southward surface flow in the Makassar Strait (Gordon et al., 2003; Susanto et al., 2012).

7.3. Material & Methods

Piston core SO 217-18517 (1°32.199' S 117°33.756' E, 699 m water depth, Fig. 2) was recovered off the Mahakam Delta during *R/V Sonne*-217 MAJA expedition in 2011 (Kuhnt et al., 2011; Fig. 2). The uppermost 400 cm of the sedimentary record consist of undisturbed, foraminifera bearing silty clay with manganese streakings within the upper 50 cm. The uppermost few centimeters of sediment were lost during coring. The record was sampled in 1-2 cm intervals providing a sample resolution of ~20 yr.

7.3.1. Age model

The age model of SO 217-18517 is based on 11 accelerator mass spectrometry (AMS) ^{14}C dates that were performed on mixed samples of the planktonic foraminifera species *Globigerinoides ruber and Globigerinoides sacculifer* (without the final sac-like chamber) at the Keck Carbon Cycle Accelerator Mass Spectrometry Facility at the University of California in Irvine, USA (Table 1). All ages were corrected for ^{13}C, and ^{14}C ages were converted to calendar years using the MARINE13 calibration curve (Reimer et al., 2013) without any local offset (Southon et al., 2002). The age-depth relation was determined by using Bayesian age modelling with the Bacon.R 2.2 software and the default settings developed by Blaauw and Christen (2011). Sedimentation rates were calculated based on the Bayesian age model.

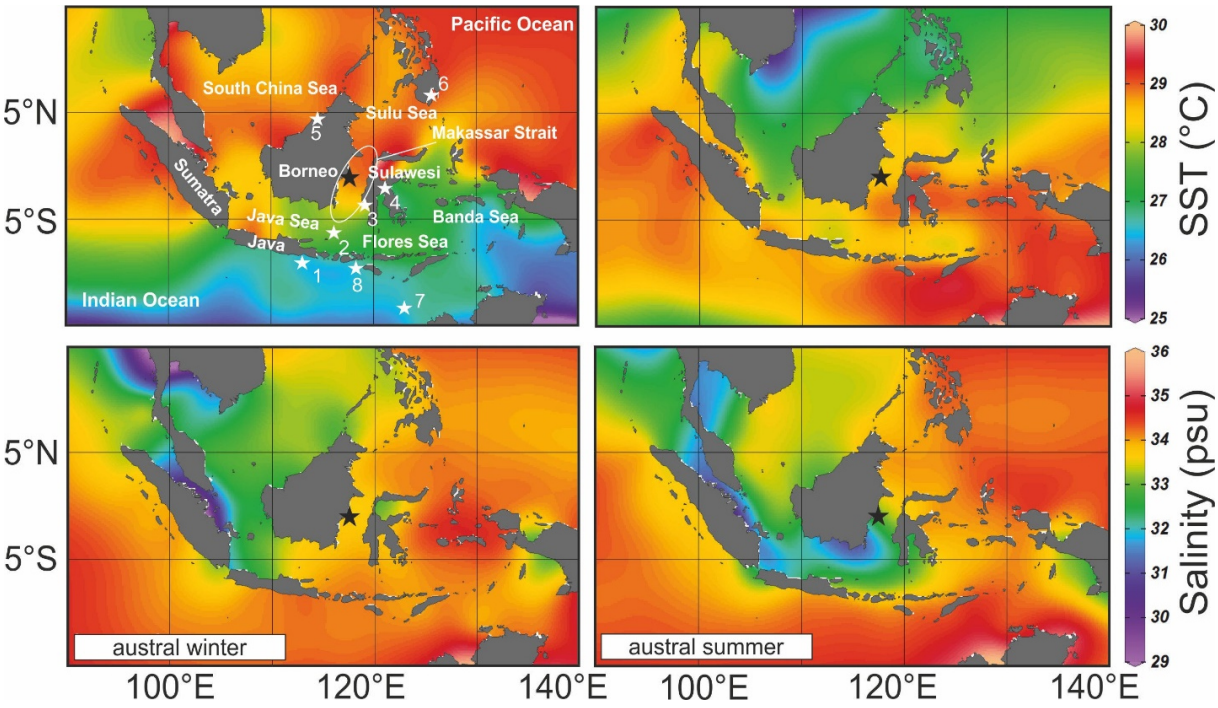

Figure 7.2: Sea surface temperature (top row) and sea surface salinity (bottom row) in Indonesia during austral winter (left) and austral summer (right). The black star indicates the core site of SO 217-18517 while the other study sites discussed here are numbered as follows: 1. Mohtadi et al. (2011), 2. Linsley et al. (2010), 3. Tierney et al. (2012), 4. Russell et al. (2014), 5. Partin et al. (2007), 6. Stott et al. (2004), 7. Kuhnt et al. (2015), and 8. Steinke et al. (2014). The maps were created by using Ocean Data View with the data of World Ocean Atlas 2013.

7.3.2. Planktic foraminiferal stable isotope and trace element analyses

Planktic foraminifera *Globigerinoides ruber* sensu stricto (*G. ruber* s.s.) were picked from the size fraction 250-355 µm. About 50 individuals were crushed and split for stable isotope and trace element analyses. The continuous occurrence of pteropod fragments allows the exclusion of dissolution effects on foraminiferal Mg/Ca.

For foraminiferal Ba/Ca and Mg/Ca analyses, crushed tests were cleaned following the protocol outlined in Barker et al. (2003) including a clay-removal using ultra-pure water and Methanol and an oxidative step using 1% NaOH-buffered H_2O_2 to eliminate additional Mg trapped in organic matter. A reductive cleaning step was applied by using hydrazine solution according to Martin and Lea (2002) in order to preclude an alternation of temperature estimates by Mg-containing authigenic phases. After the weak acid leach with 0.001M NHO_3 the samples were dissolved and centrifuged for 10 min. at 6,000 rpm. The solutions were diluted to the final volume and measured with Inductively Coupled Plasma Optical Emission Spectrometry (Agilent Technologies 700 Series ICP-OES with a Cetac ASX-520

autosampler) at the MARUM, University of Bremen. The Mg/Ca values are reported as mmol mol^{-1}. The instrumental precision of the measurements was monitored by using an external standard solution (Mg/Ca = 2.89 mmol mol^{-1}) measured after every fifth sample as well as the ECRM 752-1 standard measured after every 50 sample, with a standard deviation of 0.002 mmol mol^{-1} (0.056%) for the external standard and 0.002 mmol mol^{-1} (0.061%) for the ECRM 752-1 standard, respectively. The reproducibility of the samples was 2.31% (n = 11) corresponding to a standard deviation of 0.11 mmol mol^{-1}. Aluminum as an indicator for a contamination by silicate minerals (Barker et al., 2003) is below detection limit. The influence of additional Mg of post-depositional Mn-rich oxyhydroxides coatings altering the foraminiferal Mg/Ca could be excluded by evaluating Fe/Ca and Mn/Ca ratios in relation to Mg/Ca ratios. No relationship between Mn/Ca and Mg/Ca ratios (r^2 = 0.2) and Fe/Ca and Mg/Ca ratios (r^2 = 0.1) could be observed.

Mg/Ca ratios were converted into temperatures (T) using the all species equation proposed by Anand et al. (2003):

$$Mg/Ca = 0.38 \exp(0.09T).$$

The error of the temperature reconstructions based on *G. ruber* s.s. Mg/Ca is estimated by propagating the errors introduced by the Mg/Ca measurements and Mg/Ca-temperature calibration (see Mohtadi et al., 2014 for details). The resulting error is on average 1.13 °C. Foraminiferal Ba/Ca values are reported as μmol mol^{-1}. Due to high methodologic uncertainties only periods of very high Ba/Ca are interpreted.

Foraminiferal $\delta^{18}O$ was measured with a Finnigan MAT 251 mass spectrometer at the Isotope Laboratory of MARUM, University of Bremen. The isotopic composition of foraminiferal calcium carbonate was analyzed on CO_2 emerged by treatment with phosphoric acid. The internal standard (Solnhofen limestone) was calibrated against Pee Dee Belemnite (PDB) by using the NBS 19 standard. Consequently, all isotopic data reported here are relative to the PDB standard. The stable isotope analyses have a long-term standard deviation of 0.07‰ (Isotope Laboratory at Faculty of Geosciences, University of Bremen). Sample reproducibility is 5.61% (0.18‰) for $\delta^{18}O$ (n=15).

Changes in SSS were determined by using $\delta^{18}O_{sw}$ with more negative values indicative for a sea surface freshening. Based on foraminiferal Mg/Ca derived SST and foraminiferal $\delta^{18}O$ we calculated the $\delta^{18}O_{sw}$ values by using the low light equation proposed by Bemis et al. (1998):

$$T(°C) = 16.5\text{-}4.80*(\delta_c - \delta_w)$$

with δ_c and δ_w standing for $\delta^{18}O$ of foraminiferal carbonate and sea water,

respectively. Values were converted relative to Standard Mean Ocean Water (SMOW) by adding 0.27‰ to δ_c (Bemis et al., 1998). The error of the $\delta^{18}O_{sw}$ reconstructions is estimated by propagating the errors introduced by the SST, the error of SST, the $\delta^{18}O$ measurements, and $\delta^{18}O_{sw}$ calibration (see Mohtadi et al., 2014 for details). The resulting error is on average 0.25‰ SMOW.

7.3.3. X-Ray Fluorescence analyses

The elemental composition of the sedimentary record was measured in 1cm intervals by using the AVAATECH XRF core scanners at the Institute for Geosciences at Kiel University. The methodological approach is published in Kuhnt et al. (2015). Results are reported in natural logarithms of elemental ratios, which provide signals of relative changes in chemical composition downcore and minimize the risk of measurement artefacts from variable signal intensities and matrix effects (Weltje and Tjallingii, 2008). Variations in lnZr/Rb are interpreted as a grain size indicator since Zr resides in coarser Zircon grains and Rb mainly in clays (Croudace and Rothwell, 2015). Therefore, higher Zr/Rb ratios indicate a coarser mean grain size while lower Zr/Rb indicate finer sediments (Dypvik and Harris, 2001; Kylander et al., 2011).

7.4. Results

7.4.1. Age model

The age model of core SO 217-18517 shows a continuous sedimentary sequence from 5 to 0.5 ka (Fig, 3, Table 1). Lower sedimentation rates of ~60 cm kyr^{-1} can be observed during the mid-Holocene between 4 and 3.5 ka (Fig. 3).

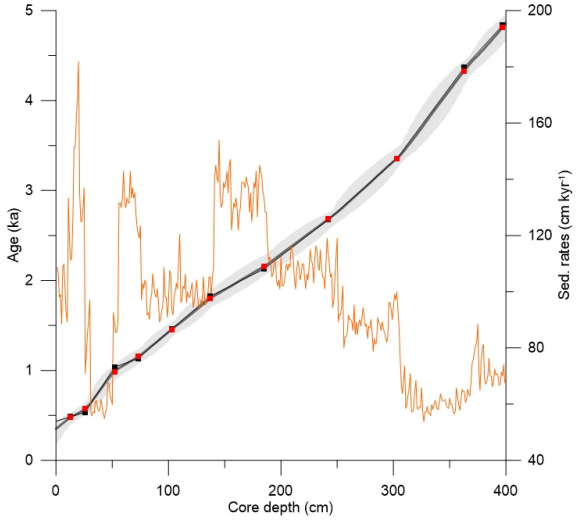

Figure 7.3: Bayesian age model (bold with red dots) compared to the linear age model (thin with black dots) of piston core SO 217-18517 with the 2σ age range (gray). The sedimentation rates are based on the Bayesian age model (orange).

Thereafter sedimentation rates increased towards two distinct periods of high sedimentation rates of ~125 cm kyr^{-1} around 2 ka and 1 ka. Between 1 and 0.5 ka, sedimentation rates decrease again (60 cm kyr^{-1}). Sedimentation rates show a short period of peak sedimentation rates around 0.5 ka (175 cm kyr^{-1}). The linear age model and the Bayesian age model do not show distinct offsets (Fig. 3).

Tabele 7.1: AMS-^{14}C ages on *G. ruber* and *G. sacculifer* and cal. ages of sedimentary record SO 217-18517

Lab. code	Sample depth (cm)	^{14}C age (ka)	cal. median age (ka)	2σ range of cal. age (ka)
133826	13	0.855 ± 0.020	0.478	0.4 – 0.52
123470	26	0.940 ± 0.020	0.578	0.51 – 0.64
133827	52	1.490 ± 0.025	0.983	0.89 – 1.06
123471	73	1.570 ± 0.020	1.153	1.07 – 1.24
133828	103	1.915 ± 0.020	1.456	1.37 – 1.54
133829	137	2.220 ± 0.025	1.796	1.69 – 1.89
123473	185	2.475 ± 0.025	2.157	2.05 – 2.28
123474	242	2.875 ± 0.020	2.681	2.56 – 2.75
133830	303	3.470 ± 0.020	3.354	3.24 – 3.48
123396	363	4.255 ± 0.020	4.329	4.17 – 4.44
123476	397	4.620 ± 0.025	4.810	4.63 – 4.92

7.4.2. Mg/Ca thermometry, foraminiferal Ba/Ca, sea surface and $\delta^{18}O_{sw}$

Foraminiferal Mg/Ca varies between 4.18 and 5.18 mmol/mol equivalent to a temperature range of 26.6 to 29 °C (Fig. 4). Higher Mg/Ca (~4.9 mmol mol^{-1}) between 4.5 and 3 ka results in higher SST of ~28.5 °C. Thereafter, Mg/Ca decreases to ~4.4 mmol mol^{-1} in the period from 2 to 1.5 ka, which is equivalent to SST of ~27.4 °C. Between 1.5 and 1 ka, Mg/Ca (~4.6 mmol mol^{-1}) points to a period of warmer temperatures of ~28°C between 1.5 and 1 ka and decreases thereafter again to 4.4 mmol mol^{-1} (27.4 °C). Foraminiferal Ba/Ca indicates no general trend over the past 5 kyr with values around ~1 µmol mol^{-1} (Fig. 4) but they show two distinct periods of high values from 2.3 to 1.8 ka and 1.2 to 0.5 ka.

The $\delta^{18}O$ data vary between -3.44‰ and -2.71‰ PDB without showing any long-term trends during the past 5 kyr (Fig. 3). The calculated $\delta^{18}O_{sw}$ values range between -0.77‰ and -0.02‰ SMOW showing more positive values of -0.3‰ SMOW between 4.5 and 3 ka. Thereafter, the $\delta^{18}O_{sw}$ values decrease to -0.6‰ SMOW between 2 and 1.8 ka. Since 1.8 ka, $\delta^{18}O_{sw}$ values vary around -0.4‰ SMOW.

7.4.3. Zircon/Rubidium as a grain size indicator

Logarithmic Zr/Rb decreases from high values of ~0.32 during the mid-Holocene to relatively low values of ~0.22 during the period between 2.2 to 1.6 ka. During the period from 1.6 to 0.4 ka the lnZr/Rb is slightly elevated to values varying around ~0.24 (Fig. 4).

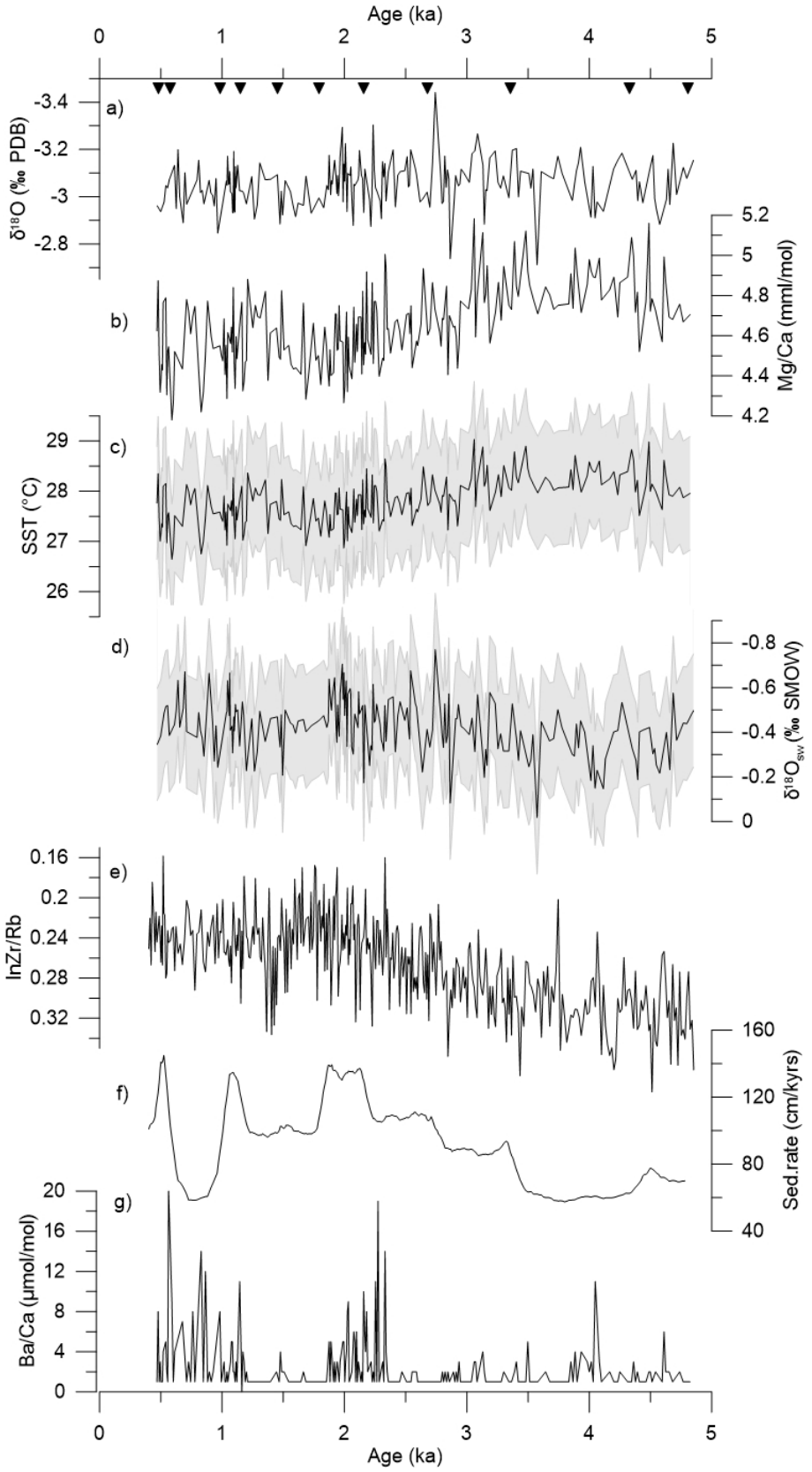

Figure 7.4: Results from sediment core SO 217-18517 from the Makassar Strait. a) Foraminiferal $\delta^{18}O$ measured on *G. ruber*, b) foraminiferal Mg/Ca measured on *G. ruber*, c) Mg/Ca-based SST estimates, d) $\delta^{18}O_{sw}$ estimates, e) Zr/Rb, f) sedimentation rates, and g) foraminiferal Ba/Ca measured on *G. ruber*. AMS ^{14}C dates are indicated by black triangles. The proxy error calculated as proposed by Mohtadi et al. (2014). Iterations were calculated by using a Monte Carlo Simulation in R and afterwards combined with the age model simulations giving the gray shading.

7.5. Discussion

Variations in rainfall in central Indonesia

Two widely used parameters to assess the terrigenous input are variations in sedimentation rates and in sediment grain size (e.g. Nizou et al., 2011). The obvious fining trend in the sediments off the Mahakam Delta as demonstrated by decreasing lnZr/Rb for the last ~3.5 kyr is largely accompanied by an increase in sedimentation rates (Fig. 3) and thus, an enhanced riverine input appears as the most likely interpretation. Delta dynamics in response to late Holocene variations in local sea level might be negligible to affect sediment composition in 700 m water depth. Moreover, the tidal and distributary channel system of the Mahakam River was very stable during the late Holocene (Storms et al., 2005).Enhanced riverine runoff, as interpreted from the fining of the sediment and the increase in sedimentation rates is further corroborated by foraminiferal Ba/Ca. As a proxy for fresh water input (Lea and Boyle, 1991), this ratio indicates two periods characterized by enhanced runoff of the Mahakam River from 2.3 to 1.8 ka and 1.2 to 0.5 ka. The runoff proxies are in agreement prior to 1 ka, however diverge between 1 and 0.5 ka indicating high Ba/Ca and lnZr/Rb but low sedimentation rates. This might be due to the short distance between the radiocarbon age determinations. Moving the two dating points prior and after the low sedimentation rate period within the 1σ error range would result in average sedimentation rates of 80-100 cm kyr^{-1} for the last 1.2 kyr, similar to the preceding period (Fig. 3). Thus, the grain size data and the sedimentation rates are interpreted to reflect an increasing terrigenous input since ~3.5 ka, with some shorter events characterized by high Ba/Ca indicating an even higher terrigenous input.

Today, southeastern Borneo is located within the global monsoon domain (Mohtadi et al., 2016). Additionally, El Niño influences precipitation pattern over eastern Borneo (Aldrian and Susanto, 2003) leading to a decrease in austral winter precipitation during El Niño years and an increase in rainfall during La Niña (Fig. 1). ENSO exerts a strong influence on the amplitude of the Australian monsoon, although it is not controlling rainfall over the Indonesian islands in peak AISM season (Hendon, 2003; Jourdain et al., 2013; Moron et al., 2015). Northern Borneo resides outside the global monsoon domain (Mohtadi et al., 2016) being mainly controlled by shifts in the mean position of the ITCZ or the ENSO state of the Pacific Ocean (Partin et al., 2007). Therefore, we suggest that the late Holocene increase in precipitation in central Borneo is primarily related to an intensified AISM as it was

already observed by Mohtadi et al. (2011) and Steinke et al. (2014) punctuated by freshwater pulses related to an intensified ENSO recorded in our foraminiferal Ba/Ca. The late Holocene intensification in rainfall is also supported by stable carbon isotopes from leaf waxes in sediments retrieved from the Lake Towuti, central Sulawesi (Russell et al., 2014), as well as speleothem records from Flores, southern Indonesia. In contrast to our proxy records indicating more humid conditions during the late Holocene, deuterium isotopes in a sedimentary record from the southern Makassar Strait indicate constant rainfall during the Holocene (Tierney et al., 2012). Moreover, the speleothem records from northern Borneo point to a decrease in rainfall during the Holocene (Partin et al. (2007). Although the isotopic composition of rainfall and dripwater from Gunung Mulu/Buda, northern Borneo, imply that speleothems record changes in the location and strength of deep convection in the western Pacific (Cobb et al., 2007), moisture residence times in the warm pool area might alter isotopic-based rainfall reconstructions (Konecky et al., 2016).

Enhanced sand content in the El Junco Crater Lake sediments, Galápagos, has been related to intensified or more frequent El Niño (Fig. 5, Conroy et al., 2008). Periods characterized by an increase in precipitation over the eastern Pacific coincide with periods of enhanced freshwater input in eastern Borneo implying a strengthening of ENSO with intensified El Niño and La Niña years, the latter being recorded in our foraminiferal Ba/Ca (Fig. 5). Thus in addition to a potential masking of dry conditions by an intense AISM, rainfall in response to La Niña might also balance the drier conditions associated with El Niño. Furthermore, a decrease in vegetation cover as a result of prolonged dry conditions related to El Niño years might result in an increase in erosion and hence, increased runoff during the following rainy season. Also intensified rainfall during La Niña induces flash floods resulting in enhanced terrigenous runoff. Therefore, our runoff proxies are probably unable to record the effect of the dry state (El Niño) but reflect the effects of the wet state (La Niña) of ENSO, indicating a strengthening ENSO from mid- to late Holocene.

Monsoonal control on Makassar Strait surface conditions

Sediment trap studies have shown that *G. ruber* occurs throughout the year with different flux rates depending on the study site, the climatic and oceanographic conditions (e.g. Kawahata et al., 2002; Yamasaki et al., 2008; Mohtadi et al., 2009). Jonkers and Kučera (2015) found relatively constant fluxes of *G. ruber* in habitats with low seasonality and SST

above 25°C. Therefore, our SST and $\delta^{18}O_{sw}$ likely recorded an annual average signal of Makassar Strait surface waters.

Sea surface conditions off the Mahakam Delta show cooler and fresher conditions during the late Holocene compared to the mid-Holocene which is generally in good agreement with the cooling and freshening trend observed in the Indo-Pacific Warm Pool (Linsley et al., 2010). The observed late Holocene cooling might be caused either by a potential spatial reduction of the warm pool area or an eastward shift of the Western Pacific Warm Pool independent of or in response to more frequent and/or intensified El Niño conditions (Linsley et al., 2010). However, the comparison of HadISST data off the Mahakam Delta from 1960 to 2010 (Fig. 1, Rayner et al., 2003) to the Nino 3.4 index (http://www.cpc.ncep.noaa.gov/data/indices/) implies no direct relationship to ENSO ($r = 0.02$, $p = 0.56$).

Variations in $\delta^{18}O_{sw}$ from the IPWP might be related to changes in the hydrological cycle controlled by the interhemispheric temperature gradient (Gibbons et al., 2014). The gradient decreased over the past 5 kyr implying a southward shift of the ITCZ (Gibbons et al., 2014).The general trend of our Zr/Rb, SST and $\delta^{18}O_{sw}$ values off the Mahakam Delta follows the December January February (DJF) cross-equatorial insolation gradient between 30°N (Tibetan High pressure cell) and 20°S (Australian Low pressure cell) supporting a strengthening of cross-equatorial winds and hence, a southward shift of the austral summer ITCZ throughout the past 5 kyr (Fig. 5). The increase in seasonality reflected by the increase in the cross-equatorial insolation gradient might have caused an intensified AISM, on one hand pushing relatively cool water from the northwestern Pacific into the Makassar Strait (c.f. Fig. 2) and on the other hand freshening the Java Sea water due to intensified rainfall over southern Indonesia (c.f. Fig. 2). These low-salinity Java Sea waters might have reached further north than the core site of SO 217-18517 in response to intensified AISM during the late Holocene relative to the mid-Holocene affecting the annual mean $\delta^{18}O_{sw}$ values off the Mahakam Delta. As already mentioned, precipitation reconstructions reveal an intensified AISM rainfall during the late Holocene in the eastern Indian Ocean (Mohtadi et al., 2011; Steinke et al., 2014; Kuhnt et al., 2015). Comparison of our Zr/Rb and SST record to the Ti/Ca from Java ($r = -0.81$, $p < 0.001$ and $r = -0.83$, $p < 0.001$ for 200-yr binned Zr/Rb and SST, respectively; Mohtadi et al., 2011) and to the Ti/Ca from Sumba ($r = -0.85$, $p < 0.001$ for 200-yr binned Zr/Rb and SST to Ti/Ca; Steinke et al., 2014) suggests that rainfall in central and eastern Borneo but also the sea surface conditions in the Makassar Strait

are mainly controlled by the same climate phenomenon controlling changes in precipitation over the eastern Indian Ocean.

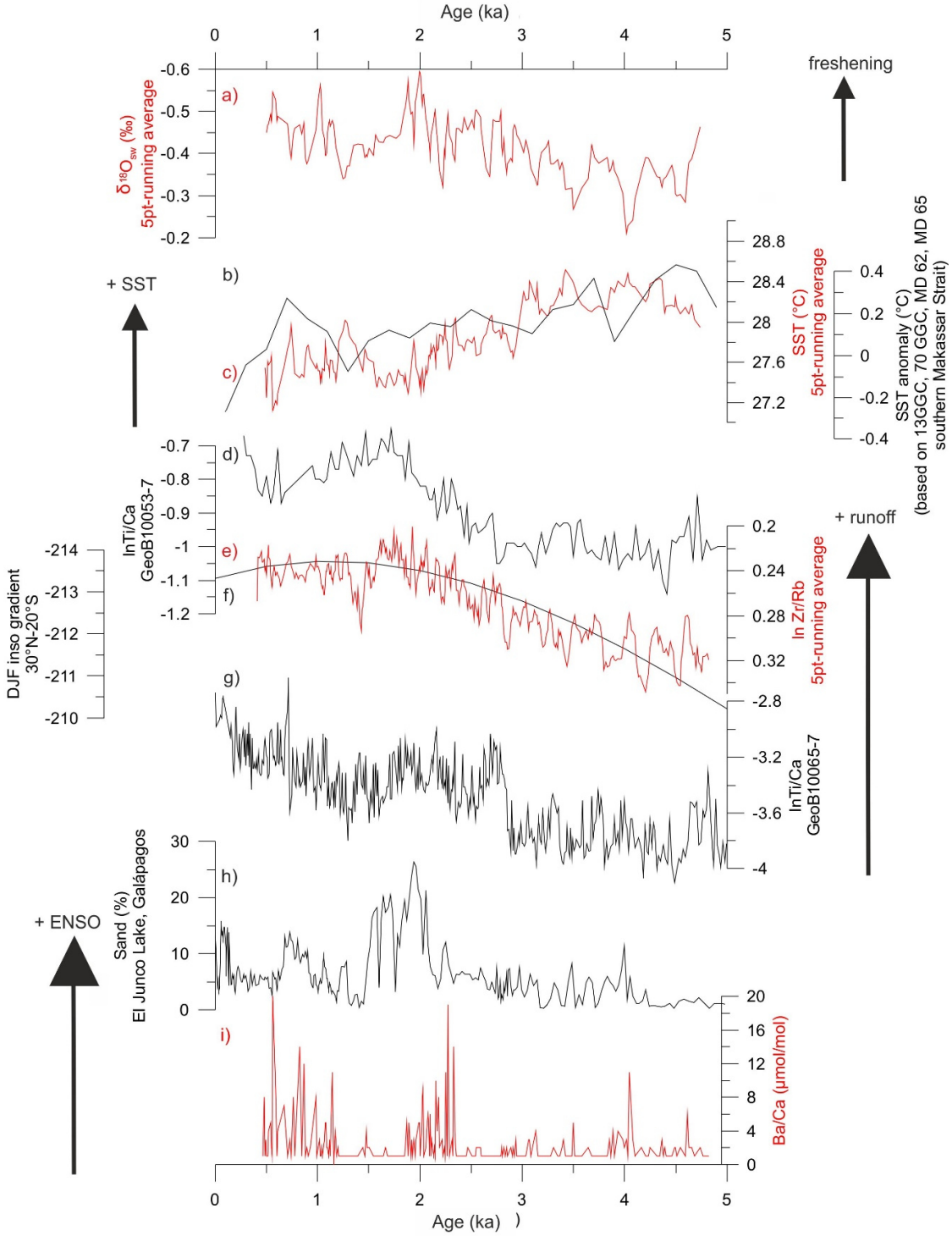

Figure 7.5: Comparison of **a)** our $\delta^{18}O_{sw}$ estimates from the Mahakam Delta, **b)** SST anomaly reconstruction from the southern Makassar Strait (Linsley et al., 2010) to **c)** a 5pt-running average of our SST estimates from the Mahakam Delta, **d)** Ti/Ca of GeoB10053-7 from the eastern Indian Ocean (Mohtadi et al., 2011), **e)** our Zr/Rb ratios following **f)** the DJF insolation gradient between 30°N and 20°S (Laskar et al., 2004), **g)** lnTi/Ca of GeoB10065-7 taken off Sumba island in the eastern Indian Ocean (Steinke et al., 2014), **h)** the sand content from the El Junco sediment record from Galapagos (Conroy et al., 2008) and **i)** our foraminiferal Ba/Ca record. Our results are plotted in a 5pt-running average to highlight the general trends.

Thus, we hypothesize that environmental conditions in the study area recorded by our proxies are mainly controlled by the AISM. The observed cooling and freshening in our record is likely caused by a strengthened AISM during the past 2.7 kyr. This is also supported by the difference in $\delta^{18}O_{sw}$ between the southern Makassar Strait and the western Pacific, which reflects a freshening in central Indonesia during the late Holocene (Linsley et al., 2010) likely related to intense monsoonal rainfall. Therefore, the first order variability in rainfall over eastern Borneo is controlled by the intensified AISM and additionally affected by ENSO resulting in intensified precipitation events over eastern Borneo in response to intense La Niña during the late Holocene.

7.6. Summary

Based on a high-resolution multi-proxy record from the Makassar Strait, Indonesia, we investigated surface water conditions off the Mahakam Delta and variations in precipitation over the Mahakam catchment area in response to the Australian-Indonesian monsoon system and El Niño Southern Oscillation over the past 5 kyr.

Variations in SST, $\delta^{18}O_{sw}$ and Zr/Rb imply a strong influence of the Australian-Indonesian summer monsoon on surface water conditions in the Makassar Strait and changes in precipitation over central Indonesia during the past 5 kyr. A strengthened Australian-Indonesian summer monsoon resulted in cooler and fresher sea surface water off the Mahakam Delta. Enhanced monsoonal rainfall over central and eastern Borneo led to an increase in riverine runoff indicated by a fining in sediment grain size. Additionally to an intensified Australian-Indonesian summer monsoon, high values of foraminiferal Ba/Ca coincident with higher sedimentation rates indicate periods characterized by intense freshwater input during the late Holocene. These freshwater pulses might be related to a strengthening ENSO during the late Holocene with intensified La Niña recorded in our foraminiferal Ba/Ca. However, the influence of El Niño usually resulting in serve droughts over Indonesia might be masked by a stronger summer monsoon or balanced by intense precipitation events during La Niña years. By providing a new dataset from central Indonesia, this study contributes to enlarge the paleo-dataset which can be used for the validation of climate models. Further high resolution records focusing especially on precipitation changes over Indonesia are needed to untangle the monsoon and ENSO signals in the past.

Acknowledgements

We acknowledge Silvana Pape, Henning Kuhnert, and Birgit Meyer-Schack for technical assistance. We are grateful to Stephan Steinke and Delia Oppo for helpful discussions. This work was funded by the BMBF projects MAJA (03G0217A), CAFINDO (03F0645A) as part of the SPICE III cluster, and supported by the DFG-Research Center / Cluster of Excellence „The Ocean in the Earth System“.

8. Late Holocene variations in precipitation pattern over Borneo and Java in response to monsoon, ENSO and northern high latitude forcing

Cornelia Kwiatkowski[1], Mahyar Mohtadi[1], Haryadi Permana[2], Susilohadi Susilohadi[3], Rina Zuraida[3], Dierk Hebbeln[1]

[1]MARUM – Center for Marine Environmental Sciences, University of Bremen, Bremen, Germany (ckwiatkowski@marum.de)

[2]LIPI – Indonesian Institute of Sciences, Bandung, Java, Indonesia

[3]Marine Geological Institute of Indonesia, Bandung, Java, Indonesia

Abstract

Precipitation reconstructions from Indonesia reveal a complex rainfall history over the Maritime Continent during the Holocene. Previous studies highlighted the strong connection of Indonesian climate variability to high northern latitude forcing via latitudinal shifts in the Intertropical Convergence Zone (ITCZ) in symphony with changes in the Australian-Indonesian monsoon system on glacial-interglacial timescales as well as during the past centuries. Here we present variations in grain size and element distribution in gravity cores from the Java Sea in order reconstruct changes in precipitation in response to the controlling climate phenomena El Niño-Southern Oscillation and the Australian-Indonesian monsoon system. The cores were taken off major river mouths, the Seruyan Delta off Borneo and the Solo Delta off Java, reflecting changes in precipitation-related runoff for the past 5.5 kyr. The records suggest a long-term decrease in rainfall culminating at ~2 ka in Borneo and relatively unchanged rainfall in Java. We suggest that drier conditions around ~2 ka are related to prolonged dry seasons in Borneo owing to intense El Niño events. These conditions are masked by a stronger Australian-Indonesian summer monsoon (AISM) in Java. Based on observational data from the past decades, we infer a strong teleconnection of the Australian-Indonesian monsoon system to North Atlantic sea surface temperature anomalies known as the Atlantic Multidecadal Oscillation (AMO). A southward shift in the austral summer ITCZ and the ensuing increase in the sensitivity of the Indonesian rainfall to AMO warm phases might have resulted in intensified AISM in Java leveling out the impact of intensified and/or more frequent El Niño events during the late Holocene.

Key words: Java Sea, Australian-Indonesian monsoon, El Niño – Southern Oscillation, Atlantic Mulitdecadal Oscillation, ITCZ, grain size, X-ray fluorescence

8.1. Introduction

The Australian-Indonesian monsoon system and the El NiñoSouthern Oscillation (ENSO) exert the main control on the seasonal and interannual variability and the spatial distribution of rainfall over the Maritime Continent (e.g. Aldrian and Susanto, 2003; Hendon, 2003). The Australian-Indonesian monsoon system provides the seasonal cycle of rainfall over the monsoonal Indonesia with a dry season during the Australian-Indonesian winter monsoon (AIWM) dominated by southeasterly winds and a wet season during the Australian-Indonesian summer monsoon (AISM) characterized by northwesterly winds. The seasonal cycle of the monsoon is most pronounced in southern and southeastern Indonesia and northern Australia and diminishes towards an all-year-round humid climate in the North and Northwest of Indonesia (Aldrian and Susanto, 2003). ENSO causes rainfall anomalies over the Maritime Continent with El Niño events which resulting in prolonged dry seasons and droughts during strong events, and La Niña events which are characterized by enhanced rainfall and flash floods.

Previous studies have shown that precipitation over Indonesia strongly fluctuates in response to climate variations in the northern high latitudes on glacial-interglacial time scales (e.g. Mohtadi et al., 2011; 2014; Russell et al., 2014) but also during the past centuries (e.g. Tierney et al., 2010). In addition, the Sunda shelf flooding and therewith a new moisture source (Griffiths et al., 2009a), the intensity of the Atlantic Meridional Overturning Circulation (Mohtadi et al., 2014), shifts and changes in the extension of the Intertropical Convergence Zone (ITCZ; Partin et al., 2007; Mohtadi et al., 2011; Griffiths et al., 2016), and the response to the Indian Walker Circulation (Tierney et al., 2012; Dubois et al., 2014) and the Pacific Walker Circulation (Partin et al., 2007; Griffiths et al., 2016) have been suggested to account for Holocene changes in Indonesian rainfall. It has been proposed that monsoonal rainfall over Indonesia is strongly controlled by precession (Lückge et al., 2009; Ayliffe et al., 2013) and solar activity (Steinke et al., 2014), which influence the hemispheric and interhemispheric distribution of insolation and hence, shift and/or strengthen/weaken the monsoon system.

Studies have shown that variations in Atlantic Multidecadal Oscillation (AMO) exert a considerable control on various monsoon systems. The AMO is an oscillatory mode of sea surface temperature (SST) anomalies in the North Atlantic with a periodicity of 65-70 yr (Schlesinger and Ramankutty, 1994). Model simulations (Wei and Lohmann, 2012) as well as

speleothem records (Knudsen et al., 2011) and climatic snapshots based on corals (Giry et al., 2012) imply that variations in AMO persisted throughout the Holocene affecting tropical rainfall

Today, intensified shallow meridional atmospheric circulation in response to warm AMO phases results in enhanced moisture flux and hence intensified African monsoonal rainfall over the Sahel (Martin and Thorncroft, 2014). Indicated by rain gauge data, warm phases of AMO strengthen the meridional tropospheric temperature gradient resulting in a prolonged Indian summer monsoon season and an increase in monsoonal rainfall over India (Goswami et al., 2006). Model simulations suggest also that the East Asian summer monsoon precipitation intensifies in response to AMO warm phases through coupled atmosphere-ocean feedback mechanisms leading to an anti-cyclonic anomaly in the western Pacific (Lu et al. (2006). However, the influence of AMO on the Australian-Indonesian monsoon rainfall has not been described yet.

We used two continuous sediment cores retrieved off two major river mouths off Borneo and Java (Fig. 1) in order to investigate changes in precipitation in southern Borneo and Java over the past 5.5 kyr. We evaluate the influence of ENSO, the Australian-Indonesian summer monsoon and related shifts in northern high latitude SST anomalies on variations in Indonesian rainfall.

8.2. Climatic conditions and river discharge in the study area

The Java Sea is a shallow sea with an average water depth of 40 m located between the islands Borneo and Java in central Indonesia. By being vertically homogeneous (Wyrtki, 1961), the current system in the Java Sea is forced by the seasonal reversal of monsoonal winds shifting the water in westward direction during AIWM and eastward direction during AISM. The Seruyan (Pembuang) River in southern Borneo and the Solo River in eastern Java discharge into the Java Sea and allow for studying climatic signals from land being recorded in Java Sea sediments. The Seruyan River has its source in the Schwaner Mountains and drains an area of 12,000 km^2 before it discharges into the northern Java Sea (Fig. 1, Itakura et al., 2015). The Solo River springs in the Sewu Mountain range in central Java and drains an area of ~16,000 km^2 before it reaches the southern Java Sea (Fig. 1, Hoekstra et al., 1988). The fluvial discharge is closely related to the monsoonal rainfall with discharge rates of 20-30 $m^3 s^{-1}$ during AIWM season and 150-500 $m^3 s^{-1}$ during AISM season (Hoekstra et al., 1988).

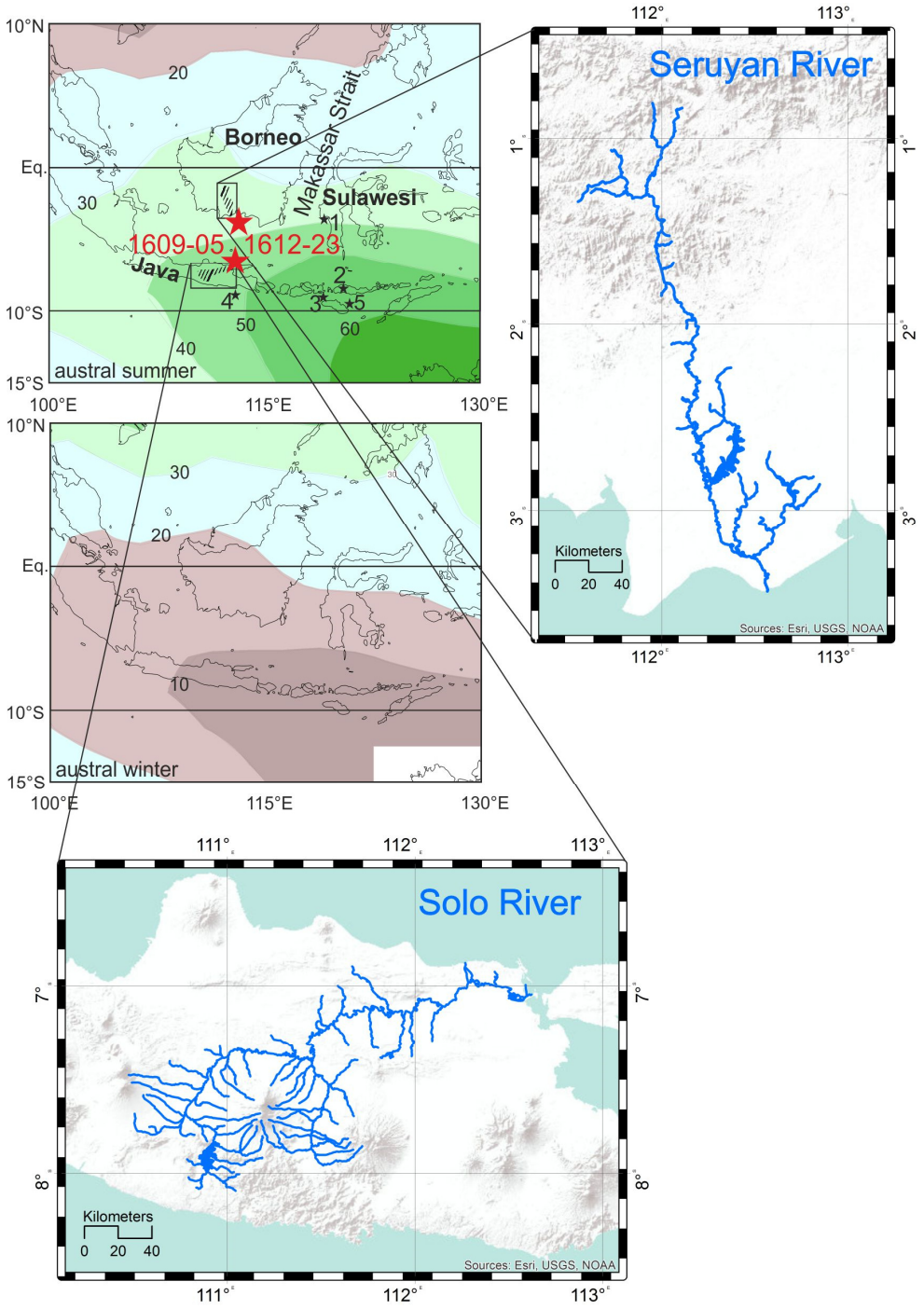

Figure 8.1: Map showing the percentage of annual precipitation that occurs during austral summer (left and austral winter (right), based upon climatological precipitation using the 1981-2010 base period from the monthly CPC Merged Analysis of Precipitation (CMAP) dataset. Regions shaded in green receive more than 30% of their annual precipitation, while areas shaded in brown receive less than 20% of their annual precipitation. Contours are drawn at intervals of 10%. Masked areas in white indicate regions that receive less than 25 mm of precipitation. The red stars indicate the core sites of 1612-23, 1612-26 and 1609-05 taken off the Seruyan River at Borneo and the Solo River of Java, with both catchment areas being indicated. The black stars show the study sites of already published records which are important for comparison; numbered as followed: 1) Speleothem record from Liang Luar, Flores (Griffiths et al., 2009; 2010), 2) GeoB10065-07 (Dubois et al., 2014; Steinke et al., 2014), 3) GeoB10053-7 (Mohtadi et al., 2011), 4) GeoB10069-03 (Dubois et al., 2014). The blow-ups show the river catchment of the Seruyan and the Solo River with all tributaries and the topograpic setting. The basemap was created by using data from ArcGis online (USGS, ESRI, TANA, AND).

Observational data indicate an additional influence of ENSO on monthly fluvial discharge with lower discharge during El Niño and enhanced discharge during La Niña years (Fig. 2).

Both rivers are located within a monsoon controlled climatic regime (Mohtadi et al., 2016; Aldrian and Susanto, 2003). Monthly precipitation over the Seruyan catchment area in Borneo shows year-round rainfall varying between 7 and 10 mm/day with slightly drier conditions during austral winter than during austral summer (Fig. 2). In El Niño years the rainfall drops by ~30% during austral winter, however, thereby hardly leaving the range of rainfall variability in 'normal' years (Fig. 2).

Also, precipitation in the Solo catchment area in Java decreases in response to El Niño events, although it remains within the range of rainfall variability typical for 'normal' years (Fig. 2). There, monthly precipitation varies between 2 and 8 mm/day showing a clear seasonal cycle according to the dry (austral winter) and wet (austral summer) season of the Austral-Indonesian monsoon system (Fig. 2). Although the Maritime Continent is located beneath the anomalously descending Pacific Walker circulation resulting in a weaker convection and less rainfall during El Niño years, model simulations do not provide any evidence that monsoonal rainfall during austral summer over the Maritime Continent is affected either by IOD nor by ENSO (Jourdain et al., 2013). However, ENSO exert a strong control on Indonesian precipitation via air-sea interactions during austral winter resulting in even lesser precipitation during the dry season (Hendon, 2003).

8.3. Material and Methods

Two marine sediment cores from the Java Sea utilized for this study were collected off the Seruyan Delta in Borneo and off the Solo Delta in Java. The cores were sampled in order to investigate runoff changes as recorded in grain size and element distribution for the time interval ~5.5 and ~0.5 ka. The gravity core 1612-23 (3°35.36' S, 112°44.23' E, 134 cm core length, ~20 m water depth) was retrieved ~24 km off the Seruyan Delta, Borneo (Fig. 1), with the Indonesian research vessel Geomarine I in 1995. The gravity core 1609-05 (6°43.15' S, 112°44.84' E, 92 cm core length, 47 m water depth) was taken also with Geomarine I 35 km off the Solo Delta system in 1993 (Fig. 1).

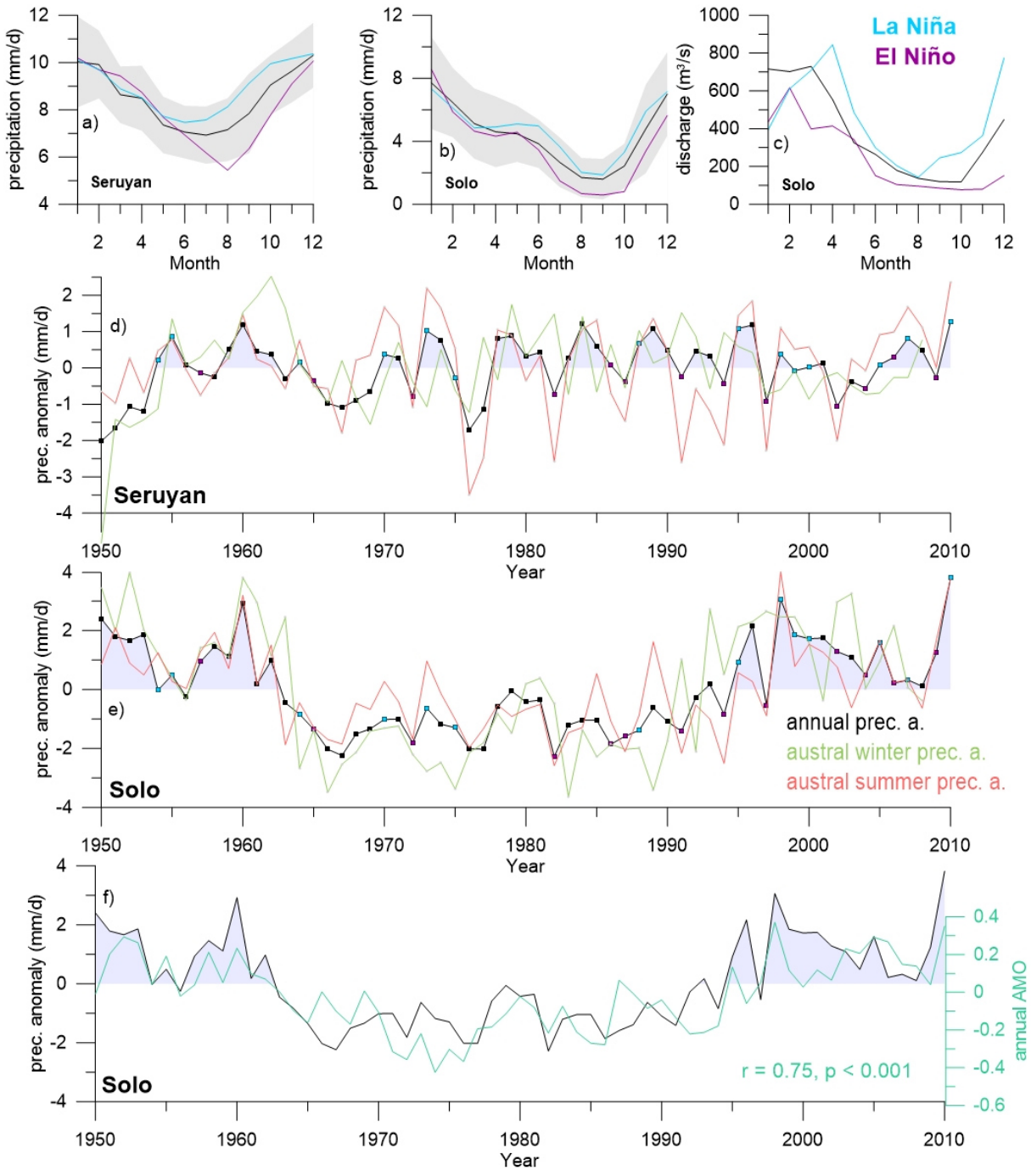

Figure 8.2: a) Rainfall variations over the Seruyan catchment area and **b)** Rainfall variations over the Solo catchment area: NCEP Reanalysis data provided by the NOAA/OAR/ESRL PSD, Boulder, Colorado, USA, indicate seasonal variations in precipitation during normal years (black), El Niño years (purple) and La Niña years (blue, Kalnay et al., 1996). The gray shading indicates the standard deviation of variations in rainfall during normal years since 1960. **c)** Seasonal variations in fluvial discharge of the Solo River during normal years (black), El Niño years (purple) and La Niña years (blue). Time series of annual (black), austral winter (JJA, green) and austral summer (DJF, pink) precipitation anomalies of the **d)** Seruyan River and **e)** the Solo River (Kalnay et al., 1996). El Niño and La Niña years are indicated by purple and blue dots, respectively. The definition of El Niño, La Niña and normal years for **a)** to **e)** is based on Ding and Li (2012) and Sprintall and Révelard (2014). **f)** Annual precipitation anomaly over the Solo catchment area (black) in comparison to the AMO index which is shown in green (http://www.esrl.noaa.gov/psd/data/timeseries/AMO/).

8.3.1. Age Model

The age models are based on 5-6 accelerator mass spectrometry (AMS) ^{14}C dates in each core, which were performed on epibenthic foraminifera and gastropods at the Keck Carbon Cycle Accelerator Mass Spectrometry Facility at the University of California in Irvine, USA (Table 1). All ages were corrected for ^{13}C. Radiocarbon ages were converted to calendar years based on the calibration curve MARINE 13 (Reimer et al., 2013) with a ΔR of zero (Southon et al., 2002). The age-depth relationship was model by using Bayesian age modelling with the Bacon.R software with default settings developed by Blaauw and Christen (2011).

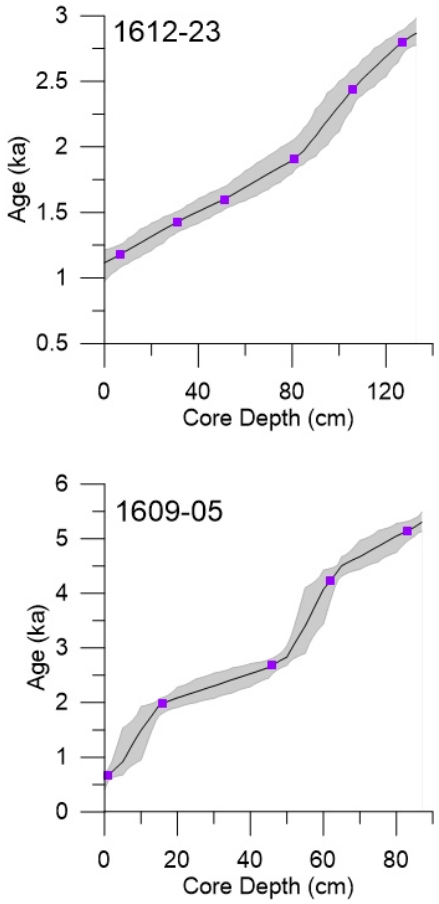

Figure 8.3: Age–depth relationship of sedimentary records 1612-23 off Borneo and 1609-05 off Java based on AMS-14C dates (purple dots) with a 2sigma error range (gray shading) years using Bayesian age modelling.

Tabele 8.1: AMS-^{14}C ages on epibenthic foraminifera and gastropods and cal. ages; AMS-^{14}C ages of core 1612-23 were used to construct a linear age model and published in Poliakova et al. (2016).

Core	Lab. code	Sample depth (cm)	^{14}C age (ka)	cal. median age (ka)	2σ range of cal. age (ka)
1612-23	123503	7	1.605 ± 0.020	1.183	1.09 – 1.26
1612-23	133821	31	1.895 ± 0.020	1.426	1.35 – 1.51
1612-23	145985	51	2.025± 0.025	1.6	1.52 – 1.69
1612-23	133822	81	2.275 ± 0.020	1.910	1.82 – 2.06
1612-23	145986	106	2.760 ± 0.025	2.44	2.31 – 2.59
1612-23	123483	127	3.060 ± 0.020	2.795	2.71 – 2.89
1609-05	145988	1	1.095 ± 0.025	0.656	0.56 – 0.77
1609-05	123489	16	2.355 ± 0.020	1.983	1.81 – 2.09
1609-05	133815	46	2.870 ± 0.020	2.682	2.53 – 2.81
1609-05	133816	62	4.220 ± 0.020	4.238	3.89 – 4.46
1609-05	123490	83	4.805 ± 0.020	5.1454	4.96 – 5.32

8.3.2. Grain size analysis

Both cores were sampled in 5 cm intervals for grain size analyses. Particle-size measurements were performed in the Particle-Size Laboratory at MARUM, University of Bremen with a Beckman Coulter Laser Diffraction Particle Size Analyzer LS 13320.

Prior to the measurements, the terrigenous sediment fractions of 1g bulk sediment were isolated by removing organic carbon, calcium carbonate, and biogenic opal by boiling the samples (in about 200 ml water) with 10 ml of H_2O_2 (35%; until the reaction stopped), 10 ml of HCl (10%; 1 min) and 6 g NaOH pellets (10 min), respectively. After every preparation step the samples were diluted (dilution factor: >25). Finally, remaining aggregates were destroyed prior to the measurements by boiling the samples with ~0.3 g tetra-sodium diphosphate decahydrate ($Na_4P_2O_7$ * $10H_2O$, 3 min) (see also McGregor et al., 2009). Sample preparation and measurements were carried out with deionized, degassed and filtered water (filter mesh size: 0.2 µm) to reduce the potential influence of gas bubbles or particles within the water. The obtained results provide the particle-size distribution of a sample from 0.04 to 2,000 µm divided in 116 size classes. The calculation of the particle sizes relies on the Fraunhofer diffraction theory and the Polarization Intensity Differential Scattering (PIDS) for particles from 0.4 to 2,000 µm and from 0.04 to 0.4 µm, respectively. The reproducibility is checked regularly by replicate analyses of three internal glass-bead standards and is found to be better than ±0.7 µm for the mean and ±0.6 µm for the median particle size (1σ). The average standard deviation integrated over all size classes is better than ±4 vol% (note that the standard deviation of the individual size classes is not distributed uniformly). All provided statistic values are based on a geometric statistic. All provided statistic values are based on a geometric statistic. Here, we use the sand, silt and clay contents and the clay-to-silt ratio as an indicator for riverine runoff in response to over-land precipitation. Higher clay-to-silt ratios indicate enhanced fluvial input as a result of intensified precipitation.

8.3.3. X-Ray Fluorescence analysis

The cores were sampled in 3 cm -intervals for XRF measurements. About 4 g of sediment was freeze-dried, homogenized via micronization and measured by using Panalytical Epsilon 3XL, an energy-dispersive X-ray fluorescence spectrometer with a high-resolution Si-drift detector, at MARUM, University of Bremen. The X-ray tube has a rhodium anode, is software controlled and operates with a maximum voltage of 30 kV. The spectrometer itself was calibrated based on various certified

and in-house standards giving a precision of < 1% and an accuracy of < 3% for all element concentrations. Values are given in mg/kg. Based on the Fe_2O_3 content of bulk and clay sediment fractions of river sediments in Borneo, Liu et al. (2012) infer an enrichment of Fe in weathering products, in this case the red soil, which is the main source of river sediments. Consequently, Fe/Ca are interpreted to reflect variations in terrigenous runoff based on the assumption that Ca mainly reflects biogenic carbonate. In addition, Ti/Ca is interpreted also as a reliable proxy for terrigenous runoff in response to precipitation as it was already used in deep-sea cores from this region by Steinke et al. (2014) and Mohtadi et al. (2011).

8.4. Results

8.4.1. Age Model

Bayesian age modelling resulted in two continuous age chronologies spanning from ~3 to ~1 ka off Borneo and ~5.5 to ~0.5 ka off Java (Fig. 3). Sedimentation rates are on average 0.09 cm/yr off Borneo and 0.03 cm/yr off Java giving an average sample resolution of ~35 (1612-23) and ~110 yr (1609-05) for XRF analysis and ~60 (1612-23) and ~180 yr (1609-05) for grain size analysis.

8.3.4. Grain size

Grain size distributions in the sediment core off Borneo is characterized by a low content in sand (< 8%), high content in silt (~60%) and a moderate content in clay (~35%; Fig. 4). The clay/silt show relatively constant ratios between 3 and 2 ka and an increase from 2 to 1 ka (Fig. 5). The sediment core taken off Java is characterized by a relatively low content of sand (< 7%), a slight decrease in silt content coincident with a slight increase in the clay content during the past 2 kyr (Fig. 4). The clay/silt indicates almost no trend from 5.5 to 2.7 ka. Thereafter, the ratio shows a distinct excursion to higher values and an increasing ratio between ~2 to ~0.5 ka off eastern Java (Fig. 5).

8.4.2. Element composition

Off Borneo, Fe contents are very similar to the Ti contents showing a decrease until ~2 ka and fluctuations around a higher mean value until ~1 ka (Fig. 4). Mirrored by the Fe and Ti contents, Ca contents increase until ~2 ka and varies around 45,000 mg/kg thereafter (Fig. 4). Off Java, the Fe content again follows the Ti content which is anti-correlated to the Ca content (Fig. 4). Variations in Fe and Ti (Ca) show centennial-scale variations between 5.5 and ~2 ka, a minimum (maximum) at ~2 ka and an increase (decrease) to mid-Holocene values thereafter.

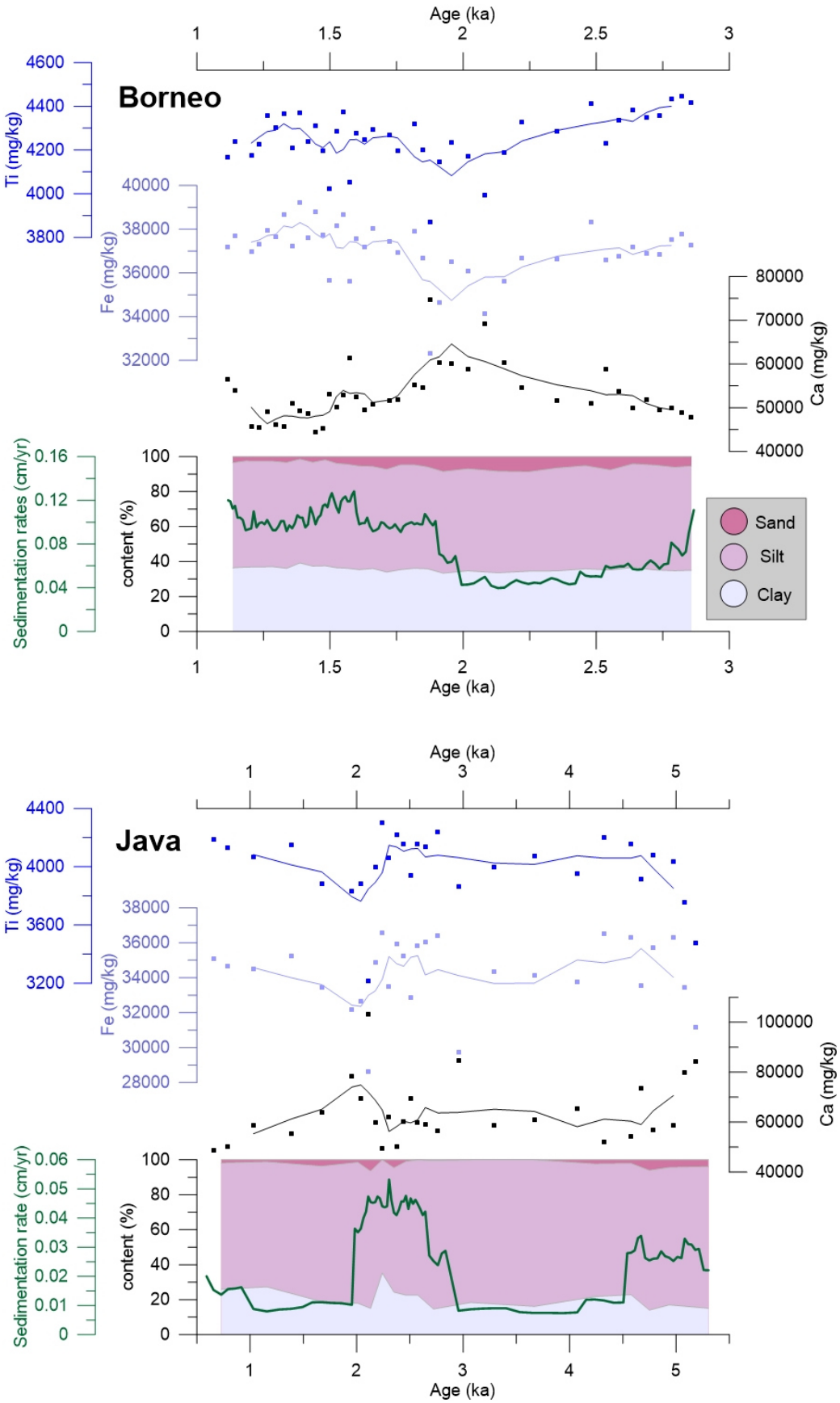

Figure 8.4: Ca, Ti, and Fe contents in mg/kg and grain size distribution in % of cores 1612-23 (top) off Borneo and 1609-05 (bottom) off Java. Sedimentation rates based on the Bayesian age model are indicated in green.

Off Borneo, both Ti/Ca and Fe/Ca indicate a decrease from ~3 to ~2 ka and an increase between ~2 to ~1 ka (Fig. 5). Off Java, Ti/Ca and Fe/Ca show constant ratios from 5.5 to 2.2 ka, a sudden drop around 2.1 ka and an increasing trend to mid-Holocene values between 1.7 and 0.5 ka (Fig. 5).

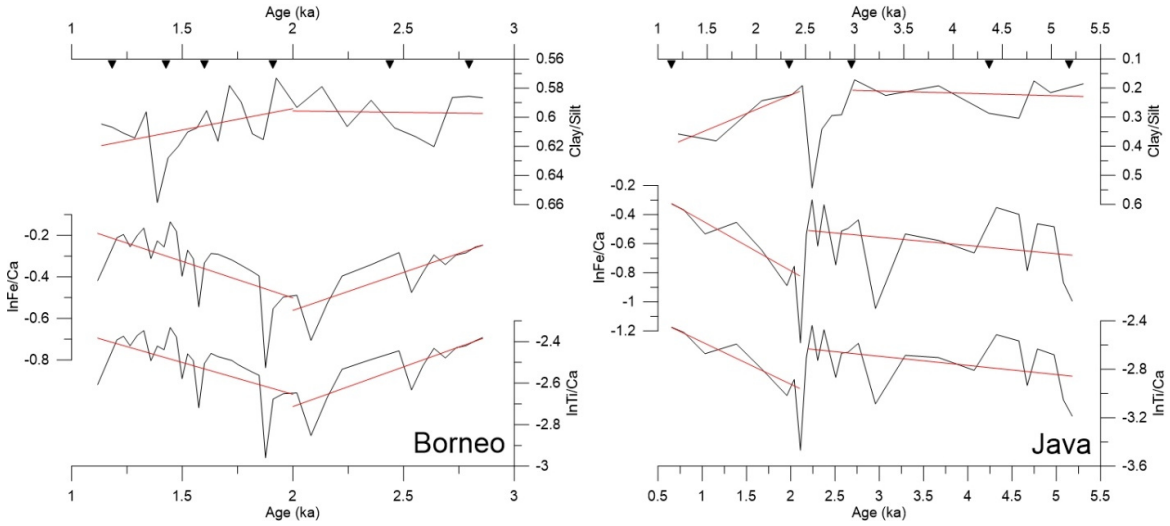

Figure 8.5: Clay/Silt, fine sand content and lnTi/Ca and lnFe/Ca indicating riverine runoff owing to changes in precipitation over the river catchment off Borneo (left) and Java (right). Red lines indicate the general trends of the proxy records. Black triangles indicate the dating points.

8.5. Discussion

Variations in the clay/silt of our records likely reflect changes in terrigenous runoff transported by the rivers Seruyan in Borneo and Solo in Java to the core sites. In addition, variations in Fe/Ca and Ti/Ca are interpreted to reflect changes in continental runoff with Fe and Ti representing the terrigenous input and Ca representing biogenic carbonate of marine origin (Fig. 4). The anti-correlation of Ca to Fe and Ti implies that the latter two are truly related to terrigenous supply in our proxy records. Within this study, we interpret the general trends in proxy data as in such near coastal settings extreme events can cause individual peak values that usually do not reflect the overall paleo-environmental development. Off Borneo, relatively constant grain size is accompanied by low sedimentation rates and decreasing Fe/Ca and Ti/Ca between ~3 and ~2 ka indicating a decrease in rainfall culminating in relatively dry conditions at ~2 ka (Fig. 4, 5). Thereafter, a decrease in grain size and a shift toward higher sedimentation rates as well as an increase in Fe/Ca and Ti/Ca suggest an increase in precipitation between ~2 and ~1 ka. Off Java, constant grain size in addition to relatively constant Fe/Ca and Ti/Ca reveal constant precipitation over Java between 5.5. and 2.5 ka (Fig. 5). A distinct period characterized by enhanced deposition of fine grained material between

2.5 and 2 ka corresponds to slightly higher Fe/Ca and Ti/Ca and is followed by again coarser sediments and a minimum in Fe/Ca and Ti/Ca pointing to drier conditions at ~2 ka (Fig. 5). Thereafter, a decrease in grain size is accompanied by an increase in Fe/Ca and Ti/Ca to mid-Holocene values which indicates an increase in precipitation between ~2 and ~1 ka.

Present-day precipitation over southern and central Indonesia is mainly controlled by the Australian-Indonesian monsoon system and to a lesser extent by ENSO (Aldrian and Susanto, 2003). This is supported by NCEP Reanalysis rainfall and river discharge data from the Seruyan and the Solo catchment areas indicating seasonal variations according to the Australian-Indonesian monsoon system as well as prolonged and more intense dry seasons related to El Niño events (Fig. 2). Although the Australian-Indonesian monsoon system is not independent from ENSO (e.g. Mohtadi et al., 2016) due to the eastward displacement of the rising branch of the Pacific Walker Circulation during El Niño years (Kumar et al., 2006), the main control of ENSO on monsoonal rainfall is detected during austral winter and spring but absent during the peak rainy season (Hendon, 2003; Moron et al., 2015). Thus, proxies that reflect annual average rainfall in southern Borneo and experience year-round rainfall with a less intense seasonal cycle in rainfall would be strongly affected by a decrease in austral winter rainfall. In contrast, the annual average rainfall over Java is mainly controlled by the AISM (Fig. 2) which might mask a potential drying during the AIWM season in response to El Niño over Java. Considering the influence of northern high latitudes on tropical rainfall, we compared present-day annual NCEP Reanalysis rainfall anomalies in Java to the AMO index. The correlation between the NCEP rainfall data and AMO index is relatively high and statistically significant ($r = 0.75$, $p < 0.01$; Fig. 2). Thus, some of the rainfall variability over Java can be attributed to changes in AMO/or northern latitude SST anomalies. Today, a positive AMO phase coincides with enhanced precipitation and a negative AMO phase is related to a decrease in precipitation over Java (Fig. 2). Based on present-day climatic teleconnections, in the following we will investigate the late Holocene evolution of Indonesian rainfall and the relationship to ENSO, the Australian-Indonesian monsoon, and AMO within the following.

An increase in sand content in the sediments of the El Junco Crater Lake on Galápagos as a result of enhanced precipitation has been suggested to reflect more frequent and/or intensified El Niño events between 2 and 1.5 ka (Fig. 6, Conroy et al., 2008). According to the El Niño dynamics these events should coincide with

drier conditions over Indonesia. Consequently, the concurrency of intensified precipitation in Galápagos (enhanced sand content) and the decrease in rainfall over Borneo supports a possible influence of ENSO on late Holocene rainfall variations over central Indonesia.

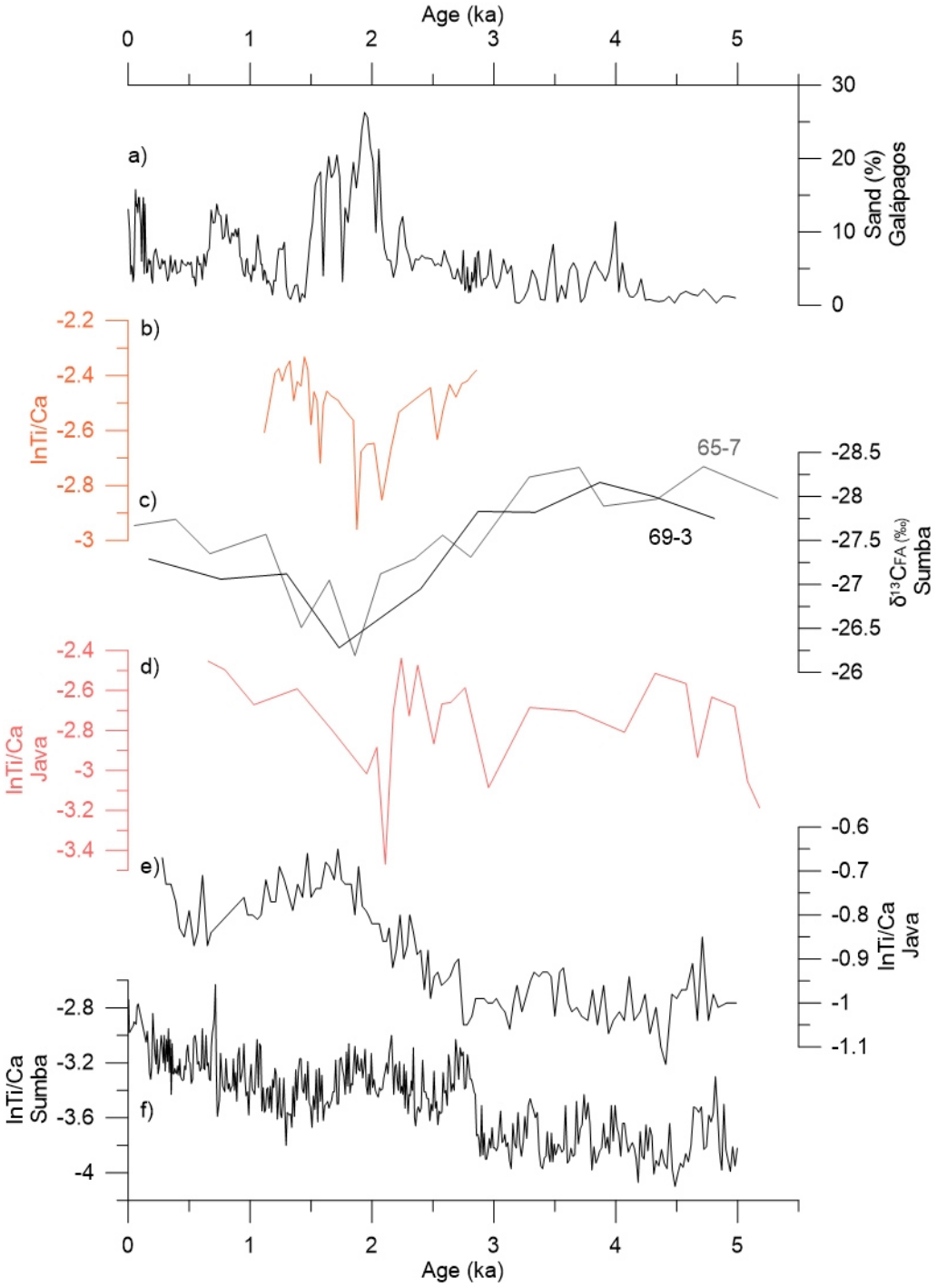

Figure 8.4: Comparison of **a)** the sand content record from the El Junco Lake on Galápagos (Conroy et al., 2008), **b)** lnTi/Ca from core 1612-23 collected off Borneo (orange; this study), **c)** δ^{13}CFA of vascular plant fatty acids as an indicator for vegetation changes from core GeoB 10065-7 and 10069-3 taken off Sumba with more negative values reflecting wetter climate conditions (Dubois et al., 2014), **d)** lnTi/Ca from core 1609-05 taken off Java (pink; this study), **e)** lnTi/Ca from core GeoB10053-7 taken off Java in the eastern Indian Ocean (Mohtadi et al., 2011), **f)** lnTi/Ca from core GeoB10065-7 taken off Sumba (Steinke et al., 2014).

The decrease in rainfall observed in southern Borneo at ~2 ka is also coincident with a decrease in rainfall recorded in speleothems in northern Australia (Denniston et al., 2013) and an abrupt increase in C_4 plants suggesting drier conditions in Sumba, southern Indonesia (Dubois et al., 2014). Vegetation changes in Sumba are interpreted to be caused by an increase in rainfall seasonality owing to a weaker AISM and enhanced water stress through prolonged dry seasons (austral winter, Fig. 6, Dubois et al., 2014). In contrast, the decrease in precipitation observed over northern Australia was explained by a decrease in pre-monsoon rainfall related to an increase in amplitude and/or frequency of El Niño events (Denniston et al., 2013). Intensified rainfall over the eastern Pacific Ocean coincident with a decrease in rainfall in southern Borneo, prolonged dry periods in Sumba and a decrease in pre-monsoonal rainfall in northern Australia around 2 ka (Fig. 6) which implies an intensified ENSO strongly affecting pre-monsoonal rainfall of the Maritime Continent during the late Holocene.

Previous studies suggest a late Holocene intensification of monsoonal rainfall in southern Indonesia (Mohtadi et al., 2011; Steinke et al., 2014). A speleothem record from Flores reflects a strengthening of the AISM during the late Holocene compared to the mid-Holocene (Griffiths et al., 2009a; 2010). This is supported by marine and lacustrine proxy records indicating a late Holocene intensification of the AISM either in response to solar activity (Fig. 6, Steinke et al., 2014), northern high latitude forcing (Mohtadi et al., 2011; Russell et al., 2014), or southern high latitude forcing (Kuhnt et al., 2015). Thus, intensified rainfall due to a strengthening AISM or enhanced precipitation related to intense La Niña might even out the decrease in rainfall related to intensified El Niño recorded in our proxy record from Java. Furthermore, a more scant vegetation cover as a result of more intense and longer dry seasons even promote strong erosion and enhanced terrigenous runoff during the following rainy season.

Previous studies suggest a significant control on Indonesian rainfall pattern by the northern high-latitudes on glacial-interglacial timescales (Mohtadi et al., 2011; Mohtadi et al., 2014; Russell et al., 2014), which is also reflected in present-day data (Fig. 2).We speculate that a potential late Holocene strengthening of the AISM observed in southern Indonesia (e.g. Mohtadi et al., 2011, Fig. 6) might result from a shift towards warmer AMO phases in the northern Atlantic from mid- to late Holocene. Today, warm phases of AMO cause a delay in monsoonal wind reversals over the Indian Ocean and hence, prolonged

Indian summer monsoon seasons (Goswami et al., 2006), positive rainfall anomalies over the Sahel during the African summer monsoon season (Martin and Thorncroft, 2014), and enhanced East Asian summer monsoon rainfall (Lu et al., 2006). By using a coupled atmosphere-ocean global general circulation model, Lu et al. (2006) suggested that positive SST anomalies in the eastern Indian Ocean and the Maritime Continent related to a positive AMO might cause positive local rainfall anomalies further leading to an anticyclonic anomaly in the lower troposphere over the western Pacific. This might have resulted in enhanced precipitation over Southeast and East Asia (Lu et al., 2006). During the past decades, summer as well as winter precipitation over Java follow variations in AMO which implies that both seasons are affected by AMO (Fig. 2).

The relationship between rainfall over Java and AMO is supported by the long-term simulations of the earth system model Community Earth System Models (COSMOS) indicating that the western Pacific Ocean is very sensitive to changes in AMO probably in response to changes in the position of the ITCZ (Wei and Lohmann, 2012). Southern Indonesia was drier during the mid-Holocene (6 ka) compared to today (Wei and Lohmann, 2012) and might reflect a direct response to AMO with enhanced (decreased) rainfall over Indonesia during warm (cold) phases. Based on a latitudinal transect of proxy records reflecting changes in precipitation in the western Atlantic, Knudsen et al. (2011) suggested north-south migrations of the ITCZ and the atmospheric polar fronts to control the sensitivity of low-latitudinal rainfall on variations in AMO. A southward shift of the ITCZ over the past 5 kyr might result in an enhanced sensitivity of the tropics to changes in AMO (Knudsen et al., 2011) and therewith probably increasing the influence of AMO on the Australian-Indonesian monsoon during the late Holocene.

8.6. Summary

A distinct decrease in rainfall in Borneo around ~2 ka corresponds to prolonged dry periods over Sumba (Dubois et al., 2014) and a decrease in pre-monsoonal rainfall over Australia (Denniston et al., 2013). These relatively dry conditions are likely related to more frequent and/or intensified El Niño events as inferred from a Galápagos precipitation record (Conroy et al., 2008). Grain size data as well as Ti/Ca and Fe/Ca off Java reflect constant precipitation-related riverine runoff owing to an intensified AISM that masks to the impact of more intense El Niño events.

Based on recent observational data from the Solo River catchment, we inferred a close relationship of rainfall in Java to sea surface

temperature anomalies in the northern Atlantic known as AMO. Supported by the model study of Wei and Lohmann (2012), Indonesia was very sensitive to changes in northern high latitudes also during the past. Via a southward shift of the ITCZ from mid- to late Holocene the sensitivity of tropical rainfall to shifts in AMO potentially increased (Knudsen et al., 2011), predominant AMO warm phases during the late Holocene might have resulted in enhanced precipitation over southern Indonesia (cf. Wei and Lohmann, 2012). A positive ocean-atmosphere feedback in response to a positive SST anomaly in the eastern Indian Ocean and the Maritime Continent (Lu et al., 2006) provides a possible link between AMO in the northern Atlantic and precipitation over the Indo-Pacific region. Further studies and climate models are necessary to investigate the underlying mechanism of the high latitude forcing on the Australian-Indonesian monsoon system in more detail.

Acknowledgements

We are grateful to Silvana Pape and Jürgen Titschack for technical assistance and to Stephan Steinke for helpful discussions. This work was funded by the BMBF project CAFINDO (03F0645A) as part of the SPICE III cluster, and supported by the DFG-Research Center / Cluster of Excellence „The Ocean in the Earth System“.

9. Synthesis

Proxy records from four marine sediment cores retrieved off Sumatra (western Indonesia), from the Makassar Strait (central Indonesia), and the Java Sea (southern Indonesia) reveal centennial- to millennial-scale variations in sea surface conditions, upper water stratification, and terrigenous supply in response to different climatic forcing mechanisms during the Holocene.

Today, the climatic control on the Maritime Continent varies with the study site due to a very complex geography and a very complex climatic system. This is also reflected by climate reconstructions drawing an inconsistent picture of Holocene climate variability in the Maritime Continent.

By using a continuous high resolution sedimentary record, variations in the upper water column stratification and changes in subsurface water temperatures off western Sumatra, a key area for studying variations of the IOD, could be related to variations in IOD. The Indian Ocean likely shifted from a more negative IOD-like mean state to a more positive IOD-like mean state at ~3 ka. A transient model simulation indicates increasing easterly winds over the equatorial Indian Ocean over the past 8 kyr and supports the interpretation of a more positive IOD-like mean state during the late Holocene.

Sea surface conditions in the Makassar Strait are mainly controlled by the AISM. The intensified AISM results in a surface cooling and freshening as well as an increase in terrigenous supply owing to enhanced precipitation. Additionally, precipitation over eastern Borneo is strongly affected by intensified ENSO during the late Holocene reflected as freshwater pulses in response to La Niña.

Precipitation reconstruction from sedimentary records retrieved from the Java Sea indicate a decrease in rainfall over southern Borneo around ~ 2 ka coincident with relatively dry conditions in northern Australia (Denniston et al., 2013) and Sumba (Dubois et al., 2014) likely related to reduced pre-monsoonal rainfall owing to intense El Niño conditions. Late Holocene intensified AISM might mask El Niño-related dry conditions in Java resulting in relatively unchanged rainfall during the late Holocene. As suggested by previous studies, precipitation over the Maritime Continent is closely related to the northern high latitudes during glacial-interglacial time scales (Mohtadi et al., 2011; Mohtadi et al., 2014; Russell et al., 2014). Supported by observational rainfall data, an intense coupling of monsoonal rainfall over Java to variations in the Atlantic Multidecadal Oscillation might have existed also during the Holocene.

The presented studies in this thesis provide essential new insights into Holocene evolution of large-scale phenomena such as IOD, ENSO, and the Australian-Indonesian monsoon system in the Maritime Continent and contribute substantially to our understanding of centennial to millennial variations in Indonesian climate history. These proxy records are conducive to build a highly resolved database of continuous environmental variations during the past to validate existing climate models and to proof developing climate simulations. Facing the global climate change, reliable climate simulations are of crucial importance to predict future climate and will help the local population to adapt to future environmental changes.

10. Outlook

Our scientific knowledge about the centennial- to millennial-scale evolution of Indonesian climate is based on scarce proxy records from the Maritime Continent. No proxy reconstructions from marine sediments exist from the eastern Maritime Continent (Banda and Arafura Sea) and also the western Maritime Continent (Karimata Strait and Java Sea) is insufficiently sampled. High-resolution sediment cores covering the past centuries as well as millennial-scale variability during the Holocene e.g. from the Java Sea would help to understand the complex interaction between the Australian-Indonesian monsoon system, ENSO and IOD. In case, piston cores or even a drilled core from the Sunda shelf would reach deep enough, the comparison of Holocene environmental variations to climate variations of the Eemian, the last Interglacial, might give some clues about how the climate in the IPWP will develop in future. Beside more high-resolution marine sediment records, also more speleothem and lacustrine proxy records are essential to reconstruct climate variations on land and in the Ocean. Additionally, more coral-based reconstructions are needed to get seasonally and interannually resolved snapshots of climate variations under different climatic controls during the past. Especially, the combination of seasonally high-resolution records from corals and long, continuous proxy records from marine sediments are essential to understand the climatic variability in the IPWP region. Furthermore, these proxy records are required to validate climate simulations and are most helpful when they fulfill all requirements such as high temporal and spatial resolution.

In addition, also climatic reconstructions representing the large-scale climate phenomena such as the Australian-Indonesian monsoon system, ENSO, and IOD controlling the environmental conditions in the IPWP as benchmark records are of crucial importance because climatic signals recorded in climate archives in the Maritime Continent need to be verified by proxy records unambiguously representing the footprint of a climate phenomenon such as ENSO during the past. To date, the evolution of ENSO during the past is still a matter of debate and benchmark records are still lacking (Mohtadi et al., 2016).

Although previous proxy records suggest a close relationship of tropical climate to the high northern latitudes, more studies are needed to investigate these teleconnections on decadal to orbital timescales during the past. In times of melting glaciers in the northern high latitudes, relationships between the poles and the deep tropics need to be identified by using model simulations. The prediction of future climatic shifts as well as the estimation of a changing frequency of climatic events is essential for the local population to adapt to a changing

environment. Therefore, the mechanism and the consequences of high latitudinal climate change on the tropics need to be understood.

References

Abram, N.J., Gagan, M.K., Cole, J.E., Hantoro, W.S., Mudelsee, M., 2008. Recent intensification of tropical climate variability in the Indian Ocean. Nature Geoscience 1, 849-853.

Abram, N.J., Gagan, M.K., Liu, Z., Hantoro, W.S., McCulloch, M.T., Suwargadi, B.W., 2007. Seasonal characteristics of the Indian Ocean Dipole during the Holocene epoch. Nature 445, 299-302.

Abram, N.J., McGregor, H.V., Gagan, M.K., Hantoro, W.S., Suwargadi, B.W., 2009. Oscillations in the southern extent of the Indo-Pacific Warm Pool during the mid-Holocene. Quaternary Science Reviews 28, 2794-2803.

Abreu, J.A., Beer, J., Ferriz-Mas, A., McCracken, K.G., Steinhilber, F., 2012. Is there a planetary influence on solar activity? Astronomy & Astrophysics 548, A88.

Aldrian, E., Susanto, R., 2003. Identification of three dominant rainfall regions within Indonesia and their relationship to sea surface temperature. International Journal of Climatology 23, 1435-1452.

Anand, P., Elderfield, H., Conte, M.H., 2003. Calibration of Mg/Ca thermometry in planktonic foraminifera from a sediment trap time series. Paleoceanography 18, 1050 - 1065.

Ashok, K., Behera, S.K., Rao, S.A., Weng, H., Yamagata, T., 2007. El Niño Modoki and its possible teleconnection. Journal of Geophysical Research: Oceans 112.

Ashok, K., Chan, W.-L., Motoi, T., Yamagata, T., 2004. Decadal variability of the Indian Ocean dipole. Geophysical Research Letters 31, L24207.

Ashok, K., Guan, Z., Yamagata, T., 2003. Influence of the Indian Ocean Dipole on the Australian winter rainfall. Geophysical Research Letters 30, 1821-1825.

Ayliffe, L.K., Gagan, M.K., Zhao, J.-x., Drysdale, R.N., Hellstrom, J.C., Hantoro, W.S., Griffiths, M.L., Scott-Gagan, H., Pierre, E.S., Cowley, J.A., Suwargadi, B.W., 2013. Rapid interhemispheric climate links via the Australasian monsoon during the last deglaciation. Nature Communications 4, 2908-2914.

Barker, S., Greaves, M., Elderfield, H., 2003. A study of cleaning procedures used for foraminiferal Mg/Ca paleothermometry. Geochemistry, Geophysics, Geosystems 4.

Battisti, D.S., Ding, Q., Roe, G.H., 2014. Coherent pan-Asian climatic and isotopic response to orbital forcing of tropical insolation. Journal of Geophysical Research: Atmospheres 119, 11997-12020.

Behera, S.K., Krishnan, R., Yamagata, T., 1999. Unusual ocean-atmosphere conditions in the tropical Indian Ocean during 1994. Geophysical Research Letters 26, 3001-3004.

Behera, S.K., Luo, J.J., Masson, S., Rao, S.A., Sakuma, H., Yamagata, T., 2006. A CGCM Study on the Interaction between IOD and ENSO. Journal of Climate 19, 1688-1705.

Bemis, B.E., Spero, H.J., Bijma, J., Lea, D.W., 1998. Reevaluation of the oxygen isotopic composition of planktonic foraminifera: Experimental results and revised paleotemperature equations. Paleoceanography 13, 150-160.

Bjerknes, J., 1969. Atmospheric Teleconnection from the equatorial Pacific. Monthly Weather Review 97, 163-172.

Blaauw, M., Christen, J.A., 2011. Flexible paleoclimate age-depth models using an autoregressive gamma process. Bayesian Analysis 6, 457-474.

Böhlke, J.K., de Laeter, J.R., De Bièvre, P., Hidaka, H., Peiser, H.S., Rosman, K.J.R., Taylor, P.D.P., 2005. Isotopic Compositions of the Elements, 2001. Journal of Physical and Chemical Reference Data 34, 57-67.

Bond, G., Kromer, B., Beer, J., Muscheler, R., Evans, M.N., Showers, W., Hoffmann, S., Lotti-Bond, R., Hajdas, I., Bonani, G., 2001. Persistent Solar Influence on North Atlantic Climate During the Holocene. Science 294, 2130-2136.

Bond, G., Showers, W., Cheseby, M., Lotti, R., Almasi, P., deMenocal, P., Priore, P., Cullen, H., Hajdas, I., Bonani, G., 1997. A Pervasive Millennial-Scale Cycle in North Atlantic Holocene and Glacial Climates. Science 278, 1257-1266.

Boulanger, J.-P., Menkes, C., 1999. Long equatorial wave reflection in the Pacific Ocean from TOPEX/POSEIDON data during the 1992–1998 period. Clim Dyn 15, 205-225.

Boyle, E.A., 1981. Cadmium, zinc, copper, and barium in foraminifera tests. Earth and Planetary Science Letters 53, 11-35.

Broccoli, A.J., Dahl, K.A., Stouffer, R.J., 2006. Response of the ITCZ to Northern Hemisphere cooling. Geophysical Research Letters 33, n/a-n/a.

Brown, S.J., Elderfield, H., 1996. Variations in Mg/Ca and Sr/Ca ratios of planktonic foraminifera caused by postdepositional dissolution: Evidence of shallow Mg-dependent dissolution. Paleoceanography 11, 543-551.

Cai, W., Pan, A., Roemmich, D., Cowan, T., Guo, X., 2009a. Argo profiles a rare occurrence of three consecutive positive Indian Ocean Dipole events, 2006–2008. Geophysical Research Letters 36, L08701.

Cai, W., Sullivan, A., Cowan, T., 2009b. How rare are the 2006–2008 positive Indian Ocean Dipole events? An IPCC AR4 climate model perspective. Geophysical Research Letters 36, L08702.

Cai, W., Zheng, X.-T., Weller, E., Collins, M., Cowan, T., Lengaigne, M., Yu, W., Yamagata, T., 2013. Projected response of the Indian Ocean Dipole to greenhouse warming. Nature Geosci 6, 999-1007.

Cane, M.A., 2005. The evolution of El Niño, past and future. Earth and Planetary Science Letters 230, 227-240.

Carton, J. A., Giese, B. S., Grodsky, S. A., 2005: Sea level rise and the warming of the oceans in the SODA ocean reanalysis. Journal of Geophysical Research **110**, C09006.

Chang, C.-P., Wang, Z., McBride, J., Liu, C.-H., 2005. Annual Cycle of Southeast Asia—Maritime Continent Rainfall and the Asymmetric Monsoon Transition. Journal of Climate 18, 287-301.

Chang, C.P., Harr, P.A., McBride, J., Hsu, H.H., 2004. Maritime continent monsoon: annual cycle and boreal winter variability, In: Chang, C.P. (Ed.), East Asian Monsoon, 2nd ed. World Scientific Publishing Co. Pte. Ltd., Singapore.

Chen, G., Fang, C., Zhang, C., Chen, Y., 2004. Observing the coupling effect between warm pool and "rain pool" in the Pacific Ocean. Remote Sensing of Environment 91, 153-159.

Chiang, J.C.H., Friedman, A.R., 2012. Extratropical Cooling, Interhemispheric Thermal Gradients, and Tropical Climate Change. Annual Review of Earth and Planetary Sciences 40, 383-412.

Clark, P.U., Shakun, J.D., Baker, P.A., Bartlein, P.J., Brewer, S., Brook, E., Carlson, A.E., Cheng, H., Kaufman, D.S., Liu, Z., Marchitto, T.M., Mix, A.C., Morrill, C., Otto-Bliesner, B.L., Pahnke, K., Russell, J.M., Whitlock, C., Adkins, J.F., Blois, J.L., Clark, J., Colman, S.M., Curry, W.B., Flower, B.P., He, F., Johnson, T.C., Lynch-Stieglitz, J., Markgraf, V., McManus, J., Mitrovica, J.X., Moreno, P.I., Williams, J.W., 2012. Global climate evolution during the last deglaciation. Proceedings of the National Academy of Sciences 109, E1134-E1142.

Clarke, A.J., 2008. An Introduction to the dynamics of El Niño and the Southern Oscillation. Academic Press Elsevier.

Clemens, S.C., Prell, W.L., Sun, Y., 2010. Orbital-scale timing and mechanisms driving Late Pleistocene Indo-Asian summer monsoons: Reinterpreting cave speleothem δ18O. Paleoceanography 25, PA4207.

Cobb, K.M., Adkins, J.F., Partin, J.W., Clark, B., 2007. Regional-scale climate influences on temporal variations of rainwater and cave dripwater oxygen isotopes in northern Borneo. Earth and Planetary Science Letters 263, 207-220.

Collins, M., 2005. El Niño- or La Niña-like climate change? Clim Dyn 24, 89-104.

Collins, W.D., Bitz, C.M., Blackmon, M.L., Bonan, G.B., Bretherton, C.S., Carton, J.A., Chang, P., Doney, S.C., Hack, J.J., Henderson, T.B., Kiehl, J.T., Large, W.G., McKenna, D.S., Santer, B.D., Smith, R.D., 2006. The Community Climate System Model Version 3 (CCSM3). Journal of Climate 19, 2122-2143.

Conroy, J.L., Overpeck, J.T., Cole, J.E., Shanahan, T.M., Steinitz-Kannan, M., 2008. Holocene changes in eastern tropical Pacific climate inferred from a Galápagos lake sediment record. Quaternary Science Reviews 27, 1166-1180.

Cravatte, S., Delcroix, T., Zhang, D., McPhaden, M., Leloup, J., 2009. Observed freshening and warming of the western Pacific Warm Pool. Clim Dyn 33, 565-589.

Croudace, I.W., Rothwell, R.G., 2015. Micro-XRF Studies of Sediment Cores - Applications of a non-destructive tool for the environmental sciences. Springer Science + Business Media Dordrecht.

Dai, A., Wigley, T.M.L., 2000. Global patterns of ENSO-induced precipitation. Geophysical Research Letters 27, 1283-1286.

Darling, K.F., Wade, C.M., 2008. The genetic diversity of planktic foraminifera and the global distribution of ribosomal RNA genotypes. Marine Micropaleontology 67, 216-238.

de Boer, E.J., Tjallingii, R., Vélez, M.I., Rijsdijk, K.F., Vlug, A., Reichart, G.-J., Prendergast, A.L., de Louw, P.G.B., Florens, F.B.V., Baider, C., Hooghiemstra, H., 2014. Climate variability in the SW Indian Ocean from an 8000-yr long multi-proxy record in the Mauritian lowlands shows a middle to late Holocene shift from negative IOD-state to ENSO-state. Quaternary Science Reviews 86, 175-189.

Debret, M., Bout-Roumazeilles, V., Grousset, F., Desmet, M., McManus, J.F., Massei, N., Sebag, D., Petit, J.-R., Copard, Y., Trentesaux, A., 2007. The origin of the 1500-year climate cycles in Holocene North-Atlantic records. Climate of the Past Discussions 3, 679-692.

Denniston, R.F., Wyrwoll, K.-H., Polyak, V.J., Brown, J.R., Asmerom, Y., Wanamaker Jr, A.D., LaPointe, Z., Ellerbroek, R., Barthelmes, M., Cleary, D., Cugley, J., Woods, D., Humphreys, W.F., 2013. A Stalagmite record of Holocene Indonesian–Australian summer monsoon variability from the Australian tropics. Quaternary Science Reviews 78, 155-168.

Deshpande, A., Chowdary, J.S., Gnanaseelan, C., 2014. Role of thermocline–SST coupling in the evolution of IOD events and their regional impacts. Clim Dyn 43, 163-174.

DiNezio, P.N., Clement, A., Vecchi, G.A., Soden, B., Broccoli, A.J., Otto-Bliesner, B.L., Braconnot, P., 2011. The response of the Walker circulation to Last Glacial Maximum forcing: Implications for detection in proxies. Paleoceanography 26, PA3217.

Ding, R., Li, J., 2012. Influences of ENSO Teleconnection on the Persistence of Sea Surface Temperature in the Tropical Indian Ocean. Journal of Climate 25, 8177-8195.

Donohoe, A., Marshall, J., Ferreira, D., McGee, D., 2012. The Relationship between ITCZ Location and Cross-Equatorial Atmospheric Heat Transport: From the Seasonal Cycle to the Last Glacial Maximum. Journal of Climate 26, 3597-3618.

Du, Y., Qu, T., 2010. Three inflow pathways of the Indonesian throughflow as seen from the simple ocean data assimilation. Dynamics of Atmospheres and Oceans 50, 233-256.

Du, Y., Qu, T., Meyers, G., 2008. Interannual Variability of Sea Surface Temperature off Java and Sumatra in a Global GCM*. Journal of Climate 21, 2451-2465.

Du, Y., Qu, T., Meyers, G., Masumoto, Y., Sasaki, H., 2005. Seasonal heat budget in the mixed layer of the southeastern tropical Indian Ocean in a high-resolution ocean general circulation model. Journal of Geophysical Research: Oceans 110, C04012.

Dubois, N., Oppo, D.W., Galy, V.V., Mohtadi, M., van der Kaars, S., Tierney, J.E., Rosenthal, Y., Eglinton, T.I., Luckge, A., Linsley, B.K., 2014. Indonesian vegetation response to changes in rainfall seasonality over the past 25,000 years. Nature Geoscience 7, 513-517.

Dypvik, H., Harris, N., 2001. Geochemical facies analysis of fine-grained siliciclastics using Th/U, Zr/Rb and (Zr+Rb)/Sr ratios. Chemical Geology 181, 131-146.

Elderfield, H., Ganssen, G., 2000. Past temperature and δ18O of surface ocean waters inferred from foraminiferal Mg/Ca ratios. Nature 405, 442-445.

Fairchild, I.J., Baker, A., 2012. Speleothem science: from process to past environments. John Wiley & Sons.

Fairchild, I.J., Frisia, S., Borsato, A., Tooth, A., 2006a. Speleothems, In: Nash, D.J., McLaren, S.J. (Eds.), Geochemical Sediments and Landscapes. Blackwells, Oxford.

Fairchild, I.J., Smith, C.L., Baker, A., Fuller, L., Spötl, C., Mattey, D., McDermott, F., E.I.M.F, 2006b. Modification and preservation of environmental signals in speleothems. Earth-Science Reviews 75, 105-153.

Fan, W., Jian, Z., Bassinot, F., Chu, Z., 2013. Holocene centennial-scale changes of the Indonesian and South China Sea throughflows: Evidences from the Makassar Strait. Global and Planetary Change 111, 111-117.

Fleitmann, D., Burns, S.J., Mangini, A., Mudelsee, M., Kramers, J., Villa, I., Neff, U., Al-Subbary, A.A., Buettner, A., Hippler, D., Matter, A., 2007. Holocene ITCZ and Indian monsoon dynamics recorded in stalagmites from Oman and Yemen (Socotra). Quaternary Science Reviews 26, 170-188.

Fleitmann, D., Burns, S.J., Mudelsee, M., Neff, U., Kramers, J., Mangini, A., Matter, A., 2003. Holocene forcing of the Indian monsoon recorded in a stalagmite from southern Oman. Science 300, 1737-1739.

Gadgil, S., 2003. The Indian monsoon and its variability. Annual Review of Earth and Planetary Sciences 31, 429-467.

Gadgil, S., Vinayachandran, P., Francis, P., Gadgil, S., 2004. Extremes of the Indian summer monsoon rainfall, ENSO and equatorial Indian Ocean oscillation. Geophysical Research Letters 31.

Garcin, Y., Melnick, D., Strecker, M.R., Olago, D., Tiercelin, J.-J., 2012. East African mid-Holocene wet–dry transition recorded in palaeo-shorelines of Lake Turkana, northern Kenya Rift. Earth and Planetary Science Letters 331–332, 322-334.

Gibbons, F.T., Oppo, D.W., Mohtadi, M., Rosenthal, Y., Cheng, J., Liu, Z., Linsley, B.K., 2014. Deglacial δ18O and hydrologic variability in the tropical Pacific and Indian Oceans. Earth and Planetary Science Letters 387, 240-251.

Giry, C., Felis, T., Kölling, M., Scholz, D., Wei, W., Lohmann, G., Scheffers, S., 2012. Mid- to late Holocene changes in tropical Atlantic temperature seasonality and interannual to multidecadal variability documented in southern Caribbean corals. Earth and Planetary Science Letters 331–332, 187-200.

Gordon, A.L., 2005. Oceanography of the Indonesian Seas and their throughflow. Oceanography 18, 14-27.

Gordon, A.L., Fine, R.A., 1996. Pathways of water between the Pacific and Indian oceans in the Indonesian seas. Nature 379, 146-149.

Gordon, A.L., Huber, B.A., Metzger, E.J., Susanto, R.D., Hurlburt, H.E., Adi, T.R., 2012. South China Sea throughflow impact on the Indonesian throughflow. Geophysical Research Letters 39, L11602.

Gordon, A.L., Susanto, R.D., Ffield, A., Huber, B.A., Pranowo, W., Wirasantosa, S., 2008. Makassar Strait throughflow, 2004 to 2006. Geophysical Research Letters 35, L24605.

Gordon, A.L., Susanto, R.D., Vranes, K., 2003. Cool Indonesian throughflow as a consequence of restricted surface layer flow. Nature 425, 824-828.

Goswami, B.N., Madhusoodanan, M.S., Neema, C.P., Sengupta, D., 2006. A physical mechanism for North Atlantic SST influence on the Indian summer monsoon. Geophysical Research Letters 33, L02706.

Gray, L.J., Beer, J., Geller, M., Haigh, J.D., Lockwood, M., Matthes, K., Cubasch, U., Fleitmann, D., Harrison, G., Hood, L., Luterbacher, J., Meehl, G.A., Shindell, D., van Geel, B., White, W., 2010. Solar influences on climate. Reviews of Geophysics 48, RG4001.

Greaves, M., Caillon, N., Rebaubier, H., Bartoli, G., Bohaty, S., Cacho, I., Clarke, L., Cooper, M., Daunt, C., Delaney, M., deMenocal, P., Dutton, A., Eggins, S., Elderfield, H., Garbe-Schoenberg, D., Goddard, E., Green, D., Groeneveld, J., Hastings, D., Hathorne, E., Kimoto, K., Klinkhammer, G., Labeyrie, L., Lea, D.W., Marchitto, T., Martínez-Botí, M.A., Mortyn, P.G., Ni, Y., Nuernberg, D., Paradis, G., Pena, L., Quinn, T., Rosenthal, Y., Russell, A., Sagawa, T., Sosdian, S., Stott, L., Tachikawa, K., Tappa, E., Thunell, R., Wilson, P.A., 2008. Interlaboratory comparison study of calibration standards for foraminiferal Mg/Ca thermometry. Geochemistry, Geophysics, Geosystems 9, Q08010.

Griffiths, M.L., Drysdale, R.N., Gagan, M.K., Frisia, S., Zhao, J.-x., Ayliffe, L.K., Hantoro, W.S., Hellstrom, J.C., Fischer, M.J., Feng, Y.-X., Suwargadi, B.W., 2010. Evidence for Holocene changes in Australian–Indonesian monsoon rainfall from stalagmite trace element and stable isotope ratios. Earth and Planetary Science Letters 292, 27-38.

Griffiths, M.L., Drysdale, R.N., Gagan, M.K., Zhao, J.x., Ayliffe, L.K., Hellstrom, J.C., Hantoro, W.S., Frisia, S., Feng, Y.x., Cartwright, I., Pierre, E.S., Fischer, M.J., Suwargadi, B.W., 2009. Increasing Australian-Indonesian monsoon rainfall linked to early Holocene sea-level rise. Nature Geoscience 2, 636-639.

Griffiths, M.L., Kimbrough, A.K., Gagan, M.K., Drysdale, R.N., Cole, J.E., Johnson, K.R., Zhao, J.-X., Cook, B.I., Hellstrom, J.C., Hantoro, W.S., 2016. Western Pacific hydroclimate linked to global climate variability over the past two millennia. Nature Communications 7, 11719.

Guan, Z., Yamagata, T., 2003. The unusual summer of 1994 in East Asia: IOD teleconnections. Geophysical Research Letters 30, 1544.

Gupta, A.K., Anderson, D.M., Overpeck, J.T., 2003. Abrupt changes in the Asian southwest monsoon during the Holocene and their links to the North Atlantic Ocean. Nature 421, 354-357.

Hallock, P., 1999. Symbiont-bearing foraminifera, In: Sen Gupta, B.K. (Ed.), Modern foraminifera. Kluwer Academic Publishers, New York, Boston, Dordrecht, London, Moscow, pp. 123-139.

Hamada, J.-I., Yamanaka, M.D., Matsumoto, J., Fukao, S., Winarso, P.A., Sribimawati, T., 2002. Spatial and Temporal Variations of the Rainy Season over Indonesia and their Link to ENSO. Journal of the Meteorological Society of Japan. Ser. II 80, 285-310.

Haug, G.H., Hughen, K.A., Sigman, D.M., Peterson, L.C., Röhl, U., 2001. Southward migration of the intertropical convergence zone through the Holocene. Science 293, 1304-1308.

Hemleben, C., Spindler, M., Anderson, O.R., 1989. Modern Planktonic Foraminifera. Springer Verlag, New York, Berlin, Heidelberg, London, Paris, Tokyo.

Hendiarti, N., Siegel, H., Ohde, T., 2004. Investigation of different coastal processes in Indonesian waters using SeaWiFS data. Deep Sea Research Part II: Topical Studies in Oceanography 51, 85-97.

Hendon, H.H., 2003. Indonesian Rainfall Variability: Impacts of ENSO and Local Air–Sea Interaction. Journal of Climate 16, 1775-1790.

Hoekstra, P., Augustinus, P.G.E.F., Terwindt, J.H.J., 1988. River Outflow and Mud Deposition in a Monsoon-Dominated Coastal Environment, In: Dronkers, J., Leussen, W. (Eds.), Physical Processes in Estuaries. Springer Berlin, Heidelberg.

Hönisch, B., Allen, K.A., Russell, A.D., Eggins, S.M., Bijma, J., Spero, H.J., Lea, D.W., Yu, J., 2011. Planktic foraminifers as recorders of seawater Ba/Ca. Marine Micropaleontology 79, 52-57.

Hu, S., Sprintall, J., 2016. Interannual variability of the Indonesian Throughflow: The salinity effect. Journal of Geophysical Research: Oceans 121, 2596-2615.

Iskandar, I., Tozuka, T., Sasaki, H., Masumoto, Y., Yamagata, T., 2006. Intraseasonal variations of surface and subsurface currents off Java as simulated in a high-resolution ocean general circulation model. Journal of Geophysical Research: Oceans 111, C12015.

Itakura, T., Nakatsugawa, M., Sugimoto, H., Watanabe, Y., 2015. Characteristics of Watershed in Central Kalimantan, In: Osaki, M., Tsuji, N. (Eds.), Tropical Peatland Ecosystems. Springer Japan.

Jin, F.-F., 1997. An Equatorial Ocean Recharge Paradigm for ENSO. Part I: Conceptual Model. Journal of the Atmospheric Sciences 54, 811-829.

Jonkers, L., Kučera, M., 2015. Global analysis of seasonality in the shell flux of extant planktonic Foraminifera. Biogeosciences 12, 2207-2226.

Jourdain, N.C., Gupta, A.S., Taschetto, A.S., Ummenhofer, C.C., Moise, A.F., Ashok, K., 2013. The Indo-Australian monsoon and its relationship to ENSO and IOD in reanalysis data and the CMIP3/CMIP5 simulations. Clim Dyn 41, 3073-3102.

Kalnay, E., Kanamitsu, M., Kistler, R., Collins, W., Deaven, D., Gandin, L., Iredell, M., Saha, S., White, G., Woollen, J., Zhu, Y., Leetmaa, A., Reynolds, R., Chelliah, M., Ebisuzaki, W., Higgins, W., Janowiak, J., Mo, K.C., Ropelewski, C., Wang, J., Jenne, R., Joseph, D., 1996. The NCEP/NCAR 40-Year Reanalysis Project. Bulletin of the American Meteorological Society 77, 437-471.

Kawahata, H., Nishimura, A., Gagan, M.K., 2002. Seasonal change in foraminiferal production in the western equatorial Pacific warm pool: evidence from sediment trap experiments. Deep Sea Research Part II: Topical Studies in Oceanography 49, 2783-2800.

Knudsen, M.F., Seidenkrantz, M.-S., Jacobsen, B.H., Kuijpers, A., 2011. Tracking the Atlantic Multidecadal Oscillation through the last 8,000 years. Nature Communications 2, 178.

Konecky, B., Russell, J., Bijaksana, S., 2016. Glacial aridity in central Indonesia coeval with intensified monsoon circulation. Earth and Planetary Science Letters 437, 15-24.

Konecky, B.L., Russell, J.M., Rodysill, J.R., Vuille, M., Bijaksana, S., Huang, Y., 2013. Intensification of southwestern Indonesian rainfall over the past millennium. Geophysical Research Letters 40, 386-391.

Koopmann, B., 1981. Sedimentation von Saharastaub im subtropischen Nordatlantik während der letzten 25.000 Jahre. " Meteor" Forschungs-Ergebnisse, C 35, 23-59.

Koutavas, A., Joanides, S., 2012. El Niño–Southern Oscillation extrema in the Holocene and Last Glacial Maximum. Paleoceanography 27, PA4208.

Kucera, M., 2007. Chapter 6: Planktonic foraminifera as tracers of past oceanic environments, In: Hillaire–Marcel, C., De Vernal, A. (Eds.), Proxies in Late Cenozoic Paleoceanography. Elsevier B.V., pp. 213-262.

Kucera, M., Darling, K.F., 2002. Cryptic species of planktonic foraminifera: their effect on palaeoceanographic reconstructions. Philosophical Transactions of the Royal Society of London. Series A: Mathematical, Physical and Engineering Sciences 360, 695-718.

Kucera, M., Weinelt, M., Kiefer, T., Pflaumann, U., Hayes, A., Weinelt, M., Chen, M.-T., Mix, A.C., Barrows, T.T., Cortijo, E., Duprat, J., Juggins, S., Waelbroeck, C., 2005. Reconstruction of sea-surface temperatures from assemblages of planktonic foraminifera: multi-technique approach based on geographically constrained calibration data sets and its application to glacial Atlantic and Pacific Oceans. Quaternary Science Reviews 24, 951-998.

Kuhnert, H., Kuhlmann, H., Mohtadi, M., Meggers, H., Baumann, K.-H., Pätzold, J., 2014. Holocene tropical western Indian Ocean sea surface temperatures in covariation with climatic changes in the Indonesian region. Paleoceanography 29, 2013PA002555.

Kuhnt, W., et, al., 2011. MAJA - Variability of the Indonesian Throughflow within the Makassar-Java Passage. Institute of Geosciences, Christian Albrechts - Universität zu Kiel, Germany

Kuhnt, W., Holbourn, A., Xu, J., Opdyke, B., De Deckker, P., Röhl, U., Mudelsee, M., 2015. Southern Hemisphere control on Australian monsoon variability during the late deglaciation and Holocene. Nature Communications 6, 5916.

Kylander, M.E., Ampel, L., Wohlfarth, B., Veres, D., 2011. High-resolution X-ray fluorescence core scanning analysis of Les Echets (France) sedimentary sequence: new insights from chemical proxies. Journal of Quaternary Science 26, 109-117.

Laskar, J., Robutel, P., Joutel, F., Gastineau, M., Correia, A.C.M., Levrard, B., 2004. A long-term numerical solution for the insolation quantities of the Earth. Astronomy & Astrophysics 428, 261-285.

Lea, D.W., Boyle, E.A., 1991. The Macalpine Hills Lunar Meteorite ConsortiumBarium in planktonic foraminifera. Geochimica et Cosmochimica Acta 55, 3321-3331.

Lea, D.W., Mashiotta, T.A., Spero, H.J., 1999. Controls on magnesium and strontium uptake in planktonic foraminifera determined by live culturing. Geochimica et Cosmochimica Acta 63, 2369-2379.

Lea, D.W., Spero, H.J., 1992. Experimental determination of barium uptake in shells of the planktonic foraminifera Orbulina universa at 22 C. Geochimica et Cosmochimica Acta 56, 2673-2680.

Lea, D.W., Spero, H.J., 1994. Assessing the reliability of paleochemical tracers: Barium uptake in the shells of planktonic foraminifera. Paleoceanography 9, 445-452.

Li, T., Wang, B., Chang, C.P., Zhang, Y., 2003. A Theory for the Indian Ocean Dipole–Zonal Mode. Journal of the Atmospheric Sciences 60, 2119-2135.

Linsley, B.K., Rosenthal, Y., Oppo, D.W., 2010. Holocene evolution of the Indonesian throughflow and the western Pacific warm pool. Nature Geoscience 3, 578-583.

Liu, Z., Wang, H., Hantoro, W.S., Sathiamurthy, E., Colin, C., Zhao, Y., Li, J., 2012. Climatic and tectonic controls on chemical weathering in tropical Southeast Asia (Malay Peninsula, Borneo, and Sumatra). Chemical Geology 291, 1-12.

Lorenz, S., Lohmann, G., 2004. Acceleration technique for Milankovitch type forcing in a coupled atmosphere-ocean circulation model: method and application for the Holocene. Clim Dyn 23, 727-743.

Lowe, J.J., Walker, M.J.C., 1997. Reconstructing Quaternary Environments - 2nd Edition. Pearson Education Limited, England.

Lu, R., Dong, B., Ding, H., 2006. Impact of the Atlantic Multidecadal Oscillation on the Asian summer monsoon. Geophysical Research Letters 33, L24701.

Lückge, A., Mohtadi, M., Rühlemann, C., Scheeder, G., Vink, A., Reinhardt, L., Wiedicke, M., 2009. Monsoon versus ocean circulation controls on paleoenvironmental conditions off southern Sumatra during the past 300,000 years. Paleoceanography 24, PA1208.

Mantsis, D.F., Lintner, B.R., Broccoli, A.J., Erb, M.P., Clement, A.C., Park, H.-S., 2014. The Response of Large-Scale Circulation to Obliquity-Induced Changes in Meridional Heating Gradients. Journal of Climate 27, 5504-5516.

Marchant, M., Hebbeln, D., Wefer, G., 1999. High resolution planktic foraminiferal record of the last 13,300 years from the upwelling area off Chile. Marine Geology 161, 115-128.

Marshall, J., Donohoe, A., Ferreira, D., McGee, D., 2014. The ocean's role in setting the mean position of the Inter-Tropical Convergence Zone. Clim Dyn 42, 1967-1979.

Martin, E.R., Thorncroft, C.D., 2014. The impact of the AMO on the West African monsoon annual cycle. Quarterly Journal of the Royal Meteorological Society 140, 31-46.

Martin, P.A., Lea, D.W., 2002. A simple evaluation of cleaning procedures on fossil benthic foraminiferal Mg/Ca. Geochemistry, Geophysics, Geosystems 3, 8401.

Matsumoto, J., Murakami, T., 2000. Annual changes of tropical convective activities as revealed from equatorially symmetric OLR data. Journal of the Meteorological Society of Japan 78, 543-561.

Matsumoto, J., Murakami, T., 2002. Seasonal migration of monsoons between the Northern and Southern Hemisphere as revealed from equatorially symmetric and asymmetric OLR data. Journal of Meteorological Society of Japan, Ser. II 80, 419-437.

McBride, J.L., Nicholls, N., 1983. Seasonal Relationships between Australian Rainfall and the Southern Oscillation. Monthly Weather Review 111, 1998-2004.

McGregor, H.V., Dupont, L., Stuut, J.-B.W., Kuhlmann, H., 2009. Vegetation change, goats, and religion: a 2000-year history of land use in southern Morocco. Quaternary Science Reviews 28, 1434-1448.

McPhaden, M.J., 1999. Genesis and Evolution of the 1997-98 El Niño. Science 283, 950-954.

McPhaden, M.J., Wang, Y., Ravichandran, M., 2015. Volume transports of the Wyrtki jets and their relationship to the Indian Ocean Dipole. Journal of Geophysical Research: Oceans 120, 5302-5317.

Mohtadi, M., Max, L., Hebbeln, D., Baumgart, A., Krück, N., Jennerjahn, T., 2007. Modern environmental conditions recorded in surface sediment samples off W and SW Indonesia: Planktonic foraminifera and biogenic compounds analyses. Marine Micropaleontology 65, 96-112.

Mohtadi, M., Oppo, D.W., Lückge, A., DePol-Holz, R., Steinke, S., Groeneveld, J., Hemme, N., Hebbeln, D., 2011a. Reconstructing the thermal structure of the upper ocean: Insights from planktic foraminifera shell chemistry and alkenones in modern sediments of the tropical eastern Indian Ocean. Paleoceanography 26, PA3219.

Mohtadi, M., Oppo, D.W., Steinke, S., Stuut, J.-B.W., De Pol-Holz, R., Hebbeln, D., Luckge, A., 2011b. Glacial to Holocene swings of the Australian-Indonesian monsoon. Nature Geosci 4, 540-544.

Mohtadi, M., Prange, M., Oppo, D.W., De Pol-Holz, R., Merkel, U., Zhang, X., Steinke, S., Lückge, A., 2014. North Atlantic forcing of tropical Indian Ocean climate. Nature 509, 76-80.

Mohtadi, M., Prange, M., Steinke, S., 2016. Palaeoclimatic insights into forcing and response of monsoon rainfall. Nature 533, 191-199.

Mohtadi, M., Steinke, S., Groeneveld, J., Fink, H.G., Rixen, T., Hebbeln, D., Donner, B., Herunadi, B., 2009. Low-latitude control on seasonal and interannual changes in planktonic foraminiferal flux and shell geochemistry off south Java: A sediment trap study. Paleoceanography 24, PA1201.

Mohtadi, M., Steinke, S., Lückge, A., Groeneveld, J., Hathorne, E.C., 2010. Glacial to Holocene surface hydrography of the tropical eastern Indian Ocean. Earth and Planetary Science Letters 292, 89-97.

Mook, W.G., 1986. Recommendations/resolutions adopted by the Twelfth International Radiocarbon Conference. Radiocarbon 28, 799.

Moron, V., Robertson, A.W., Qian, J.-H., 2010. Local versus regional-scale characteristics of monsoon onset and post-onset rainfall over Indonesia. Clim Dyn 34, 281-299.

Moron, V., Robertson, A.W., Qian, J.-H., Ghil, M., 2015. Weather types across the Maritime Continent: from the diurnal cycle to interannual variations, In: Ramos, A.M., Barriopedro, D., Dutra, E. (Eds.), Circulation weather types as a tool in atmospheric, climate abd environmental research. Frontiers Media SA.

Moy, C.M., Seltzer, G.O., Rodbell, D.T., Anderson, D.M., 2002. Variability of El Nino/Southern Oscillation activity at millennial timescales during the Holocene epoch. Nature 420, 162-165.

Murtugudde, R., Busalacchi, A.J., 1999. Interannual Variability of the Dynamics and Thermodynamics of the Tropical Indian Ocean. Journal of Climate 12, 2300-2326.

Murtugudde, R., McCreary, J.P., Busalacchi, A.J., 2000. Oceanic processes associated with anomalous events in the Indian Ocean with relevance to 1997–1998. Journal of Geophysical Research: Oceans 105, 3295-3306.

Naidu, C.V., Durgalakshmi, K., Muni Krishna, K., Ramalingeswara Rao, S., Satyanarayana, G.C., Lakshminarayana, P., Malleswara Rao, L., 2009. Is summer monsoon rainfall decreasing over India in the global warming era? Journal of Geophysical Research: Atmospheres 114, D24108.

Naylor, R.L., Battisti, D.S., Vimont, D.J., Falcon, W.P., Burke, M.B., 2007. Assessing risks of climate variability and climate change for Indonesian rice agriculture. Proceedings of the National Academy of Sciences 104, 7752-7757.

New, M., Hulme, M., Jones, P., 1999. Representing Twentieth-Century Space–Time Climate Variability. Part I: Development of a 1961–90 Mean Monthly Terrestrial Climatology. Journal of Climate 12, 829-856.

Newton, A., Thunell, R., Stott, L., 2011. Changes in the Indonesian Throughflow during the past 2000 yr. Geology 39, 63-66.

Niedermeyer, E.M., Sessions, A.L., Feakins, S.J., Mohtadi, M., 2014. Hydroclimate of the western Indo-Pacific Warm Pool during the past 24,000 years. PNAS 111, 9402-9406.

Ningsih, N.S., Rakhmaputeri, N., Harto, A.B., 2013. Upwelling variability along the southern coast of Bali and in Nusa Tenggara waters. Ocean Science Journal 48, 49-57.

Nizou, J., Hanebuth, T.J.J., Vogt, C., 2011. Deciphering signals of late Holocene fluvial and aeolian supply from a shelf sediment depocentre off Senegal (north-west Africa). Journal of Quaternary Science 26, 411-421.

Norris, R.D., 1996. Symbiosis as an evolutionary innovation in the radiation of Paleocene planktic foraminifera. Paleobiology 22, 461-480.

Oppo, D.W., Rosenthal, Y., Linsley, B.K., 2009. 2,000-year-long temperature and hydrology reconstructions from the Indo-Pacific warm pool. Nature 460, 1113-1116.

Pachauri, R.K., Allen, M.R., Barros, V., Broome, J., Cramer, W., Christ, R., Church, J., Clarke, L., Dahe, Q., Dasgupta, P., Dubash, N.K., Edenhofer, O., Elgizouli, I., Field, C.B., Forster, P.,

Friedlingstein, P., Fuglestvedt, J., Gomez-Echeverri, L., Hallegatte, S., Hegerl, G., Howden, M., Jiang, K., Jimenez Cisneroz, B., Kattsov, V., Lee, H., Mach, K.J., Marotzke, J., Mastrandrea, M.D., Meyer, L., Minx, J., Mulugetta, Y., O'Brien, K., Oppenheimer, M., Pereira, J.J., Pichs-Madruga, R., Plattner, G.K., Pörtner, H.O., Power, S.B., Preston, B., Ravindranath, N.H., Reisinger, A., Riahi, K., Rusticucci, M., Scholes, R., Seyboth, K., Sokona, Y., Stavins, R., Stocker, T.F., Tschakert, P., van Vuuren, D., van Ypserle, J.P., 2014. Climate change 2014: synthesis Report. Contribution of working groups I, II and III to the fifth assessment report of the intergovernmental panel on climate change. IPCC, Geneva, Switzerland.

Partin, J.W., Cobb, K.M., Adkins, J.F., Clark, B., Fernandez, D.P., 2007. Millennial-scale trends in west Pacific warm pool hydrology since the Last Glacial Maximum. Nature 449, 452-455.

Pearson, P.N., 2012. Oxygen isotopes in foraminifera: Overview and historical review. Paleontological Society Papers 18, 1-38.

Peeters, F.J.C., Acheson, R., Brummer, G.-J.A., de Ruijter, W.P.M., Schneider, R.R., Ganssen, G.M., Ufkes, E., Kroon, D., 2004. Vigorous exchange between the Indian and Atlantic oceans at the end of the past five glacial periods. Nature 430, 661-665.

Pena, L.D., Calvo, E., Cacho, I., Eggins, S., Pelejero, C., 2005. Identification and removal of Mn-Mg-rich contaminant phases on foraminiferal tests: Implications for Mg/Ca past temperature reconstructions. Geochemistry, Geophysics, Geosystems 6, Q09P02.

Philander, S.G.H., 1983. El Nino Southern Oscillation phenomena. Nature 302, 295-301.

Philander, S.G.H., 1985. El Niño and La Niña. Journal of the Atmospheric Sciences 42, 2652-2662.

Poliakova, A., Zonneveld, K.A.F., Herbeck, L.S., Jennerjahn, T.C., Permana, H., Kwiatkowski, C., Behling, H., 2016. High-resolution multi-proxy reconstruction of environmental changes in coastal waters of the Java Sea, Indonesia, during the late Holocene. Palynology, 1-14.

Ponton, C., Giosan, L., Eglinton, T.I., Fuller, D.Q., Johnson, J.E., Kumar, P., Collett, T.S., 2012. Holocene aridification of India. Geophysical Research Letters 39, L03704.

Prins, M.A., Weltje, G.J., 1999. End-member modeling of siliciclastic grain-size distributions: the late Quaternary record of eolian and fluvial sediment supply to the Arabian Sea and its paleoclimatic significance, Numerical Experiments in Stratigraphy: Recent Advances in Stratigraphic and Sedimentologic Computer Simulations. SEPM Special Publication.

Qian, J.-H., Robertson, A., Moron, V., 2013. Diurnal cycle in different weather regimes and rainfall variability over Borneo associated with ENSO. Journal of Climate 26, 1772-1790.

Qian, J.-H., Robertson, A.W., Moron, V., 2010. Interactions among ENSO, the Monsoon, and Diurnal Cycle in Rainfall Variability over Java, Indonesia. Journal of the Atmospheric Sciences 67, 3509-3524.

Qiu, Y., Cai, W., Li, L., Guo, X., 2012. Argo profiles variability of barrier layer in the tropical Indian Ocean and its relationship with the Indian Ocean Dipole. Geophysical Research Letters 39, L08605.

Qu, T., Meyers, G., 2005. Seasonal variation of barrier layer in the southeastern tropical Indian Ocean. Journal of Geophysical Research: Oceans 110, C11003.

Ramage, C.S., 1968. Role of a tropical "Maritime Continent" in the atmospheric circulation 1. Monthly Weather Review 96, 365-370.

Rao, K.G., Goswami, B.N., 1988. Interannual Variations of Sea Surface Temperature over the Arabian Sea and the Indian Monsoon: A New Perspective. Monthly Weather Review 116, 558-568.

Rao, S.A., Behera, S.K., Masumoto, Y., Yamagata, T., 2002. Interannual subsurface variability in the tropical Indian Ocean with a special emphasis on the Indian Ocean Dipole. Deep Sea Research Part II: Topical Studies in Oceanography 49, 1549-1572.

Rasmusson, E.M., Carpenter, T.H., 1982. Variations in Tropical Sea Surface Temperature and Surface Wind Fields Associated with the Southern Oscillation/El Niño. Monthly Weather Review 110, 354-384.

Rayner, N.A., Parker, D.E., Horton, E.B., Folland, C.K., Alexander, L.V., Rowell, D.P., 2003. Global analyses of sea surface temperature, sea ice, and night marine air temperature since the late nineteenth century. Journal of Geophysical Research 108, 4407.

Reimer, P.J., Bard, E., Bayliss, A., Beck, J.W., Blackwell, P.G., Bronk Ramsey, C., Buck, C.E., Cheng, H., Edwards, R.L., Friedrich, M., Grootes, P.M., Guilderson, T.P., Haflidason, H., Hajdas, I., Hatté, C., Heaton, T.J., Hoffmann, D.L., Hogg, A.G., Hughen, K.A., Kaiser, K.F., Kromer, B., Manning, S.W., Niu, M., Reimer, R.W., Richards, D.A., Scott, E.M., Southon, J.R., Staff, R.A., Turney, C.S.M., van der Plicht, J., 2013. IntCal13 and Marine13 Radiocarbon Age Calibration Curves 0–50,000 Years cal BP. Radiocarbon 55, 1869-1887.

Robertson, A., Moron, V., Qian, J.-H., Chang, C.P., Tangang, F., Aldrian, E., Koh, T.Y., Juneng, L., 2011. The Maritime Continent Monsoon, In: Chang, C.P., Ding, Y., Lau, N.C., Johnson, R., Wang, B., Yasunari, T. (Eds.), The Global Monsoon System - Research and Forcast 2nd ed. World Scientific Publishing Co. Pte. Ltd., Singapore.

Rosenthal, Y., Linsley, B.K., Oppo, D.W., 2013. Pacific Ocean Heat Content During the Past 10,000 Years. Science 342, 617-621.

Rosenthal, Y., Oppo, D.W., Linsley, B.K., 2003. The amplitude and phasing of climate change during the last deglaciation in the Sulu Sea, western equatorial Pacific. Geophysical Research Letters 30, 1428.

Rostek, F., Ruhlandt, G., Bassinot, F.C., Muller, P.J., Labeyrie, L.D., Lancelot, Y., Bard, E., 1993. Reconstructing sea surface temperature and salinity using δ18O and alkenone records. Nature 364, 319-321.

Russell, J.M., Vogel, H., Konecky, B.L., Bijaksana, S., Huang, Y., Melles, M., Wattrus, N., Costa, K., King, J.W., 2014. Glacial forcing of central Indonesian hydroclimate since 60,000 y B.P. PNAS 111, 5100–5105.

Saji, N.H., Goswami, B.N., Vinayachandran, P.N., Yamagata, T., 1999. A dipole mode in the tropical Indian Ocean. Nature 401, 360-363.

Saji, N.H., Yamagata, T., 2003. Structure of SST and Surface Wind Variability during Indian Ocean Dipole Mode Events: COADS Observations. Journal of Climate 16, 2735-2751.

Sarachik, E.S., Cane, M.A., 2010. The El Niño-Southern Oscillation Phenomenon. Cambrige University Press, New York.

Sarnthein, M., Tetzlafil, G., Koopmann, B., WolterT, K., Pflaumann, U., 1981. Glacial and interglacial wind regimes over the eastern. Nature 293, 193.

Schiebel, R., Hemleben, C., 2005. Modern planktic foraminifera. Paläontologische Zeitschrift 79, 135-148.

Schlesinger, M.E., Ramankutty, N., 1994. An oscillation in the global climate system of period 65-70 years. Nature 367, 723-726.

Schneider, T., Bischoff, T., Haug, G.H., 2014. Migrations and dynamics of the intertropical convergence zone. Nature 513, 45-53.

Schott, F.A., Xie, S.-P., McCreary, J.P., 2009. Indian Ocean circulation and climate variability. Reviews of Geophysics 47, RG1002.

Shinoda, T., Han, W., Metzger, E.J., Hurlburt, H.E., 2012. Seasonal Variation of the Indonesian Throughflow in Makassar Strait. Journal of Physical Oceanography 42, 1099-1123.

Shinoda, T., Hendon, H.H., Glick, J., 1998. Intraseasonal Variability of Surface Fluxes and Sea Surface Temperature in the Tropical Western Pacific and Indian Oceans. Journal of Climate 11, 1685-1702.

Sirocko, F., 1991. Deep-sea sediments of the Arabian Sea: A paleoclimatic record of the southwest-Asian summer monsoon. Geologische Rundschau 80, 557-566.

Southon, J., Kashgarian, M., Fontugne, M., Metivier, B., Yim, W.W.-S., 2002. Marine reservoir corrections for the Indian Ocean and Southeast Asia. Radiocarbon 44, 167-180.

Spintall, J., Tomczak, M., 1992. Evidence of the Barrier Layer in the Surface Layer of the Tropics. Journal of Geophysical Research 97, 7305-7731.

Sprintall, J., Révelard, A., 2014. The Indonesian Throughflow: Response to Indo-Pacific climate variability. Journal of Geophysical Research: Oceans 119, 1161-1175.

Steinke, S., Glatz, C., Mohtadi, M., Groeneveld, J., Li, Q., Jian, Z., 2011. Past dynamics of the East Asian monsoon: No inverse behaviour between the summer and winter monsoon during the Holocene. Global and Planetary Change 78, 170-177.

Steinke, S., Mohtadi, M., Prange, M., Varma, V., Pittauerova, D., Fischer, H.W., 2014. Mid- to Late-Holocene Australian–Indonesian summer monsoon variability. Quaternary Science Reviews 93, 142-154.

Storms, J.E.A., Hoogendoorn, R.M., Dam, R.A.C., Hoitink, A.J.F., Kroonenberg, S.B., 2005. Late-Holocene evolution of the Mahakam delta, East Kalimantan, Indonesia. Sedimentary Geology 180, 149-166.

Stott, L., Cannariato, K., Thunell, R., Haug, G.H., Koutavas, A., Lund, S., 2004. Decline of surface temperature and salinity in the western tropical Pacific Ocean in the Holocene epoch. Nature 431, 56-59.

Stuiver, M., Polach, H.A., 1977. Discussion; reporting of C-14 data. Radiocarbon 19, 355-363.

Susanto, R., Ffield, A., Gordon, A.L., Adi, T.R., 2012. Variability of the Indonesian throughflow within Makassar Strait, 2004-2009. Journal of Geophysical Research 117, C09013.

Susanto, R.D., Gordon, A.L., Zheng, Q., 2001. Upwelling along the coasts of Java and Sumatra and its relation to ENSO. Geophysical Research Letters 28, 1599-1602.

Susanto, R.D., Moore, T.S., Marra, J., 2006. Ocean color variability in the Indonesian Seas during the SeaWiFS era. Geochemistry, Geophysics, Geosystems 7.

Swapna, P., Krishnan, R., 2008. Equatorial undercurrents associated with Indian Ocean Dipole events during contrasting summer monsoons. Geophysical research letters 35.

Tierney, J.E., deMenocal, P.B., 2013. Abrupt Shifts in Horn of Africa Hydroclimate Since the Last Glacial Maximum. Science 342, 843-846.

Tierney, J.E., Oppo, D.W., LeGrande, A.N., Huang, Y., Rosenthal, Y., Linsley, B.K., 2012. The influence of Indian Ocean atmospheric circulation on Warm Pool hydroclimate during the Holocene epoch. Journal of Geophysical Research: Atmospheres 117, D19108.

Tierney, J.E., Oppo, D.W., Rosenthal, Y., Russell, J.M., Linsley, B.K., 2010. Coordinated hydrological regimes in the Indo-Pacific region during the past two millennia. Paleoceanography 25, PA1102.

Tierney, J.E., Russell, J.M., Huang, Y., Damsté, J.S.S., Hopmans, E.C., Cohen, A.S., 2008. Northern Hemisphere Controls on Tropical Southeast African Climate During the Past 60,000 Years. Science 322, 252-255.

Tierney, J.E., Smerdon, J.E., Anchukaitis, K.J., Seager, R., 2013. Multidecadal variability in East African hydroclimate controlled by the Indian Ocean. Nature 493, 389-392.

Tomczak, M., Godfrey, J.S., 1994. Regional Oceanography: An Introduction. Elsevier Science.

Varma, V., Prange, M., Merkel, U., Kleinen, T., Lohmann, G., Pfeiffer, M., Renssen, H., Wagner, A., Wagner, S., Schulz, M., 2012. Holocene evolution of the Southern Hemisphere westerly winds in transient simulations with global climate models. Climate of the Past 8, 391-402.

Von Storch, H., Zwiers, F.W., 2004. Statistical analysis in climate research. Cambridge university press.

Walker, M., Johnsen, S., Rasmussen, S.O., Popp, T., Steffensen, J.-P., Gibbard, P., Hoek, W., Lowe, J., Andrews, J., Björck, S., Cwynar, L.C., Hughen, K., Kershaw, P., Kromer, B., Litt, T., Lowe, D.J., Nakagawa, T., Newnham, R., Schwander, J., 2009. Formal definition and dating of the GSSP (Global Stratotype Section and Point) for the base of the Holocene using the Greenland NGRIP ice core, and selected auxiliary records. Journal of Quaternary Science 24, 3-17.

Wang, B., Liu, J., Kim, H.-J., Webster, P.J., Yim, S.-Y., Xiang, B., 2013. Northern Hemisphere summer monsoon intensified by mega-El Niño/southern oscillation and Atlantic multidecadal oscillation. Proceedings of the National Academy of Sciences 110, 5347-5352.

Wang, P., 2009. Global monsoon in a geological perspective. Chinese Science Bulletin 54, 1113-1136.

Wang, Y., Cheng, H., Edwards, R.L., He, Y., Kong, X., An, Z., Wu, J., Kelly, M.J., Dykoski, C.A., Li, X., 2005. The Holocene Asian Monsoon: Links to Solar Changes and North Atlantic Climate. Science 308, 854-857.

Wanner, H., Beer, J., Bütikofer, J., Crowley, T.J., Cubasch, U., Flückiger, J., Goosse, H., Grosjean, M., Joos, F., Kaplan, J.O., Küttel, M., Müller, S.A., Prentice, I.C., Solomina, O., Stocker, T.F., Tarasov, P., Wagner, M., Widmann, M., 2008. Mid- to Late Holocene climate change: an overview. Quaternary Science Reviews 27, 1791-1828.

Webster, P.J., Moore, A.M., Loschnigg, J.P., Leben, R.R., 1999. Coupled ocean-atmosphere dynamics in the Indian Ocean during 1997-98. Nature 401, 356-360.

Wei, W., Lohmann, G., 2012. Simulated Atlantic Multidecadal Oscillation during the Holocene. Journal of Climate 25, 6989-7002.

Weltje, G.J., Tjallingii, R., 2008. Calibration of XRF core scanners for quantitative geochemical logging of sediment cores: Theory and application. Earth and Planetary Science Letters 274, 423-438.

Wiedicke-Hombach, M., et, al., 2007. SUMATRA - The hydrocarbon system of the Sumatra forearc. Federal Institute for Geosciences and Natural Resources (BGR) Hannover Vol. Archive No. 0126492

Wyrtki, K., 1961. Physical Oceanography of the Southeast Asian Waters, NAGA Report. Scripps Institution of Oceanography.

Wyrtki, K., 1973. An Equatorial Jet in the Indian Ocean. Science 181, 262-264.

Yamasaki, M., Sasaki, A., Oda, M., Domitsu, H., 2008. Western equatorial Pacific planktic foraminiferal fluxes and assemblages during a La Niña year (1999). Marine Micropaleontology 66, 304-319.

Yan, H., Wei, W., Soon, W., An, Z., Zhou, W., Liu, Z., Wang, Y., Carter, R.M., 2015. Dynamics of the intertropical convergence zone over the western Pacific during the Little Ice Age. Nature Geoscience 8, 315-320.

Yeager, S.G., Shields, C.A., Large, W.G., Hack, J.J., 2006. The Low-Resolution CCSM3. Journal of Climate 19, 2545-2566.

Yu, W., Xiang, B., Liu, L., Liu, N., 2005. Understanding the origins of interannual thermocline variations in the tropical Indian Ocean. Geophysical Research Letters 32, L24706.

Zhang, C., 2005. Madden-Julian Oscillation. Reviews of Geophysics 43, RG2003.

Zhang, R., Delworth, T.L., 2005. Simulated Tropical Response to a Substantial Weakening of the Atlantic Thermohaline Circulation. Journal of Climate 18, 1853-1860.

Zhao, Y., Nigam, S., 2015. The Indian Ocean Dipole: A Monopole in SST. Journal of Climate 28, 3-19.